University of Minnesota
St. Anthony Falls Hydraulic Laboratory

Project Report No. 276

HYDRAULIC TRANSIENT ANALYSIS OF TARP PHASE II O'HARE SYSTEM

by

Qizhong Guo

and

Charles C. S. Song

Prepared for

U.S. Army Corps of Engineers
Chicago District
Chicago, Illinois 60604

CONTRACT NO. DACW25-88-M-4080

September 1988
Minneapolis, Minnesota

CONTENTS

LIST OF FIGURES

I. INTRODUCTION

A. PURPOSE OF THE STUDY

The O'Hare System of the Tunnel and Reservoir Plan (TARP), which services 11.2 square miles of combined sewers, as shown in Fig. 1, is the smallest of the four systems comprising the 352–square mile combined sewer service area operated by the Metropolitan Sanitary District of Greater Chicago (MSDGC). After completion of this system in 1980, the O'Hare System area has still experienced problems, including basement flooding from sewer back–up and foundation seepage, overbank flooding, transportation delays caused by flooded streets, water quality degradation of area watercourses from combined sewer overflow, and public health hazards resulting from sewer back–ups. The average annual damage due to flooding in the O'Hare System are estimated to be in excess of $2.5 million [1].

The Chicago District Corps of Engineers, representing the Federal interest in the TARP, has investigated over years the water and related land resource problems and needs in O'Hare combined sewer service area with respect to the MSDGC TARP Phase 2 proposal, and has investigated alternative flood damage reduction plans for the area. The MSDGC TARP Phase 2 proposal of reservoirs is favored by the Corps against traditional improvement of channel capacity [1]. Size, shape, number and location of the reservoir have to be determined for a National Economic Development (NED) Plan. The purpose of this study is to investigate the effectiveness of the recommended plan from the transient flow point of view.

B. METHODS OF THE STUDY

The traditional approach to sewer hydraulic analysis based on steady flow assumption is valid only when flow is small and the sewer never pressurizes. When inflow exceeds the sewer capacity, or when the sewer is designed to store as well as convey water, such as in the case of the TARP system, the network would undergo changes in flow regimes. Typically, the flow would initially be free surface type everywhere. As the sewer continues to fill, the system will pressurize somewhere, such as at a junction or at the downstream end. The flow shortly thereafter is characterized by the existence of a free surface flow regime and a pressurized flow regime separated by one or more moving surge fronts. The magnitude of such a surge may build up to a significant amount as it moves upstream and would generate severe waterhammer pressure upon its collision with an upstream boundary. Clearly, a steady state or a kinematic wave type model is not suitable in these cases. The St. Anthony Falls Hydraulic Laboratory has developed a dynamic model capable of simulating unsteady mixed flow [2] and the model has been applied to a number of sewer networks. One recent example is its application to the TARP Mainstream System sponsored by

MSDGC, where the modeled results match quite well with the measured downstream water level [3]. Due to the strong surge movement in the Mainstream System following heavy storm events, the water level in the sewer network often exceeded the level of combined sewer connection pipe, resulting in sewer back–up or combined sewer overflow.

In addition to sewer back–up and combined sewer overflows, manhole (or dropshaft) cover blow–off and geysering problems have been experienced by many sewer systems including the TARP Main Stream System. Manhole cover blow–off and geysering are violent transient phenomena usually triggered by a pressurization surge and sometimes magnified by the resonant response of a dropshaft and drift tube system. Sudden increase in inflow and lack of ventilation capacity may also cause some problems. A separate mathematical model was established to study these mysterious phenomena in the Mainstream System [3], and further study on this subject is carried out for the O'Hare System.

C. SCOPE OF THE WORK

Overflow, sewer back–up, manhole cover blow–off, and geysering problems were analyzed using a mathematical modeling approach. An overall mixed transient flow model was used to simulate the tunnel fill–up process and the generation of surges. A separate local model was used to analyze the possibility of the blow–off and geysering problems. The mathematical models were also used to determine engineering solution alternatives to the surge problems.

II. TRANSIENT FLOW IN THE MAIN TUNNEL

A. THE MIXED TRANSIENT FLOW MODEL

As pointed out in the Introduction, the flow to be simulated is very unsteady and contains highly dynamic phenomena such as pressurization surge. The model used, then, must be able to simultaneously calculate unsteady open channel flows and unsteady pressurized flows, including the abrupt change that occurs at the shock or the surge front.

The well–known St. Venant equations:

$$\frac{\partial y}{\partial t} + v \frac{\partial y}{\partial x} + \frac{c^2}{g} \frac{\partial v}{\partial x} = 0 \qquad \text{(II–1)}$$

$$g \frac{\partial y}{\partial x} + \frac{\partial v}{\partial t} + v \frac{\partial v}{\partial x} + g(S_f - S_o) = 0 \qquad \text{(II–2)}$$

are used to represent the unsteady open channel flow. In the above equations, y is the flow depth, v is the flow velocity, c is the gravity wave speed, S_o is the channel slope, S_f is the energy slope, and g is the acceleration due to gravity.

The corresponding equations for unsteady pressurized flow are

$$\frac{\partial y}{\partial t} + v \frac{\partial y}{\partial x} + \frac{a^2}{g} \frac{\partial v}{\partial x} = 0 \qquad \text{(II–3)}$$

$$g \frac{\partial y}{\partial x} + \frac{\partial v}{\partial t} + v \frac{\partial v}{\partial x} + g(S_f - S_o) = 0 \qquad \text{(II–4)}$$

in which a is the pressure wave speed, while y takes the meaning of piezometric head measured from the tunnel invert. The system of Eqs. (II–1) ~ (II–4) are solved by the method of characteristics.

Because the transition from the open channel flow condition to pressurized flow condition must be abrupt, as in the case of the hydraulic jump, the special shock boundary conditions must be applied. It was shown by Song [4] that three characteristic equations plus two shock boundary conditions can be used to calculate five unknowns at the pressurization surge or at positive surge. These five unknowns are v and y on both sides of the interface and the speed of the interface movement. The model can also simulate the negative surge which occurs during the depressurization process. A number of other boundary conditions representing junctions, dropshafts, upstream end, downstream end, reservoirs, and other accessories have been developed.

Sewer network geometry, e.g. size and shape of the tunnel, location of dropshafts and junctions were specified in the input data file. Inflow hydrographs, outflow conditions, and other active or passive flow control methods can also be included in the input data file. Velocity, depth, discharge, and other variables at any location and any time may be specified as outputs. In principle, if all input data are accurate, the model should require no calibration. In practice, however, there may be some uncertainties in the input data, especially in estimated inflow hydrographs.

B. APPLICATION OF THE MODEL TO THE TARP O'HARE SYSTEM

1. System Configuration for Modeling Purpose

For the mathematical modeling purpose, the simplified O'Hare system configuration, as shown in Fig. 2, is used. Numbers shown in Fig. 2 are the station numbers used in the model for the purpose of defining different segments of the system. Each junction is represented by three stations for identification of three connecting segments. The entire system is divided into 76 segments of 500 feet each. Locations of eight dropshafts or inflow points are also shown in Fig. 2. Each shaft is assumed to be directly attached to the tunnel, and the detailed geometry including the drift tube is ignored. Dropshaft No. 6 is lumped into the junction represented by Station Nos. 25, 41, and 42. The O'Hare Water Reclamation Plant (WRP) is combined into Dropshaft No. 7 by imposing a negative inflow.

2. Treatment of the Downstream Boundary Condition

The existing TARP phase 1 tunnel system is connected to the proposed terminal reservoir through a 170–foot long concrete conduit at the mainshaft, as shown in Fig. 3. The hydraulics of the terminal reservoir, the connecting conduit, and the main shaft are represented by downstream boundary condition. There are three different flow regimes possible at the downstream end. When the water level in the main shaft is below the crown of the tunnel, the main shaft acts as a reservoir and there is a free surface flow at the downstream end. If the water level in the main shaft is above the crown of the tunnel but below the water level in the reservoir, there is a pressurized flow at the downstream end and the main shaft is still treated as a reservoir. If the water level in the main shaft exceeds the water level in the terminal reservoir, then water is conveyed to the terminal reservoir according to the following equation.

$$Q = cA\sqrt{2g(H_t - H_R)} \qquad \text{(II–5)}$$

where Q is the flowrate, A the cross–sectional area of the connecting conduit, H_t the water level in the tunnel system at main shaft, H_R the water level in the terminal reservoir, and c is the discharge coefficient, estimated to be equal to 0.524.

3. Other Input Data

The main tunnel that extends from St. 1, through Sts. 20 and 50, to St. 76, as shown in Fig. 2, is a 20–foot diameter tunnel. The branch tunnel between St. 26 and St. 49 is a 16–foot diameter tunnel. Finally, the diameter of the branch between St. 21 and St. 25 is 9 feet. The tunnel slope is 0.001 everywhere except for the last segment between St. 71 and St. 76, where an adverse slope of – 0.002 exists. The Manning's coefficient (n) is assumed to be equal to 0.013.

There are eight dropshafts in the system, as shown in Figs. 1 and 2. A typical dropshaft structure (DS–4) is shown in Fig. 4. To simulate transient flow in the main tunnel, inflow hydrographs, dropshaft diameter, and the level at which water flows out of the system (overflow or outfall) are provided. The design hydrographs and hydrographs for several historical storms are shown in Figs. 5 to 15. Dropshaft diameter, outfall level, and other dropshaft parameters are summarized in Table I.

TABLE I. Dropshaft Parameters

No.	Diameter (ft)	Bottom Elevation (ft)	Outfall Elevation (ft)	Surface Ground Elevation (ft)	Drift tube Length (ft)	Drift tube Size	Sewer Q_{max} (cfs)	Design Inflow Rate (cfs)
1	9'x9'	–58.06*	+73.80	+95.00	65'	(13'x28')	1716	1450
2	5'	–61.17	+62.08	+84.00	80'	5'x5' (8'x11')	96	96
3	7'2"	–65.07	+48.00	+80.50	80'	9'x11' (9'x16')	192	270
6	9'	–66.16	+64.60	+81.50	106'	11'x15' (11'x22')	200	811
5	9'	–56.14	+61.50	+73.00	65'	(12'x28')	214	620
6	7'2"	–65.08	+60.81	+73.50	74'	9'x9' (9'x10')	146	200
7	5'	–79.68	+79.50	+79.50	108'	5'x5' (8'x11')	133	133
8	9'	–57.23	+61.75	+74.50	64'	(12'x24')	220	916

* elevation with Chicago city datum
( ) = size of the deaeration chamber

The terminal reservoir sizes under the Corps' consideration include 450 acre–feet, 1,050 acre–feet, and 1,650 acre–feet. The reservoir area is calculated by assuming a cylindrical volume and by knowing the total depth. The diameter of the main shaft at the lower level is 25 feet. The O'Hare Treatment Plant capacity is taken to be 170 cfs during the whole filling process.

C. TRANSIENT CHARACTERISTICS IN THE MAIN TUNNEL

To illustrate the transient characteristics, a pilot study is carried out at first. The design inflow hydrograph, as shown in Fig. 9, a pumping rate of 170 cfs, and the 1,050 acre–feet terminal reservoir are inputted. To save the computer cost, pressure wave speed of 200 cfs is assumed. At the beginning of the simulation, 27 percent of the total tunnel volume is assumed to be filled with water and the terminal reservoir is assumed to be empty.

Computed instantaneous hydraulic gradelines at various stations are shown in Figs. 16 through 20. At the beginning of the filling process, the tunnel near the pumping station gets pressurized first and a moving hydraulic jump forms (Fig. 16). The surge or the hydraulic jump continuously moves upstream until it reaches the junction at Station 50. Then, the surge breaks in half, and later one of these divides into two again at Station 42. Therefore, at $t = 245.653$ minutes, for example, there are three pressurization surges each moving upstream. When a surge reaches an upstream end, a strong pressure is produced due to the lack of surge relief capacity. The instantaneous hydraulic gradeline at $t = 246.835$, shown in Fig. 16, represents the sharp rise in pressure after the main surge reaches Station 1. The other two surges arriving at upstream ends at later times also produce rapid pressure increase. The pressure surge is relatively weaker at DS–5 because the tunnel diameter is smaller and the original pressurization surge is weaker.

The surge produced at DS–1 moves back and forth in the tunnel from Station 1 to Station 20 (No. 50) and to the downstream end at the main shaft, as shown in Fig. 17., until it is joined by the strong reflected surge from DS–8, as shown in Fig. 18. Each reflection rapidly increases the pressure until the water level in the main shaft reaches the terminal reservoir level, as shown in Fig. 19. After the flow to the terminal reservoir is established, the reservoir begins to damp the surge and the flow becomes much less dynamic, as shown in Fig. 20. Time variations of water level at several dropshaft locations are shown in Figs. 21 to 26. Sudden rise in water depth and the severe oscillations following the arrival of the surge are clearly indicated in these figures. The time variation of flow from the tunnel system to the terminal reservoir is shown in Fig. 27. A highly dynamic condition in the initial stage of outflow followed by a gradual damping and slow rise is clearly shown.

From the above illustrations, especially from Figs. 21 to 26, it can be seen that the reservoir does play the role of eliminating the sewer back–up or overflow since the reservoir provides a much lower outfall level than rivers. But the strong surge movements does also exist in the early filling process, which is due to i) high inflow rate, ii) lack of surge relief capacities

at three upstream ends, and iii) relatively high reservoir bottom elevation, making it impossible to regulate the strong surge at the early stage. Whether or not these strong surges will cause some other transient problems, such as dropshaft or manhole cover blow–off and geyser requires further analysis in the following chapter.

III. DROPSHAFT DYNAMICS

A. INTRODUCTION

The purpose of a dropshaft is to drop water from a higher level to a tunnel below without causing too much impact pressure and without entrapping too much air. Its shape and size, as illustrated by Fig. 4, is usually determined by physical modeling based on a constant design flow rate. Its responses to transient conditions, such as surges in the main tunnel, are seldom considered.

The mathematical model of an overall system as described in the previous chapter does not give the true response of the dropshaft to the transient flows because the detailed geometry of the dropshaft plus the drift tube is usually not considered. For this reason, a more detailed analysis of the dropshaft dynamics is given in this chapter.

B. THE DROPSHAFT COVER BLOW–OFF PROCESS

Water level in a dropshaft will rise rapidly if the pressurization surge causes the pressure in the tunnel to rise rapidly. The rising water will push air inside the dropshaft upward exerting pressure on the cover. The magnitude of the air pressure depends on the speed of the rise and the type of grating on the cover. However, because the air density is so small, air pressure is unlikely to lift a cover unless it is air tight.

When water touches the cover, there are two mechanisms that may produce large enough force to lift the cover. The first mechanism is the impact force produced by the water surface hitting the cover. The second type is the steady state force due to water flowing through the grating.

The impact force F is given by

$$F = \rho a V A_s (1 - f) \qquad \text{(III–1)}$$

where A_s is the area of the cover, f is the ratio of the opening to the cover area, and ρ, a, and V, are, respectively, the density, pressure wave velocity, and the flow velocity of water. The impact force given by Eq. III–1 lasts for only a brief time period ΔT. This is the amount of time needed for the pressure wave created by the impact to be relieved by the atmospheric pressure that prevails at the openings. If D_c is the average distance between the openings, then the impact time is approximately

$$\Delta T \approx \frac{D_c}{a} \qquad \text{(III–2)}$$

For the blow–off to occur (or for the cover to fly away), the cover must accelerate to the water velocity within the time interval ΔT. The criterion for the cover blow–off can be shown to be

$$V \geq \frac{gD_c\gamma_c}{a[g\rho D_c(1 - f) - 2\gamma_c]} \qquad \text{(III–3)}$$

where γ_c is the weight of the cover per unit area. In order for Eq. III–3 to be satisfied, the denominator must be positive. But this is not possible if the cover is grated and D_c is small. However, if the cover is not grated, then D_c becomes twice the dropshaft height and blow–off is quite possible. Assuming a typical dropshaft to be 140 feet high, ρ = 1.93 slug/ft^3, γ_c = 100 lb/ft^2, and a = 200 fps, then the minimum water speed for the blow–off is 0.26 fps.

The drag force due to a steady flow of water through the grating is

$$F = \frac{1}{2}\rho V^2 C_D A_s(1 - f) \qquad \text{(III–4)}$$

where

$$C_D = \frac{(1 - 0.7\sqrt{1 - f})^2}{f^2} \qquad \text{(III–5)}$$

If the force given by Eq. III–4 exceeds the weight of the cover, then the rising water will lift the cover due to drag. Assuming γ_c = 70 lb/ft^2 and f = 0.54, then the minimum velocity required to lift the cover is 4.6 fps.

C. THE GEYSER PROCESS

When a water column in a dropshaft rises very slowly to the levels of the connecting pipe, the water may back up into the connecting pipe. But, if the water column rises too rapidly, it may overshoot the connecting pipe, impact the cover, and rise out of the dropshaft, forming a geyser.

An independent mathematical model of a dropshaft–drift tube system, as sketched in Fig. 28, was constructed and used to quantify the geyser when the Mainstream System was modeled [3]. Further analyses are carried out in this study.

The motion of water column in the dropshaft can be described by the following continuity and momentum equations

$$\rho_1 A_s \frac{dH}{dt} = \rho_1 Q_i - V_d A_d \rho_2 \qquad \text{(III–6)}$$

$$\rho_1 A_s \frac{d}{dt}\left[H\frac{dH}{dt} - \frac{Q_i H}{A_s}\right] + \rho_1 Q_i V_i = -\rho_1 g H A_s - \tau_0 A_p + p_d A_s \qquad \text{(III–7)}$$

where

A_s = cross–sectional area of dropshaft,

A_d = cross–sectional area of drift tube,

A_p = wetted area of dropshaft,

H = water column height,

p_d = pressure at the bottom of the dropshaft,

V_d = velocity at the bottom of the dropshaft

V_i = inflow velocity

τ_0 = shear stress on the dropshaft wall

Q_i = inflow rate from the feeder pipe,

ρ_1 = water density in the dropshaft, and

ρ_2 = water density in the drift tube.

Assuming inflow Q_i to be zero, and ρ_1 equal to ρ_2, the above equations simplify to

$$A_s \frac{dH}{dt} = - V_d A_d \qquad \text{(III–8)}$$

$$\rho A_s \frac{d}{dt}\left[H \frac{dH}{dt}\right] = - \rho g H A_s - \tau_0 A_p + p_d A_s \qquad \text{(III–9)}$$

In Eq. III–9, τ_0 is set equal to $1/8\ \rho\ f_0(dH/dt)^2$, where f_0 is the Darcy–Weisbach friction factor, and P_d is assumed to be equal to piezometric pressure in the drift tube. The flow in the drift tube is governed by Eqs. II–3 to II–4.

The modified Euler's method is employed to solve Eq. III–8 to III–9, the method of characteristics is used to solve the partial differential equations for the drift tube. The time–dependent pressure in the main tunnel resulting from surge movements, as described in the last chapter, is set as the downstream end boundary condition of the drift tube–dropshaft model.

Figures 29 through 34 show the dropshaft–drift tube system model outputs. In all cases, main tunnel water level rising speed is set to 8 fps and the time interval of the rising is set close to half of the dropshaft water column oscillation period, which results in a maximum oscillation magnitude. It is clearly shown that even with the same main tunnel water level speed, different dropshaft–drift tube systems give different periods and magnitudes of water column oscillation. This microscale oscillation should be superimposed on the macroscale main tunnel water level variation simulated in the last chapter to obtain total water column height. Whenever the

water column exceeds the surface ground level, a geyser shows up, even if the water level in the main tunnel is lower than the outfall level.

The dropshaft–drift tube system in Fig. 28, considered above, is different from that of the O'Hare System shown in Fig. 4, in that the latter has a separate air vent. Another independent model is also set up based on Eqs. III–6, II–3, and II–4. Anderson [5] studied the stability of two shafts in tandem in a pumped storage scheme and found that the system may become unstable if the exit loss is small. To test his finding, the following equation is used for the downstream boundary condition of the double shafts–drift tube model:

$$Yp(J) = Hm - \frac{Vp^2(J)}{2g} + \xi \frac{Vp(J)|Vp(J)|}{2g} \qquad \text{(III–10)}$$

where Yp(J) and Vp(J) are, respectively, pressure head and velocity at the connection point between the main tunnel and the drift tube, Hm is the main tunnel water level, and ξ is the loss coefficient.

Figures 35 and 36 show the response of dropshaft No. 3 to the pressure rise in the main tunnel for two different sets of assumed energy loss coefficients. It can be seen that both cases are stable and that the double barrel shafts respond to rising pressure in the main tunnel in much the same way as the corresponding single shaft system. Figures 37 to 40 show the response of dropshaft No. 3 to sudden change in inflow rate assuming different energy loss coefficients. As indicated by Figs. 38 and 39, the system can be unstable to a sudden change in inflow rate if energy loss coefficients are small. Since the energy loss coefficients of dropshaft No. 3 are not likely to be small, and since the O'Hare System is designed to avoid sudden gate opening or closing, this type of instability is not considered any further.

D. ANALYTICAL SOLUTIONS TO DROPSHAFT DYNAMICS

The detailed mathematical model of a dropshaft–drift tube system is quite complex and some uncertainties exist in required parameters. For example, the pressure wave speed a is very sensitive to air content, which is not readily available. For this reason, there may be an advantage to developing a simplified analytic solution containing certain coefficients to be calibrated.

Observations of results from Figs. 29 to 34 and other results not included herewith show that the period of water column oscillation, T, can be expressed as follows:

$$T \geq \max\{T_1, T_2, T_3\} \qquad \text{(III–11)}$$

where

$$T_1 = 2\pi \sqrt{\frac{H_m}{g}} = \text{period of water column free oscillation} \qquad \text{(III–12)}$$

$$T_2 = 2\pi \sqrt{\frac{LA_s}{gA_d}} = \text{period of a surge tank oscillation} \qquad \text{(III–13)}$$

$$T_3 = \frac{4L}{a} = \text{period of water hammer oscillation} \qquad \text{(III–14)}$$

in which

H_m = the main tunnel water level,

L = the drift tube length,

A_s = cross–sectional area of the dropshaft,

A_d = cross–sectional area of the drift tube,

a = pressure wave speed in the drift tube, and

g = gravitational acceleration.

A surge tank is widely used in the hydropower development to relieve the surge created by a load change on a turbine. In the surge tank analysis [6], the compressibility of water and the inertial force of water in the tank are neglected. The analysis led to the natural period given by Eq. III–13 and the maximum height of oscillation given by the following equation.

$$h_{max_2} = 2U_m \sqrt{\frac{LA_s}{gA_d}} \qquad \text{(III–15)}$$

where U_m is the water level rising speed in the main tunnel.

The assumptions used to derive Eqs. III–13 and III–15 may not be applicable to the O'Hare System because the drift tubes are not very long and the dropshaft is not very short. The inertial force of the water column in the dropshaft is not negligible in this case.

Let

$$H = H_m + h \qquad \text{(III–16)}$$

and

$$p_d = \rho g(H_m + y') \qquad \text{(III–17)}$$

where H and H_m are the instantaneous and the mean values of the water depth in the dropshaft and p_d is the instantaneous pressure at the base of the dropshaft. In this way, h and y' are the fluctuating components of the water depth and the pressure head, respectively. By substituting Eqs. III–16 and III–17 into Eqs. III–8 and III–9 and linearizing, the following equation is obtained.

$$\frac{d^2h}{dt^2} + 2\,\xi\,\frac{dh}{dt} + k^2h = \frac{gy'}{H_m} \qquad \text{(III–18)}$$

where

$$\xi = \frac{f_0}{4D_s}\frac{dh}{dt} + \frac{1}{2H_m}\left[1 - \frac{h}{H_m}\right]\frac{dh}{dt},$$

$$k = \sqrt{\frac{g}{H_m}},$$

f_0 = Darcy–Weisbach friction factor, and

D_s = dropshaft diameter.

Equation III–18 is the differential equation of a typical vibrating mass–spring system with a variable damping factor. If we ignore the damping and assume free oscillation, then the water column oscillates with period

$$T_1 = \frac{2\pi}{k} = 2\pi\sqrt{\frac{H_m}{g}} \qquad \text{(III–19)}$$

and with magnitude

$$h_{max_1} = 2\,\frac{U_m}{k} = 2U_m\sqrt{\frac{H_m}{g}} \qquad \text{(III–20)}$$

if the water level in the main tunnel rises from one level to another in the time interval of half of the period ($T_1/2$) with the speed of U_m. Substituting parameters as used in Fig. 29 gives $h_{max_1} = 40$ ft, which is the same as the numerically simulated one.

If compressibility is high and the inertial of both drift tube and dropshaft are relatively low, and furthermore, the inertial in the dropshaft is smaller than that of the drift tube, the compressible flow equations II–3 and II–4 should be considered. By integrating spatially along the drift tube and ignoring the friction and slope (which is also suggested by Anderson in his study of the interaction of surge shafts (surge tanks) and penstocks for hydropower development [7]) the following ordinary equation is obtained:

$$\frac{d^2(Y_p - H_m)}{dt^2} + \left[\frac{\pi a}{2L}\right]^2\frac{Y_p - H_m}{L} = 0 \qquad \text{(III–21)}$$

The solution to Eq. III–21 yields the period of oscillation given by Eq. III–14 and the magnitude given by the following equation

$$h_{max_3} = \frac{4LU_m}{a\pi} \qquad \text{(III–22)}$$

if the water level in the main tunnel rises from one level to another within a time interval of half of the oscillation period ($T_3/2$) with a speed of U_m.

E. SAFETY CRITERIA

1. Derivation

Referring to Fig. 28, the oscillatory water column described above will touch the cover, forming a geyser if

$$H_m + h_{max} \geq H_s \qquad \text{(III–23)}$$

where H_s is the dropshaft height. Depending on the oscillation mode, the following three safety criteria exist:

1) Free oscillation ($T_1 \gg T_2$ and T_3)

$$N_f = \frac{2}{H_s - H_m}\sqrt{\frac{H_m}{g}}\, U_m < 1 \qquad \text{(III–24)}$$

2) Surge tank oscillation ($T_2 \gg T_1$ and T_3)

$$N_s = \frac{2}{H_s - H_m}\sqrt{\frac{LA_s}{gA_d}}\, U_m < 1 \qquad \text{(III–25)}$$

3) Water hammer oscillation ($T_3 \gg T_2$ and T_1)

$$N_w = \frac{4}{H_s - H_m}\frac{L}{\pi a}\, U_m < 1 \qquad \text{(III–26)}$$

2. Tests and Remarks

During the October 3, 1986, storm event, geysers were observed at DS–113 at the upstream end and at DS–53 in the middle portion of the mainstream system. Since the geometrical parameters at DS–113 are the same as those used in Fig. 29, then T_1 = 15.7 sec., T_2 = 9.7 sec., and T_3 = 1.79 sec., and, therefore, the water column is most likely in free oscillation and the oscillation magnitude can be estimated by Eq. III–20. Using the calibrated main tunnel rising speed and water level at DS–113, the predicted geyser height is 47 feet, which is in the range of observable height from a distance. Since the geometrical parameters at DS–53 are the same as those used in Fig. 33, then T_1 = 15.7 sec., T_2 = 35.6 sec., and T_3 = 52.4 sec., which indicates that the water hammer oscillation is more likely to occur at this location. If water hammer oscillation is assumed, for the geyser to occur, and by using criteria III–26, very low pressure wave speed is required, which corresponds to the air content on the order of 10 percent, which is not possible in the drift tube, as suggested by the model study [8]. Some other mechanisms might exist for geysers to occur in this location, such as resonance and existence of cavity, etc., but they are unlikely in the O'Hare System, and are not studied in detail.

IV. IDENTIFICATION OF AND SOLUTIONS TO THE TRANSIENT PROBLEMS

A. INTRODUCTION

Transient flows in the main tunnel and in the dropshaft–drift tube system have been described in the last two chapters. Effects of different storm events are to be described in the following. Three different storm events are requested by the Corps of Engineers for identification of transient problems, namely a 25–year, 6–hour storm, a 100–year, 6–hour storm, as used in the pilot study, and the design maximum dropshaft inflow. Since the strongest surges occur before the reservoir bottom level is reached, as indicated in the pilot study, there is no necessity to test the effects of three relatively large reservoir sizes and initial water levels in the reservoir. In the following, the reservoir size of 1,050 acre–feet and zero initial reservoir depth are inputted.

All dropshafts in the O'Hare System have relatively short drift tubes, as shown in Table I. Assuming the main tunnel water depth to be 100 ft, as indicated in the 100–year, 6–hour storm event in the pilot study, the free oscillation period (T_1) will be the longest of all three natural periods. Therefore, the safety criteria (III–24) can be applied to identify the transient problems, such as manhole cover blow–off and geysering. On the other hand, sewer back–up and overflow problems can be identified directly from the main tunnel model output, as mentioned before.

B. 100–YEAR, 6–HOUR STORM

The total inflow hydrograph is shown in Fig. 9. In the study described in Chapter II, an initial storage of 27 per cent full was assumed. Results of the main tunnel modeling are shown in Figs. 16 to 27. The surge oscillation numbers, N_f, at DS–1, DS–5, and DS–8 are, respectively, 2.52, 2.21, and 2.23, indicating geyser problems at these locations. The surge oscillation numbers at other dropshafts are smaller than 1.0.

Assuming the initial storage of 10 per cent full, the main tunnel modeling results are shown in Figs. 41 to 44. The surge oscillation numbers at DS–1, DS–5, and DS–8 are 0.34, 1.61, and 1.55, respectively, which indicates geyser problems at DS–5 and DS–8.

A result for the initially 50 per cent full case is shown in Fig. 45. There is no geysering problem in this case.

For this 100–year, 6–hour storm, an operational measure can be taken to prevent the transient problems, i.e. by filling the system initially

beyond 50 per cent, as illustrated above. Other structural methods are described below. Since 27 per cent of the initial storage creates the most severe transient problems, the following control methods are based on this initial storage.

The direct reason for the transient problems is the lack of surge relief capacity at three upstream ends. If diameters of dropshafts at DS–1, DS–5, and DS–8 are all expanded to 18 ft, the transient problems can be eliminated. The time variation of the main tunnel water depth at DS–8 in this case is shown in Fig. 46.

Alternately, the transient problem can also be solved by increasing the diameter of either DS–1 or the diameter of the mainshaft to 150 feet. The modeling results for these two cases are shown in Figs. 47 to 50.

C. 25–YEAR, 6–HOUR STORM

The total inflow hydrograph is shown in Fig. 6. The initial storage is assumed to be 27 per cent full. Model outputs are shown in Figs. 51 to 55.

There are no transient problems existing for this storm event.

D. DROPSHAFT DESIGN INFLOW

The design inflow rate for all dropshafts are shown in Table I. The inflow is assumed to rise from zero to the maximum within two hours, which is the time of concentration interpreted from other hydrographs provided by the Corps of Engineers. The total inflow hydrograph is shown in Fig. 56. The initial storage is assumed to be 27 per cent full. Model outputs are shown in Figs. 57 to 62.

As shown in Fig. 62, severe back–up or overflow will occur for this extremely large inflow rate. The overflow is not caused by the surge movements but it is due to the lower outfall level (+48 ft) at dropshaft No. 3 rather than the design high water level at the reservoir (+58 ft). The surge oscillation numbers at DS–1, DS–5, and DS–8, are 2.60, 2.31, and 2.44, respectively, indicating the existence of surge problems. Even though this storm event is unlikely to occur, the transient problems can still be solved by expanding the main shaft diameter to 180 feet. There is no way to eliminate the outfall at DS–3 unless the outfall level is raised for this storm event.

V. CONCLUSIONS

The Corps of Engineers has recommended three reservoir sizes to capture storm runoffs. This study has simulated the filling process and the associated surge problems for three different size storms. The following list of conclusions are offered as the results of this study.

1. Manhole cover blow–off and geysering problems are likely to occur at dropshafts No. 1, No. 5, and No. 8 under 100–year storms and the dropshaft capacity storm. No such problems occur for 25–year storms. Overflow may take place at dropshaft No. 3 under the dropshaft capacity flow condition even when the reservoir is empty at the beginning of the storm.

2. The occurrence of blow–off and geysering problems is caused by the pressurization surge and occurs independent of the water level in the reservoir at the beginning of the storm.

3. The surge intensity is dependent on the amount of water initially stored in the main tunnel. The worst conditions occur when the tunnel is initially about 27 per cent full. The problem does not exist if the tunnel is initially more than 50 per cent full.

4. There are four ways to prevent the blow–off and geysering problems for 100–year storms. These are listed below:

   (i) Maintain the tunnel at a 50 per cent or more full condition before the storm.

   (ii) Increase the diameters of DS–1, DS–5, and DS–8 to 20 feet.

   (iii) Increase the diameter of DS–1 to 150 feet.

   (iv) Either increase the diameter of the main shaft to 150 feet or connect the tunnel to the reservoir directly with a 150–foot diameter conduit.

5. The cover blow–off and geysering problems can be prevented for the dropshaft capacity inflow if the main shaft diameter is increased to 180 feet or the tunnel is directly connected to the reservoir with a 180–foot diameter conduit.

6. Overflow from DS–3 will not occur for storms equal to or less than a 100–year storm if the reservoir is initially empty.

7. There may be a special transient problem for the double–barreled dropshafts of the O'Hare System. However, a detailed study of this situation is out of the scope of the present study.

REFERENCES

1. U.S. Army Corps of Engineers, "Chicago Underflow Plan, Phase I GDM, O'Hare System Interim Report," Chicago District, Nov. 1983.

2. Song, Charles C. S., James A. Cardle, and Kim Sau Leung, "Transient Mixed–Flow Models For Storm Sewers," *J. of Hydraulic Engineering*, ASCE, Vol. 109, No. 11, Nov. 1983.

3. Song, Charles C. S., Qizhong Guo, and Yifan Zheng, "Hydraulic Transient Modelling of the TARP Systems," Project Report No. 270, St. Anthony Falls Hydraulic Laboratory, March 1988.

4. Song, Charles C. S., "Modelling of Mixed–Transient Flow," *Proceedings, Vol. I, SECTAM XII*, Auburn University, May 10–11, 1984.

5. Anderson, A., "A Novel Type of Surge Shaft Instability," *Proceedings of Institution of Civil Engineers*, Vol. 67, Part 2, 1979, p. 695–706.

6. Chaudhry, M. Hanif, *Applied Hydraulic Transients*, Second Edition, Van Nostrand Reinhold Co., New York, 1987.

7. Anderson, A., "Interaction of Surge Shafts and Penstocks," presented at 4th International Conference on Pressure Surges, Bath, England, September 21–23, 1983.

8. Dahlin, W. Q., J. M. Wetzel, and K. K. Nesbeitt, "Hydraulic Modelling of Vertical Dropshaft Structures," presented at International Conference on the Hydraulic Modelling of Civil Engineering Structures, Coventry, England, September 22–24, 1982.

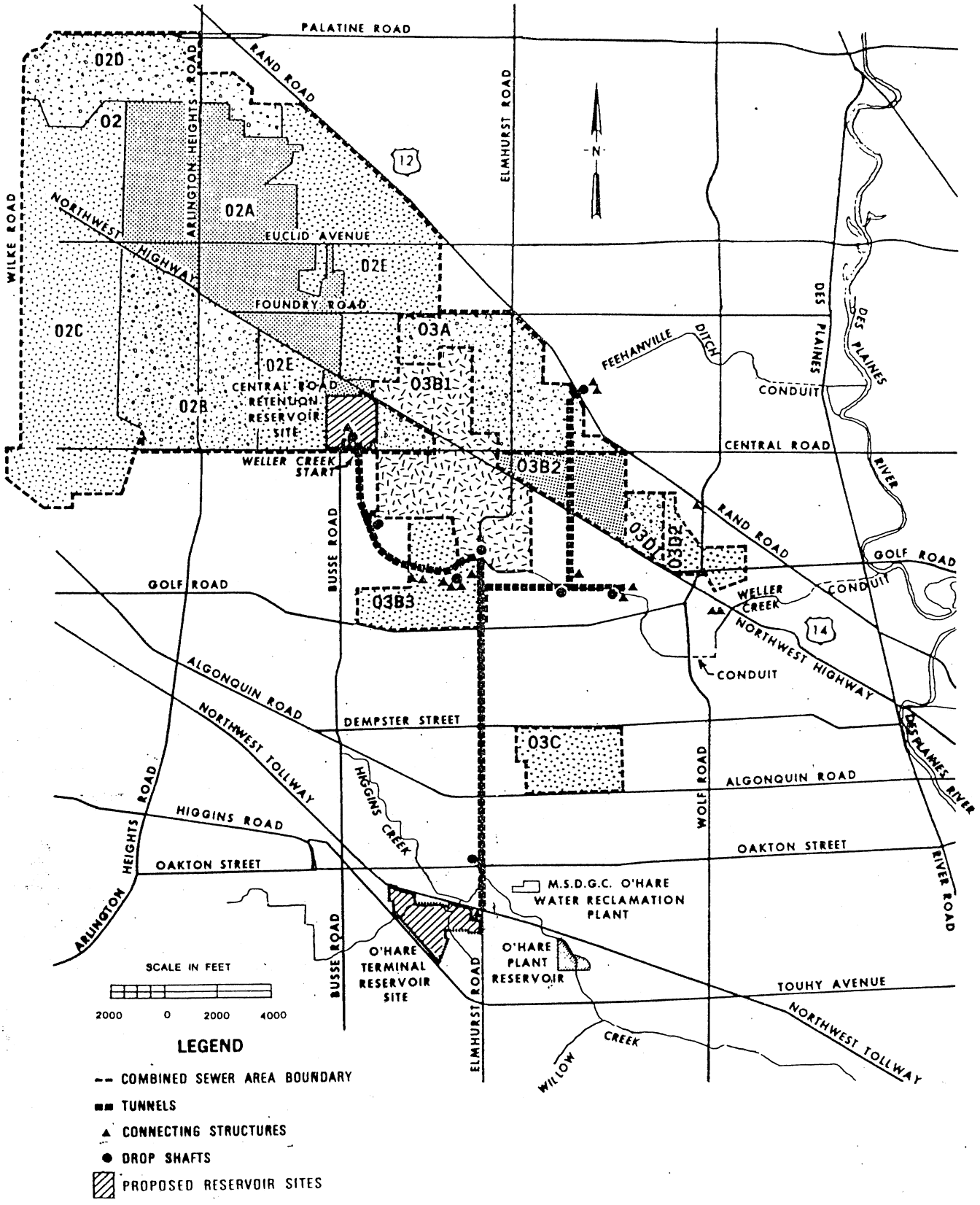

Fig. 1. TARP O'Hare System.

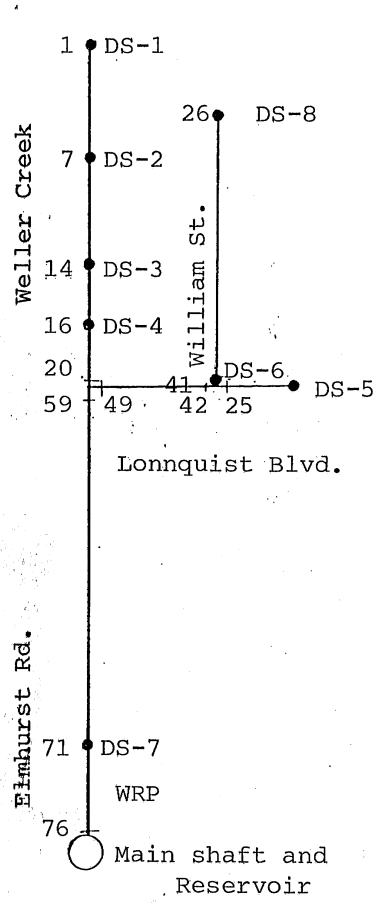

Fig. 2. O'Hare System configuration for modeling purpose.

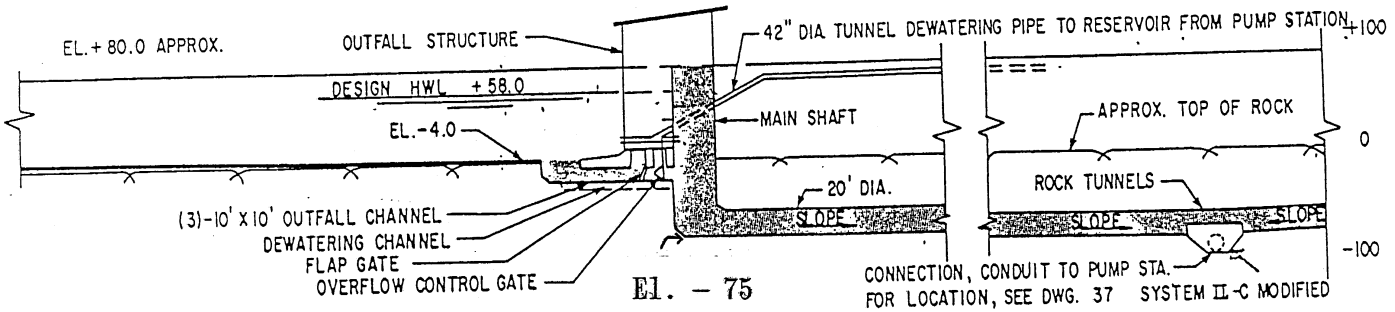

Fig. 3. Connection between the TARP Phase I tunnel system and the proposed terminal reservoir.

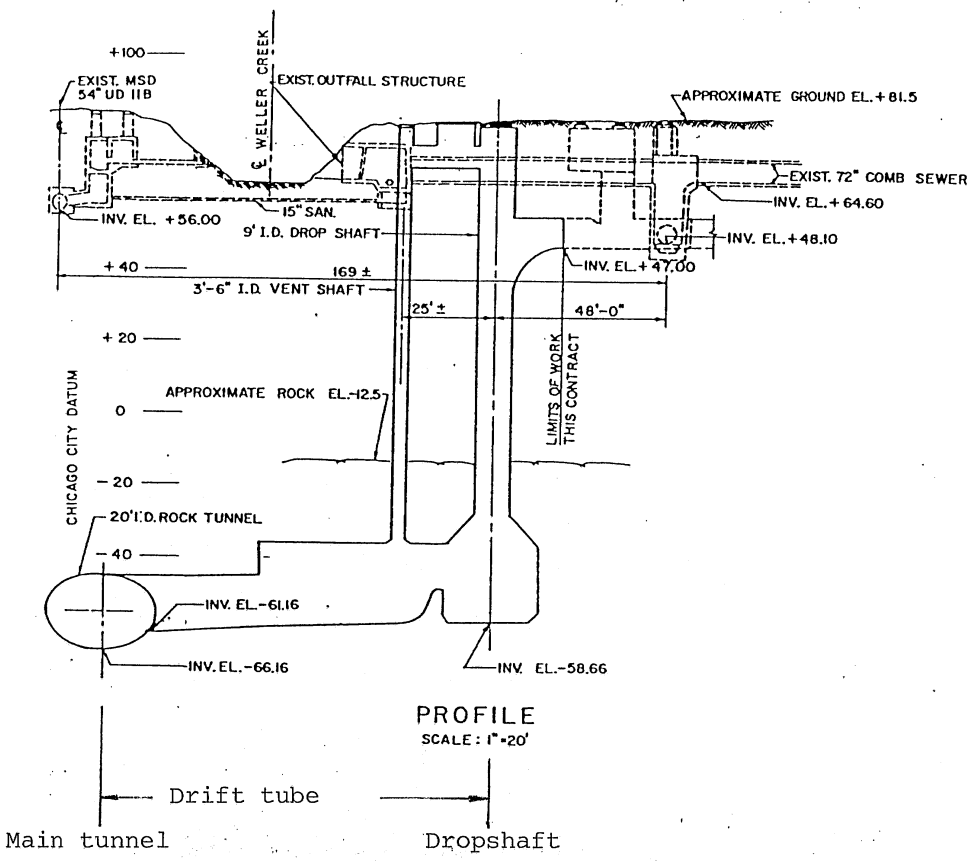

Fig. 4. A typical dropshaft structure (DS–4).

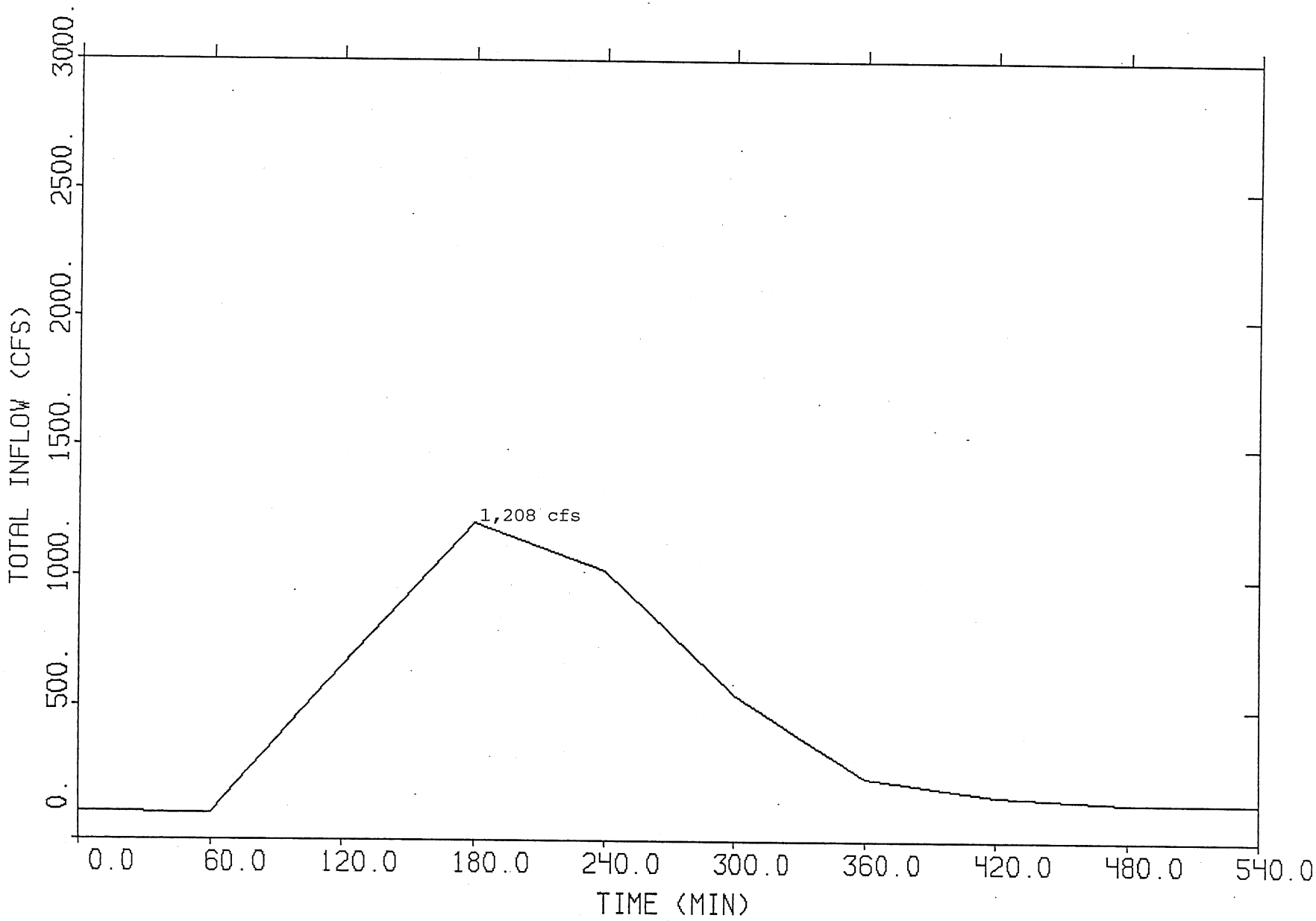

Fig. 5. Total inflow hydrograph for 25 year 2 hour storm.

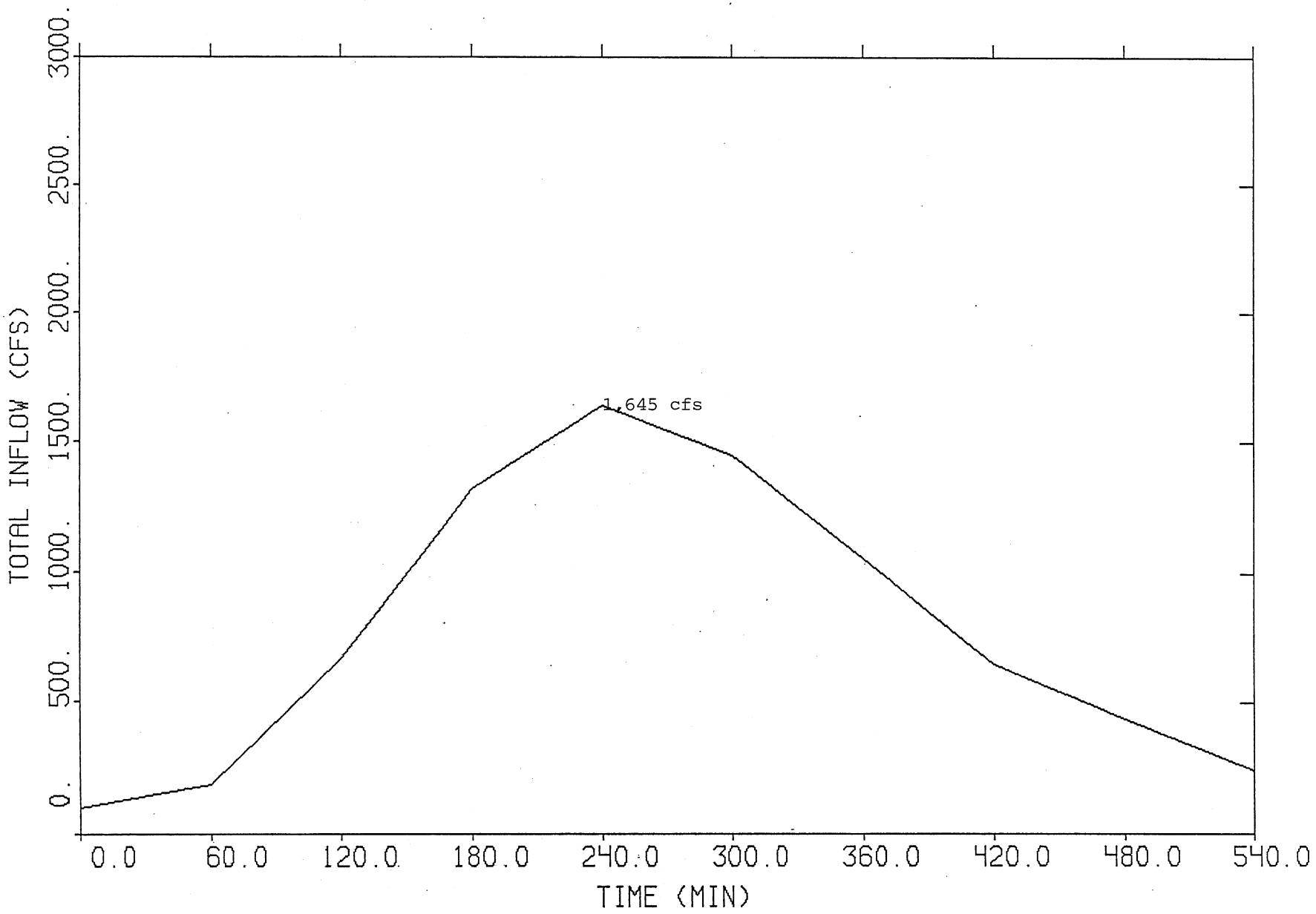

Fig. 6. Total inflow hydrograph for 25 year 6 hour storm.

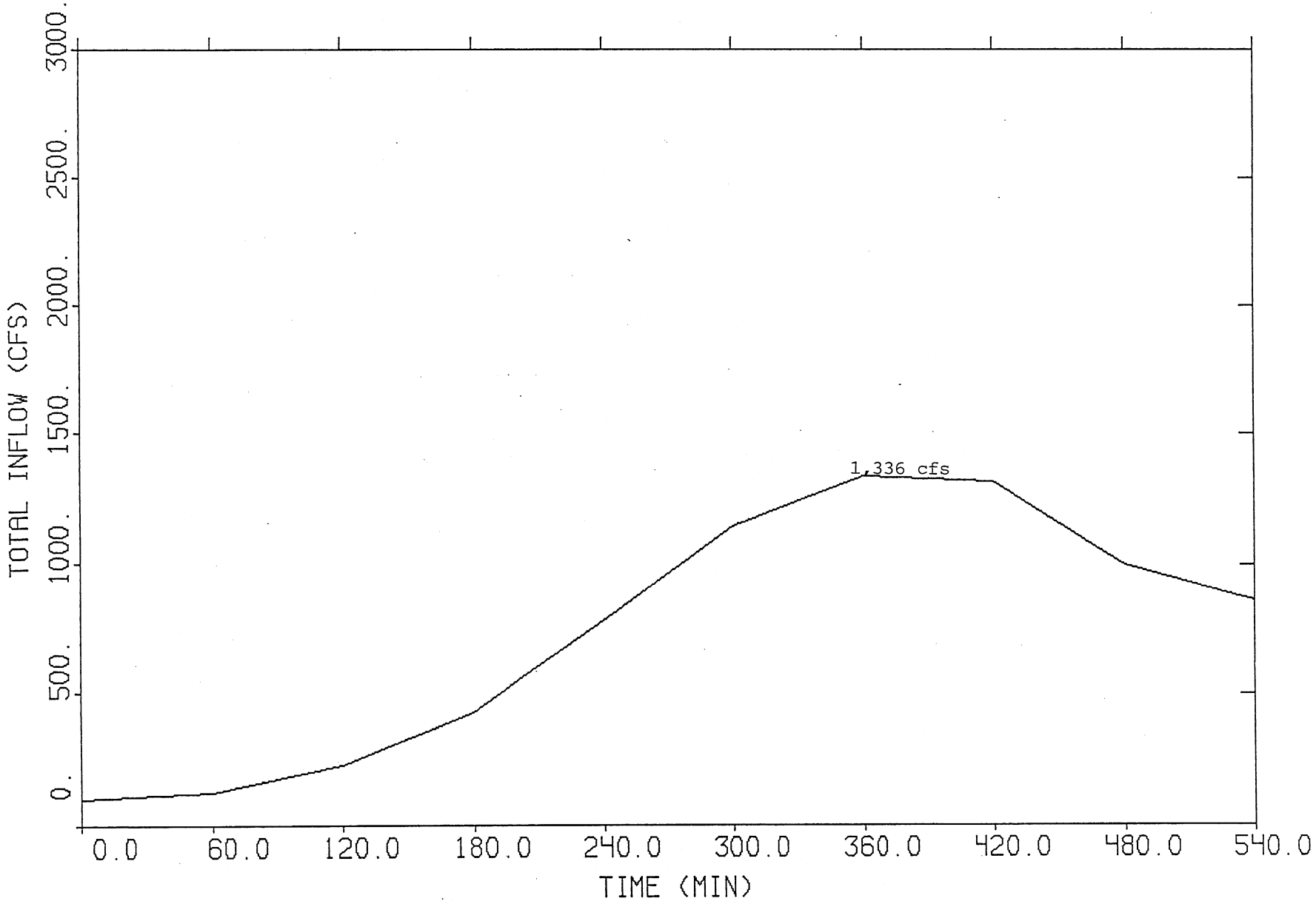

Fig. 7. Total inflow hydrograph for 25 year 12 hour storm.

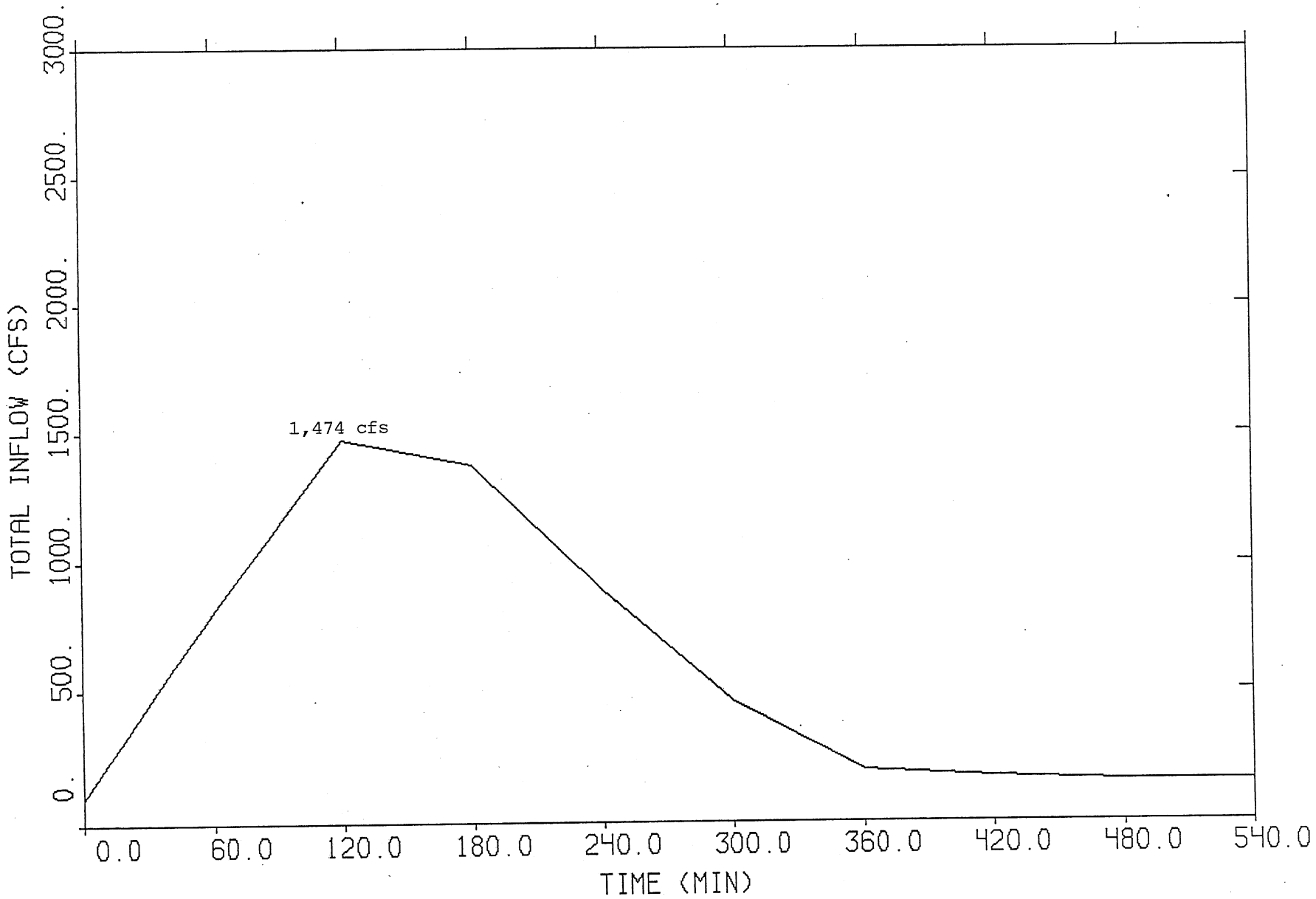

Fig. 8. Total inflow hydrograph for 100 year 2 hour storm.

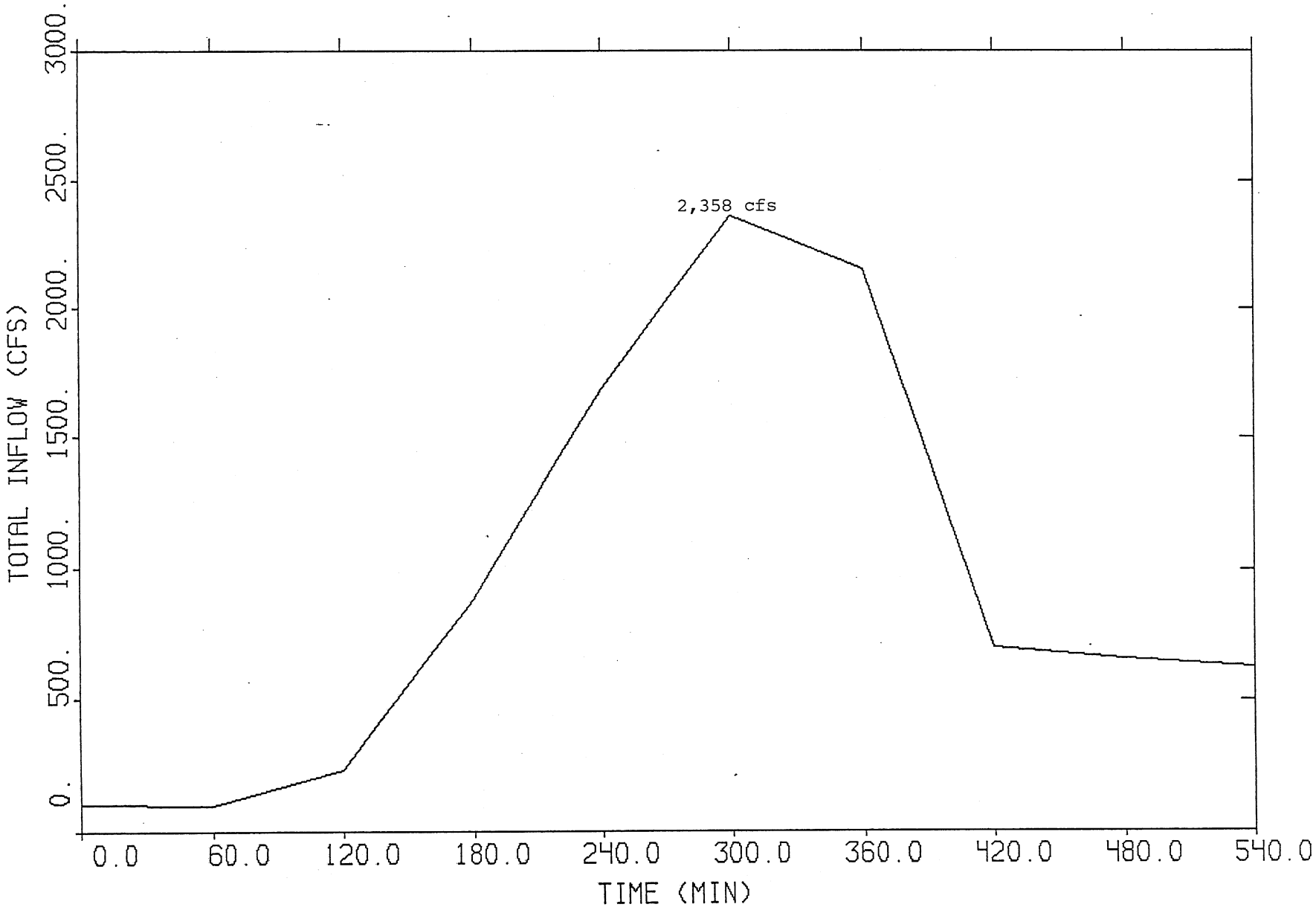

Fig. 9. Total inflow hydrograph for 100 year 6 hour storm.

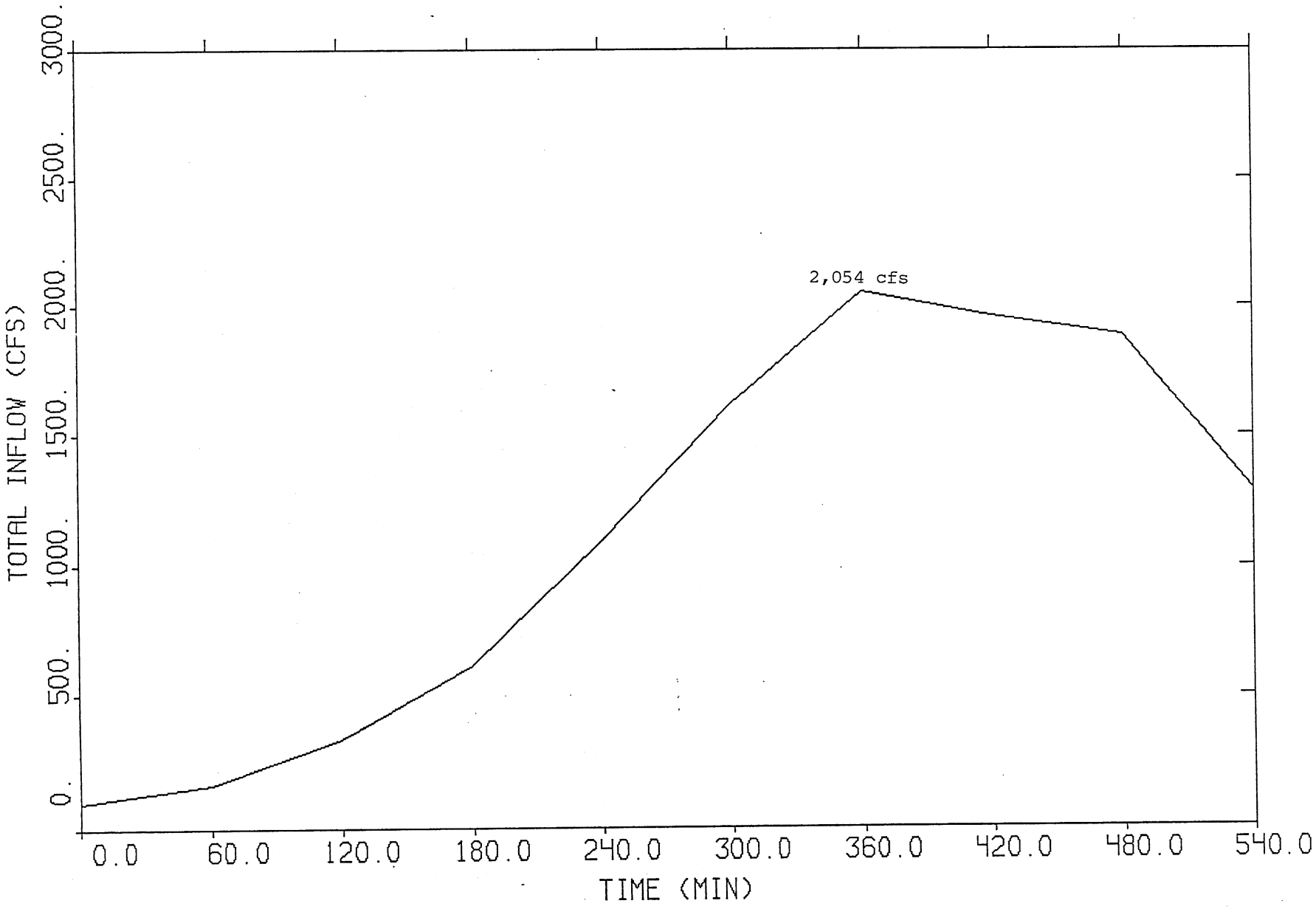

Fig. 10. Total inflow hydrograph for 100 year 12 hour storm.

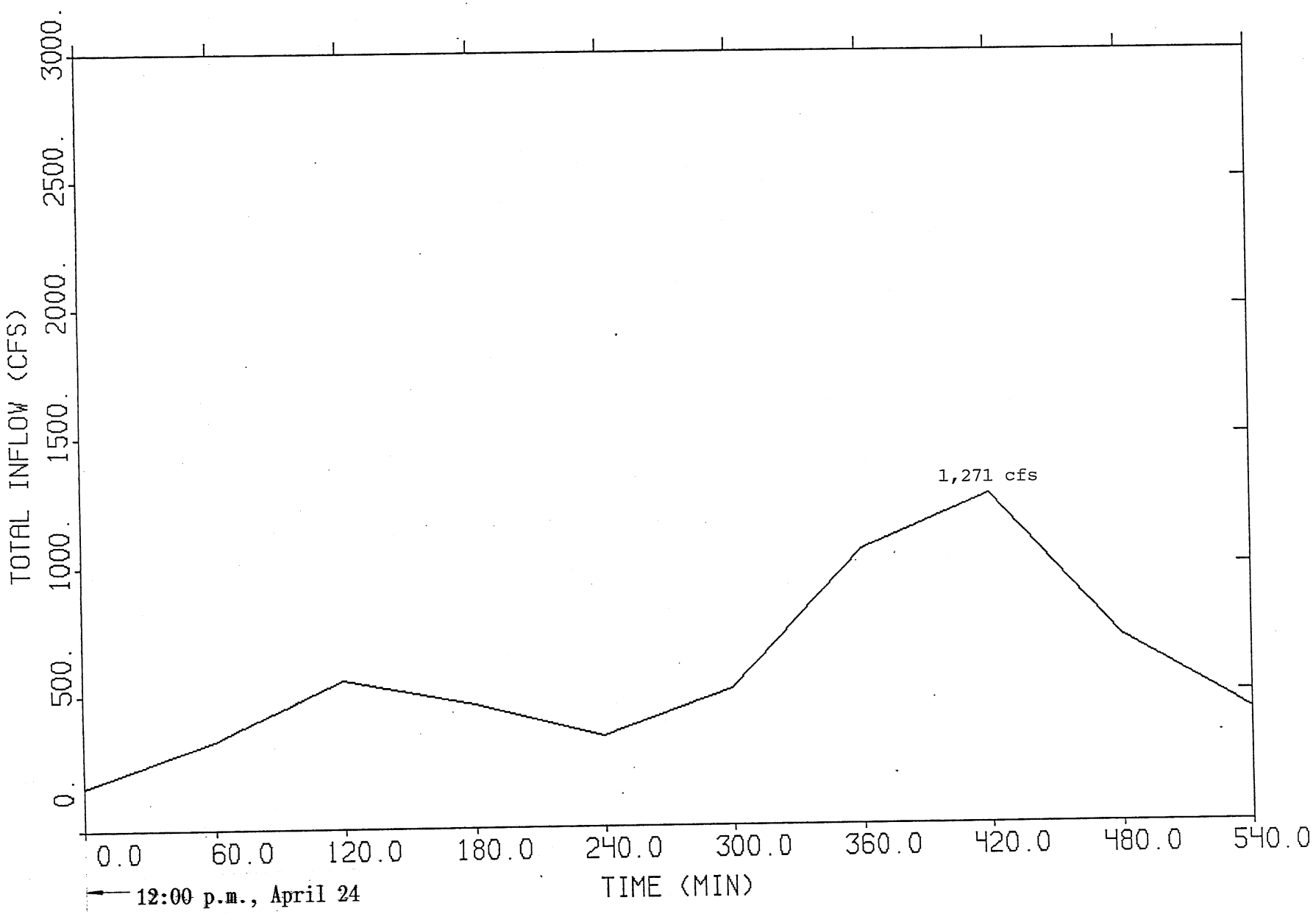

Fig. 11. Total inflow hydrograph of 1950 historical storm.

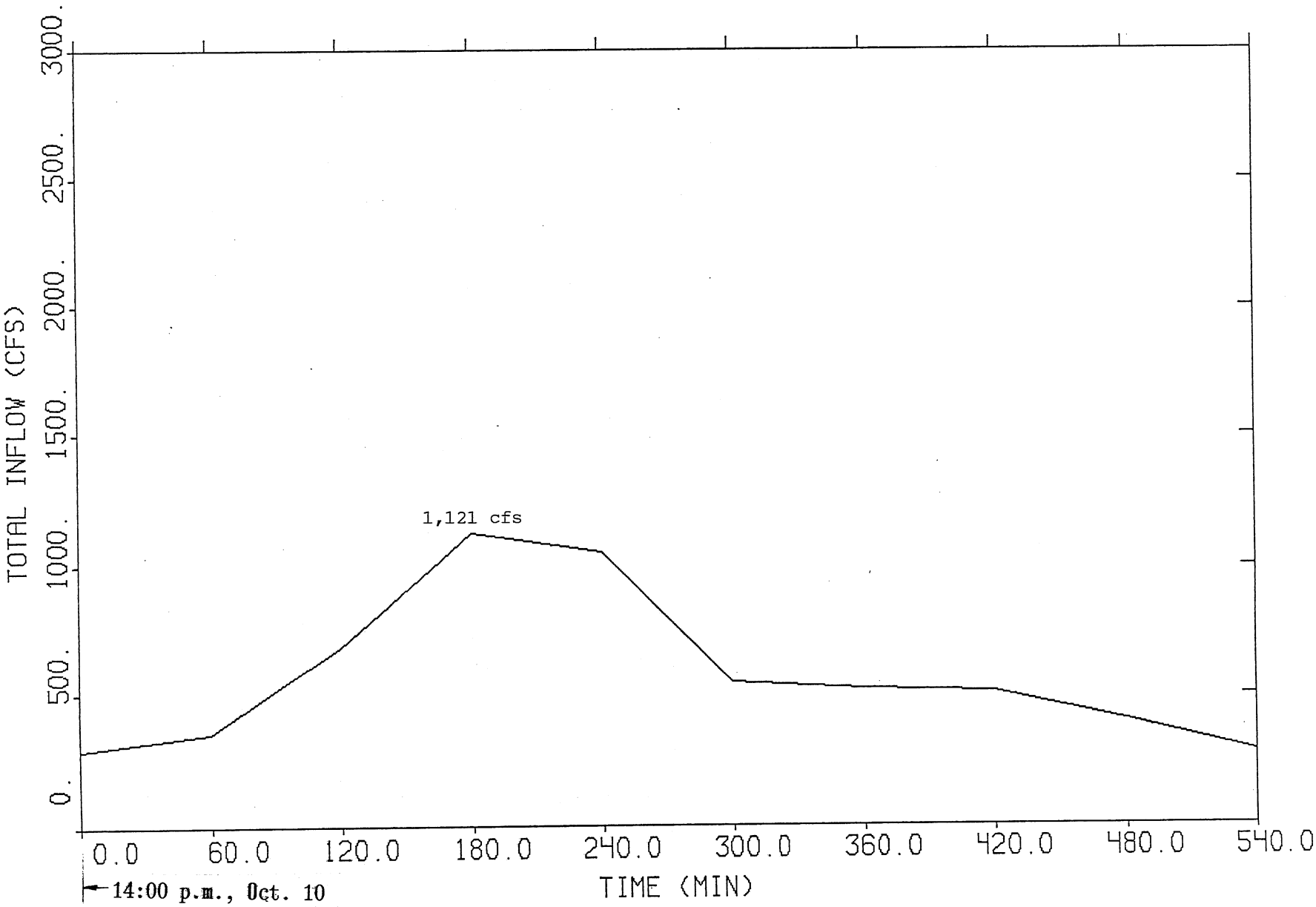

Fig. 12. Total inflow hydrograph of 1954 historical storm.

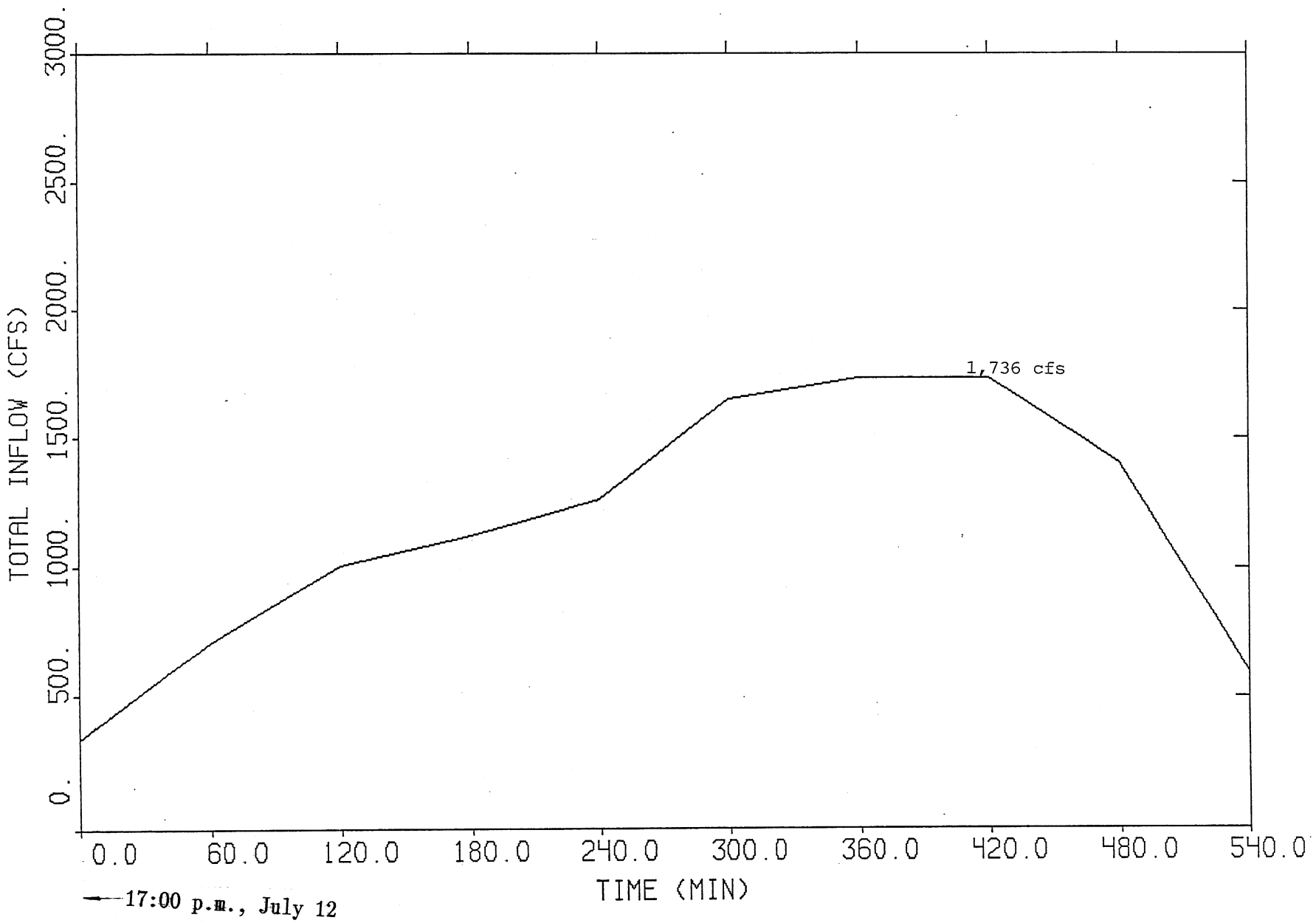

Fig. 13. Total inflow hydrograph of 1957 historical storm.

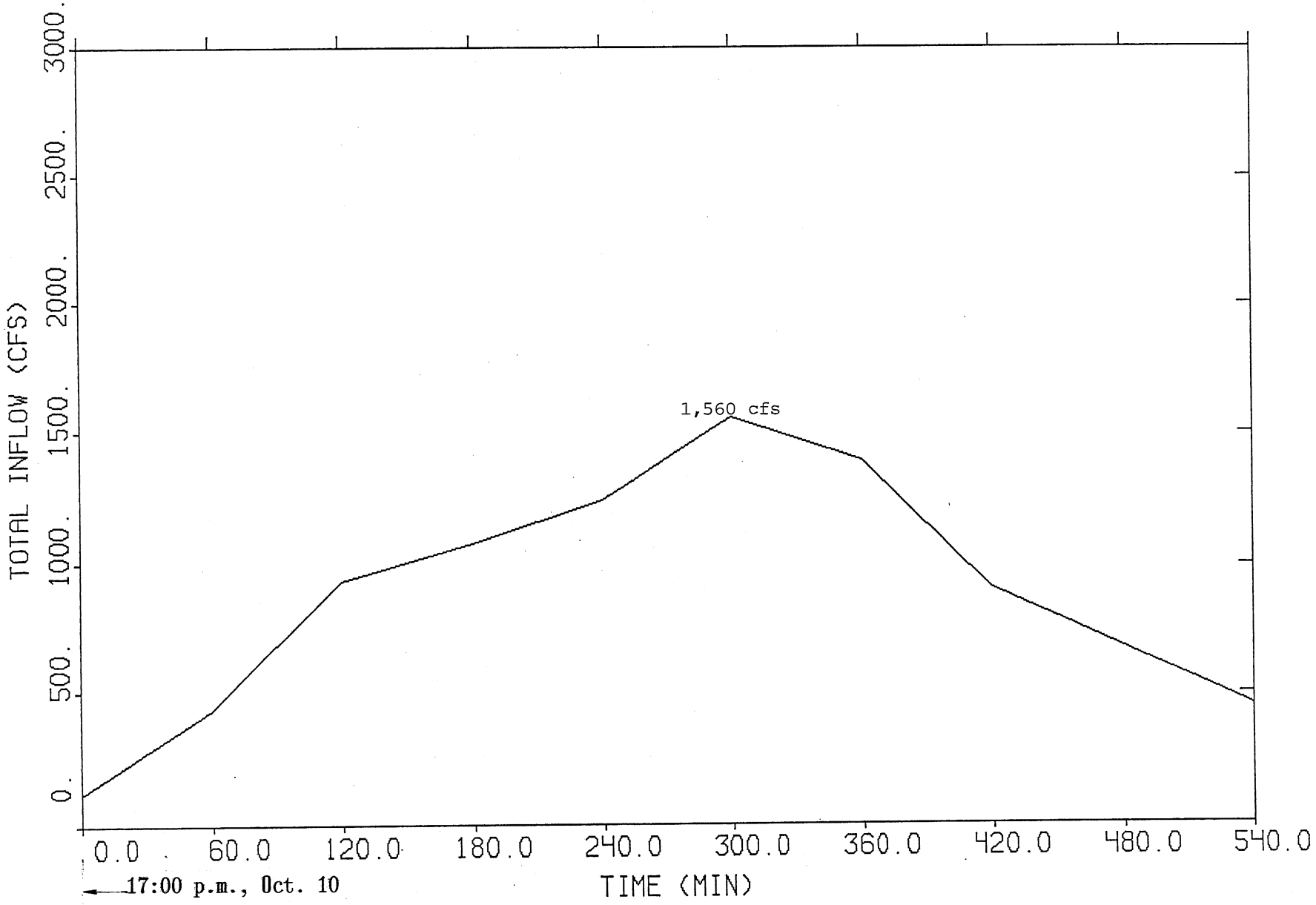

Fig. 14. Total inflow hydrograph of 1969 historical storm.

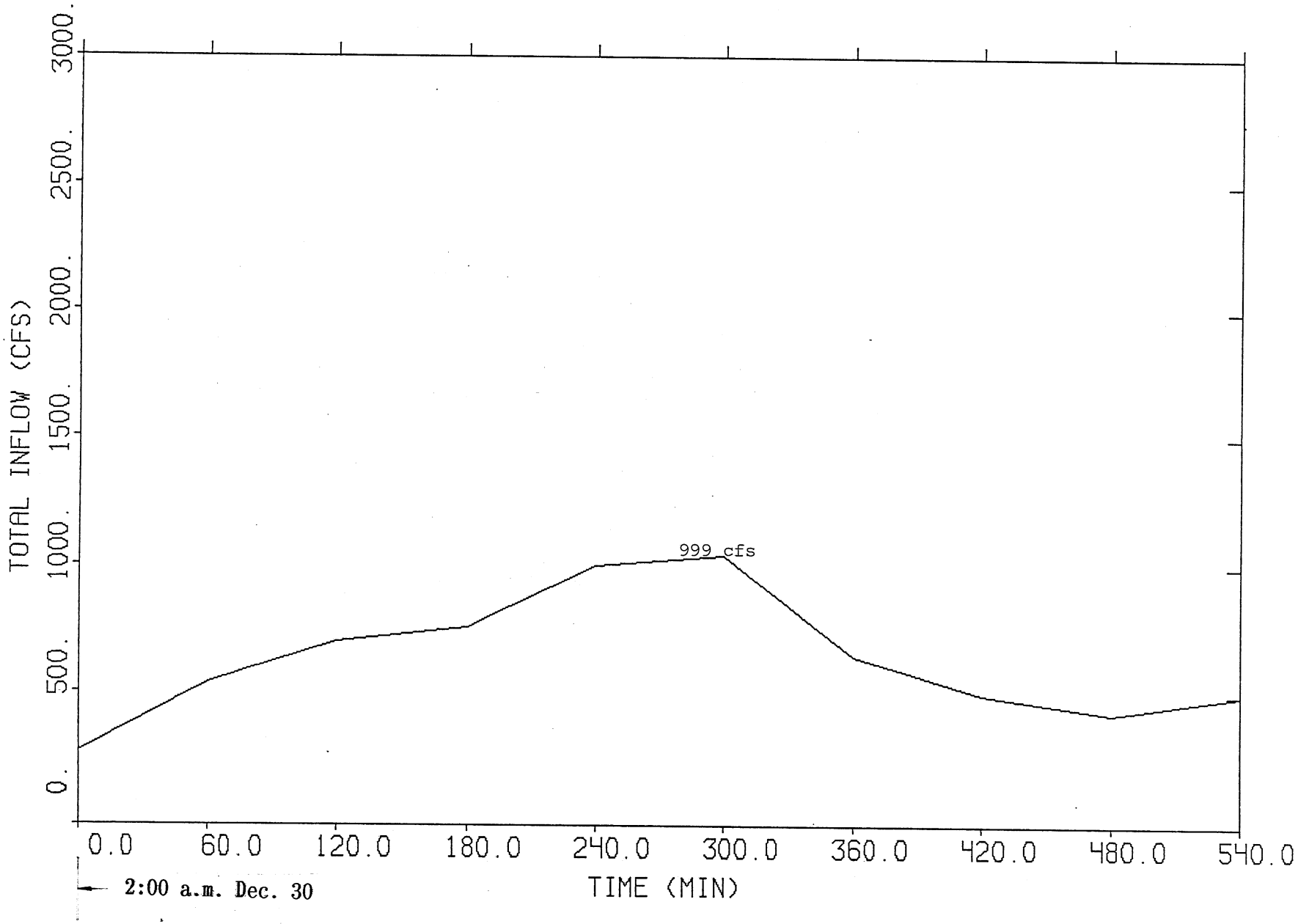

Fig. 15. Total inflow hydrograph of 1972 historical storm.

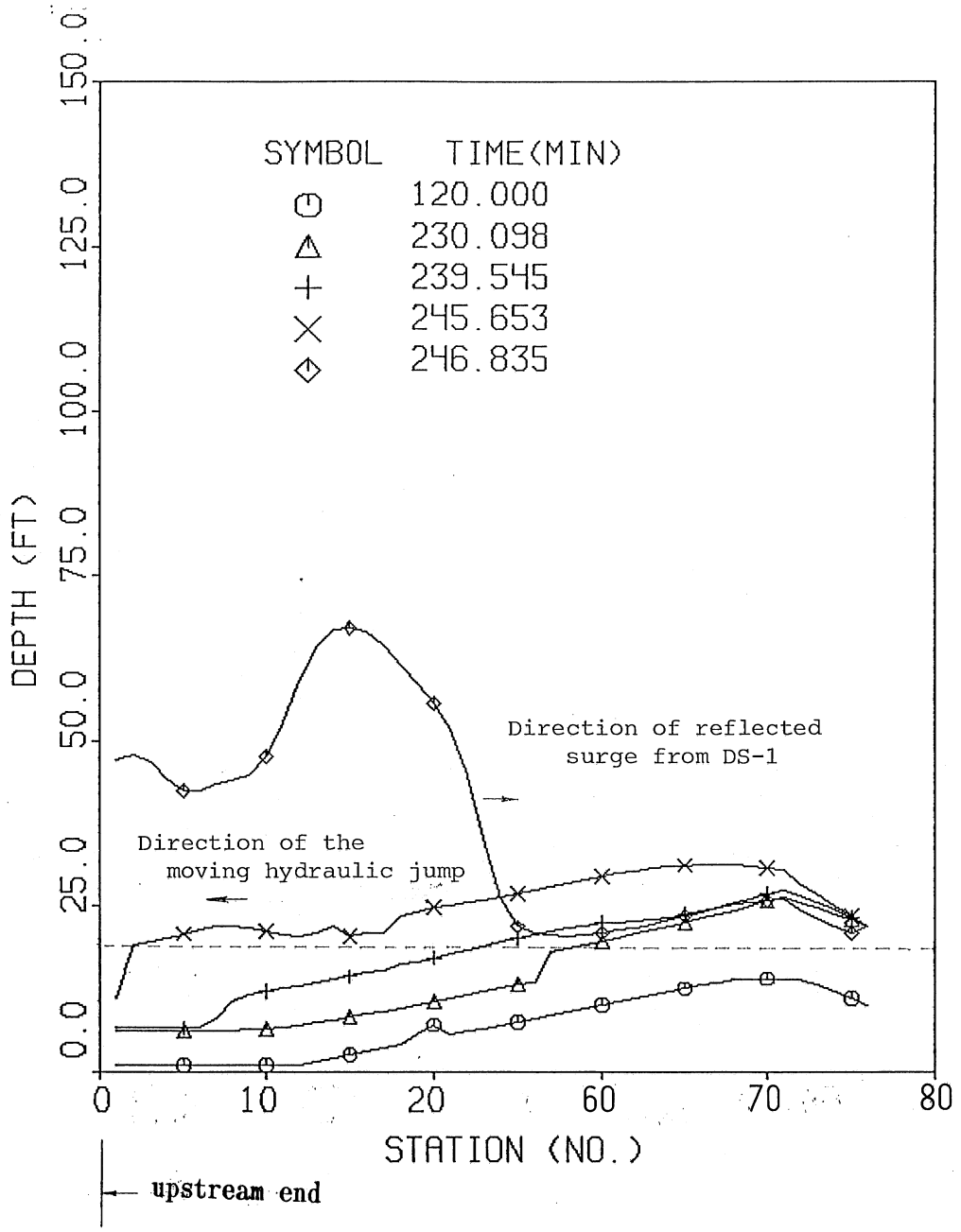

Fig. 16. Instantaneous hydraulic gradelines (measured from the tunnel invert) at the beginning of the filling process.

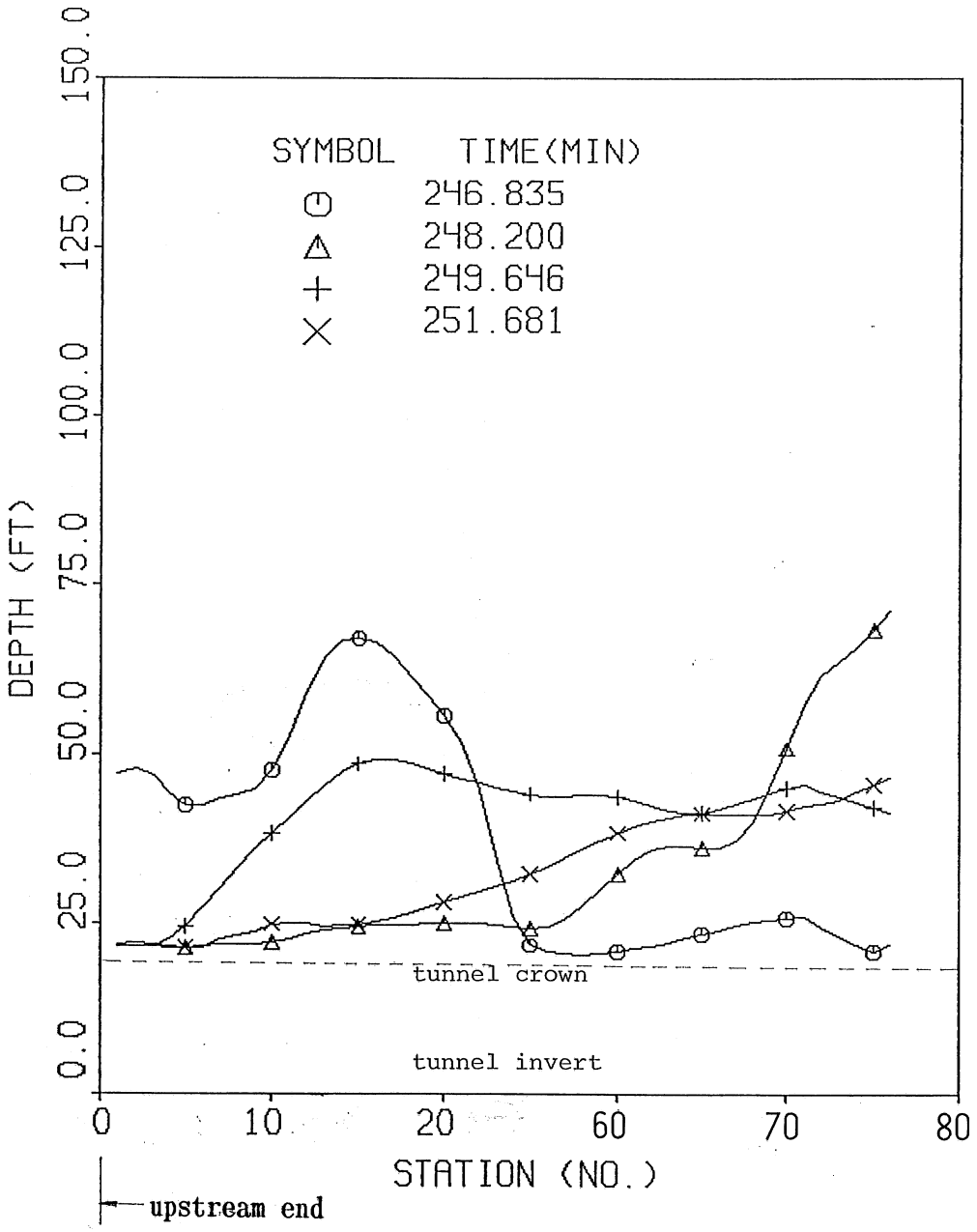

Fig. 17. Instantaneous hydraulic gradelines before the reflected surge from DS–8 reaches the junction at Stations 20, 49, and 50.

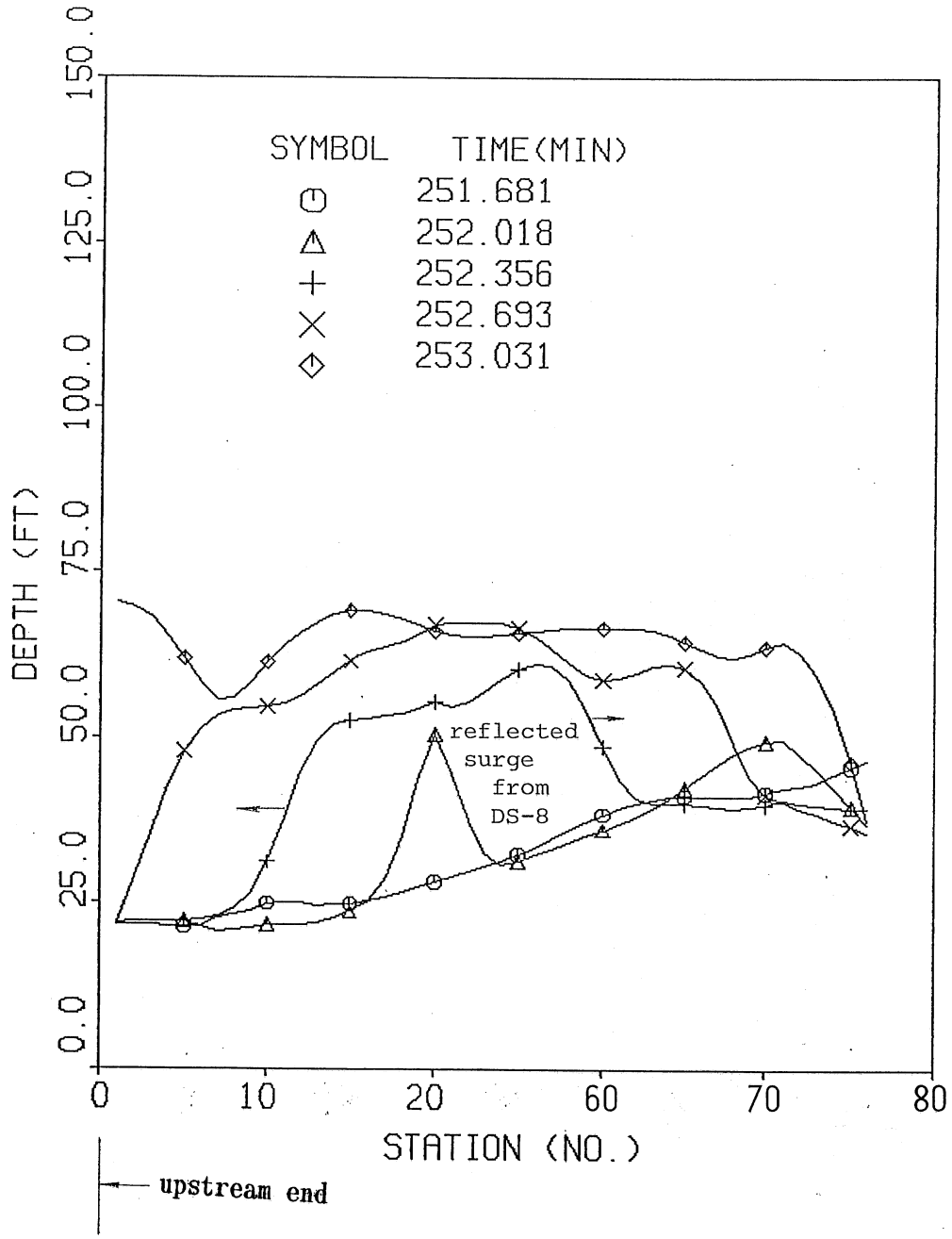

Fig. 18. Instantaneous hydraulic gradelines after the reflected surge from DS–8 reaches the junction at Stations 20, 49, and 50.

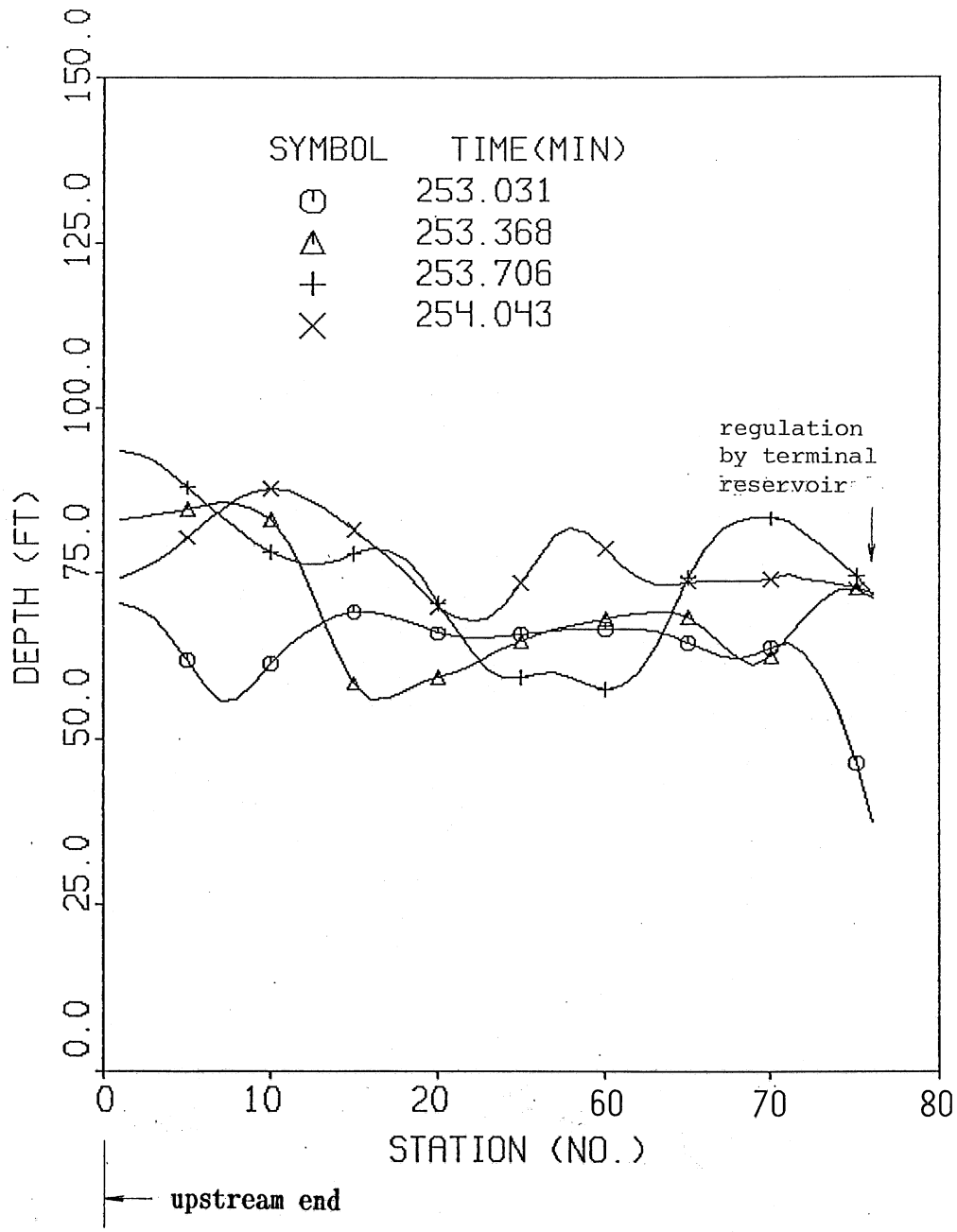

Fig. 19. Instantaneous hydraulic gradelines after outflow to the terminal reservoir begins.

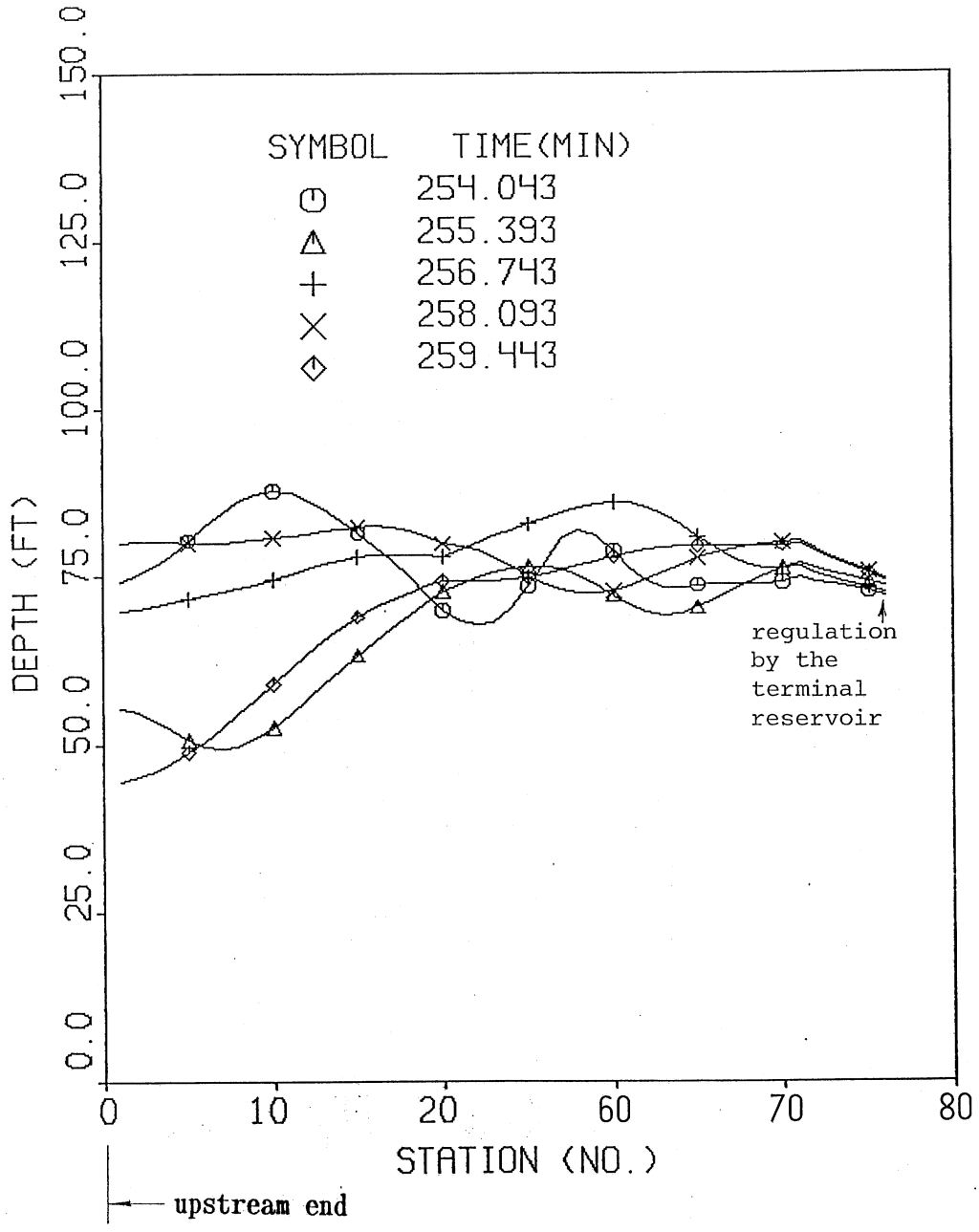

Fig. 20. Instantaneous hydraulic gradelines during the final filling process.

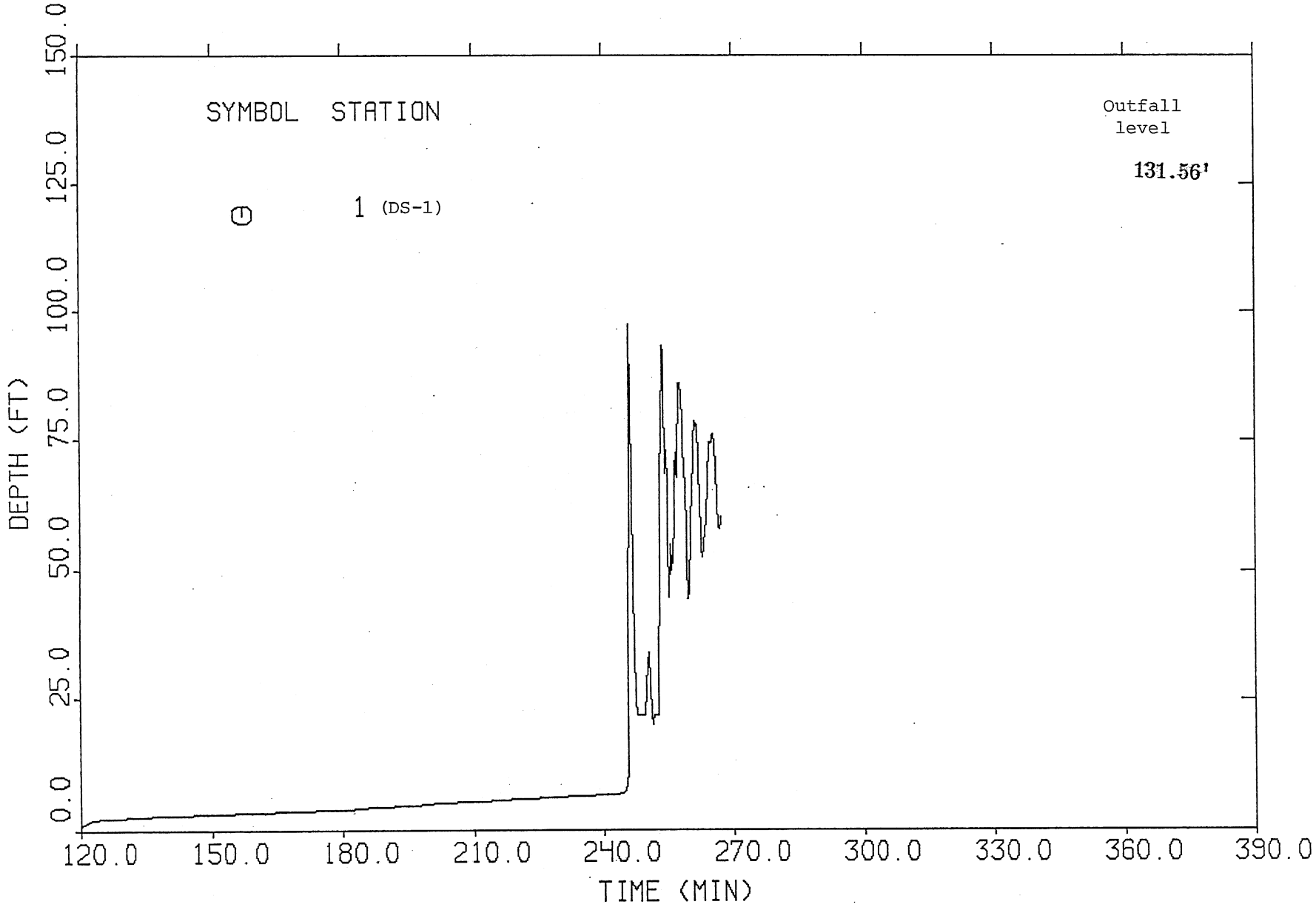

Fig. 21. Time variation of water depth at Station No. 1 (DS–1).

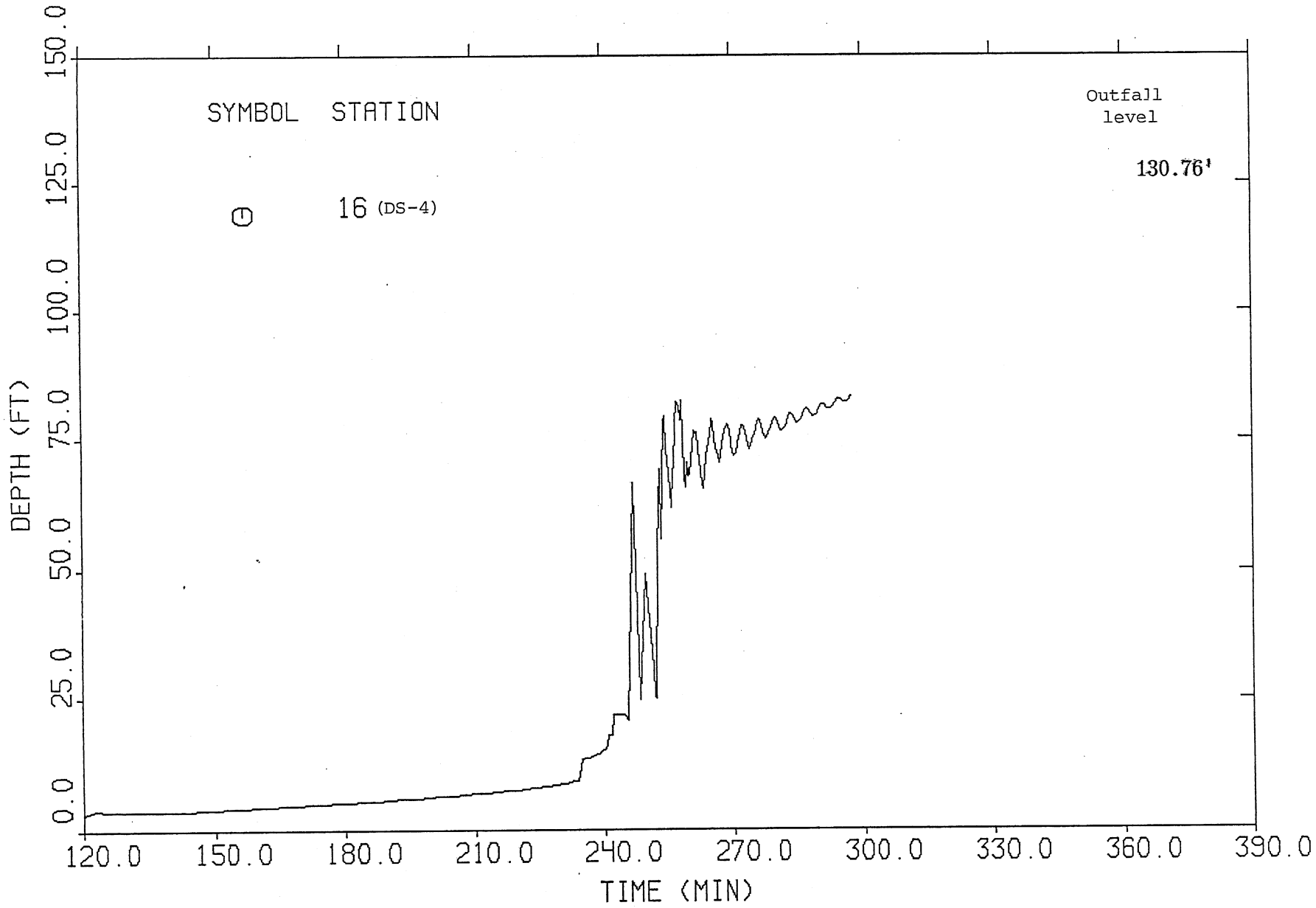

Fig. 22. Time variation of water depth at Station No. 16 (DS–4).

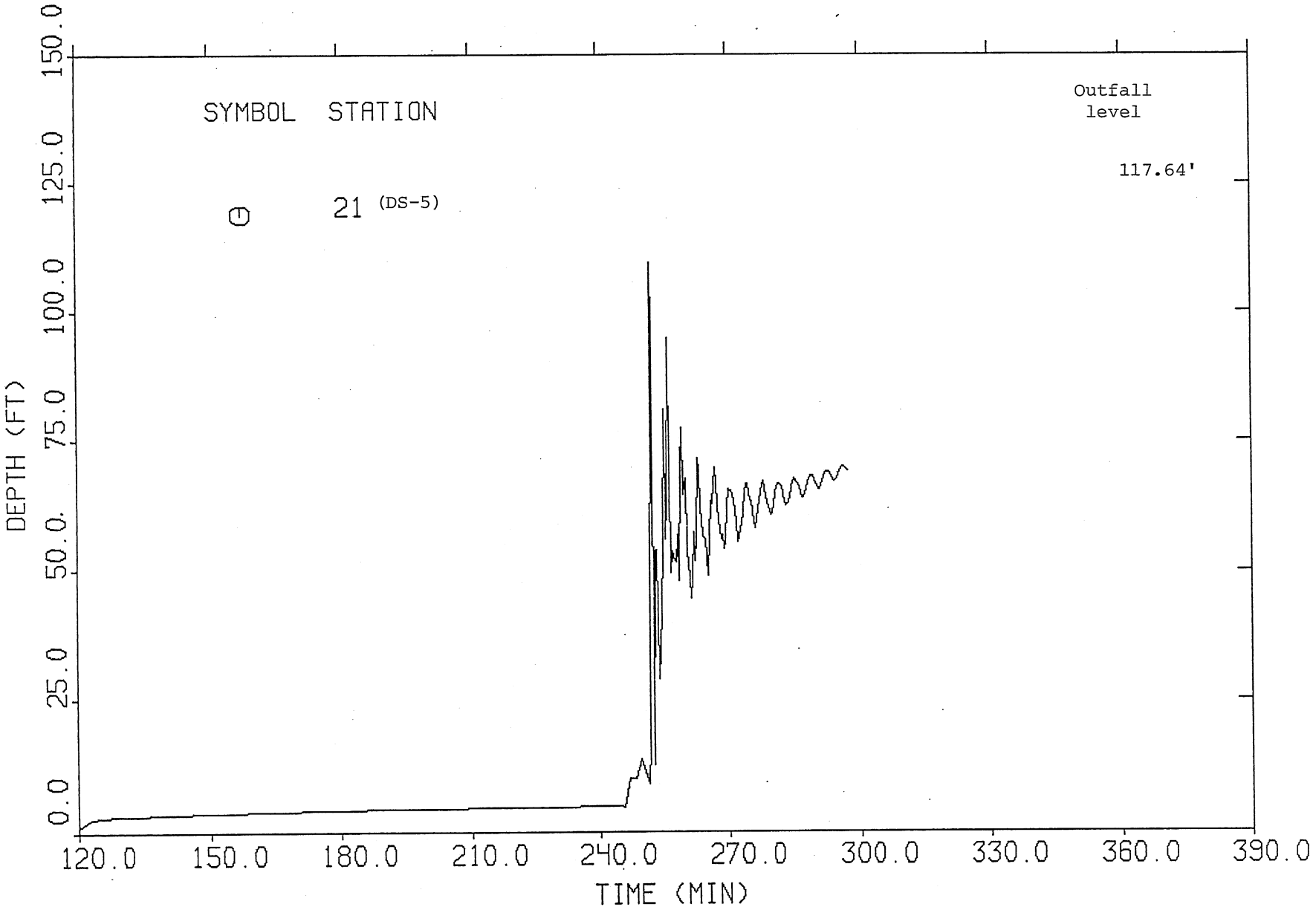

Fig. 23. Time variation of water depth at Station No. 21 (DS–5)

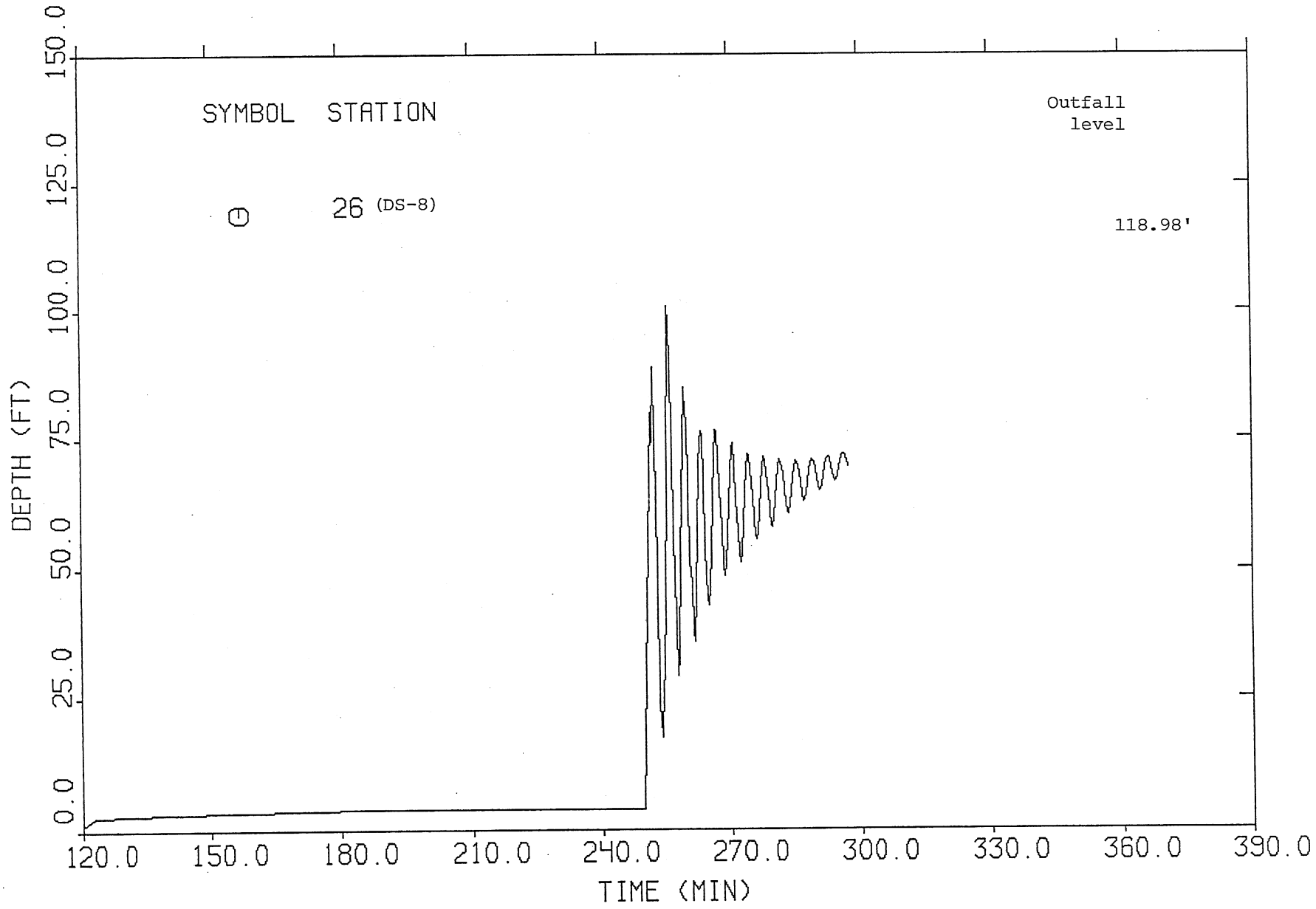

Fig. 24. Time variation of water depth at Station No. 26 (DS–8)

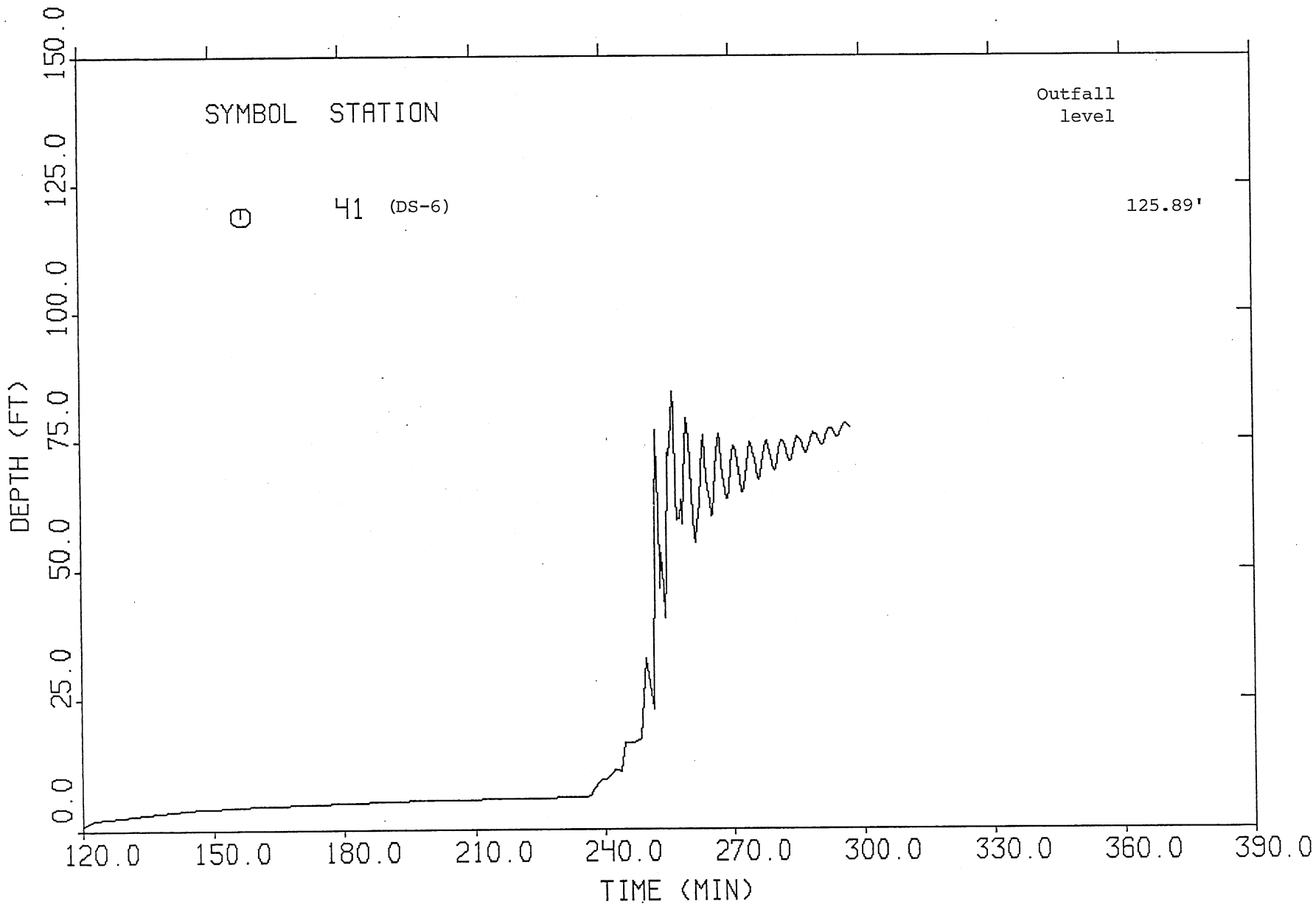

Fig. 25. Time variation of water depth at Station No. 41 (DS–6)

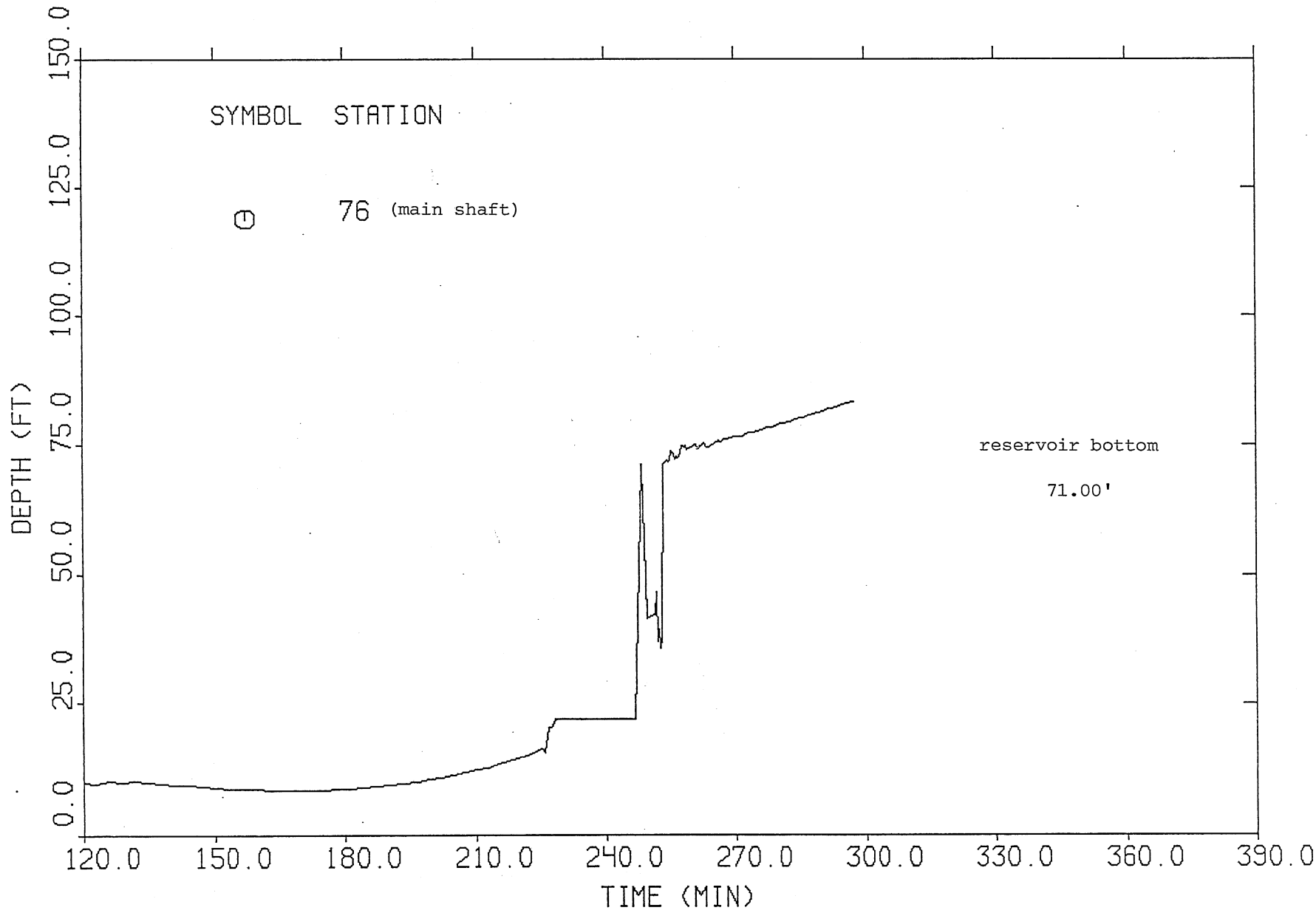

Fig. 26. Time variation of water depth at Station No. 76 (main shaft)

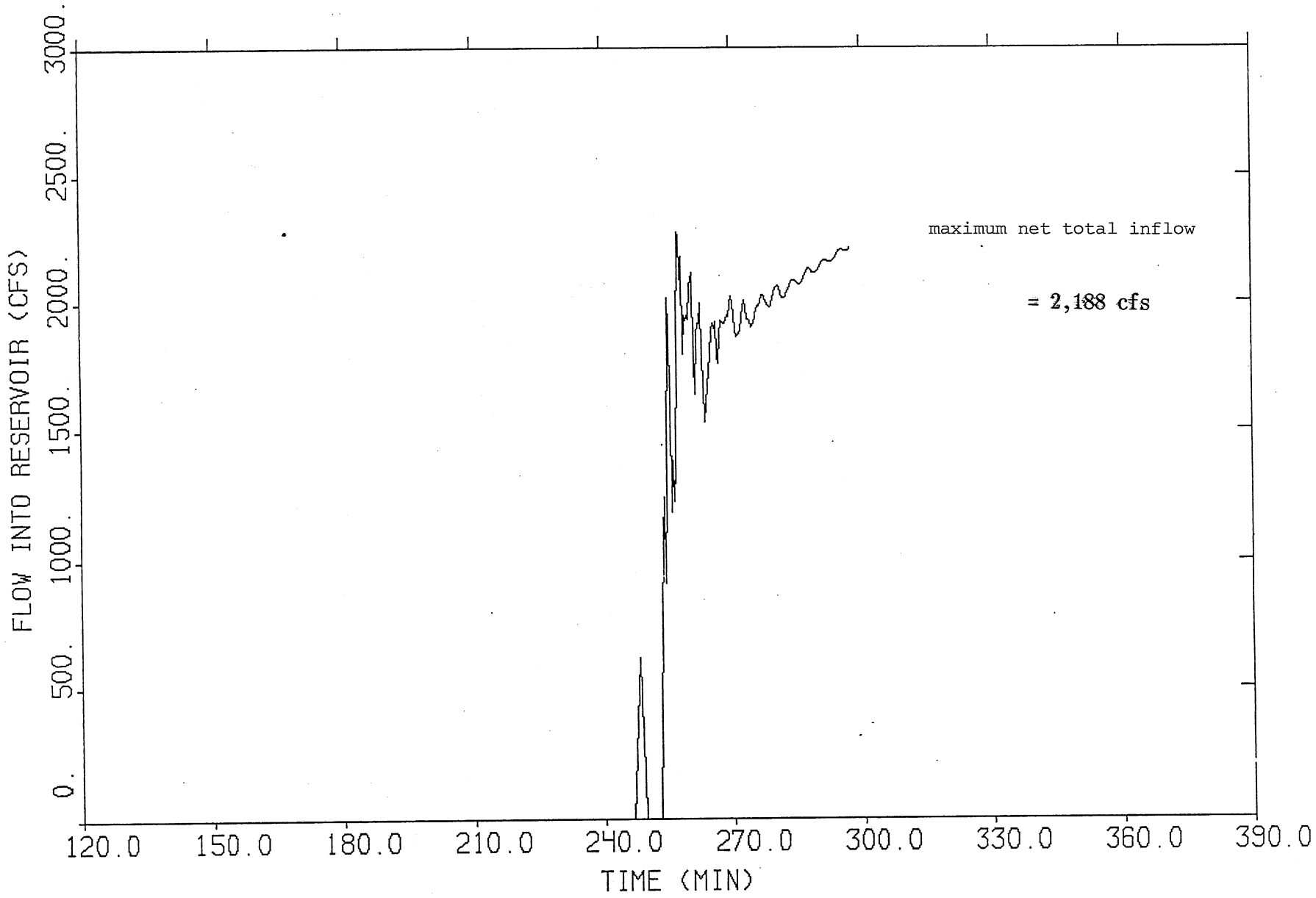

Fig. 27. Outflow hydrograph to the terminal reservoir.

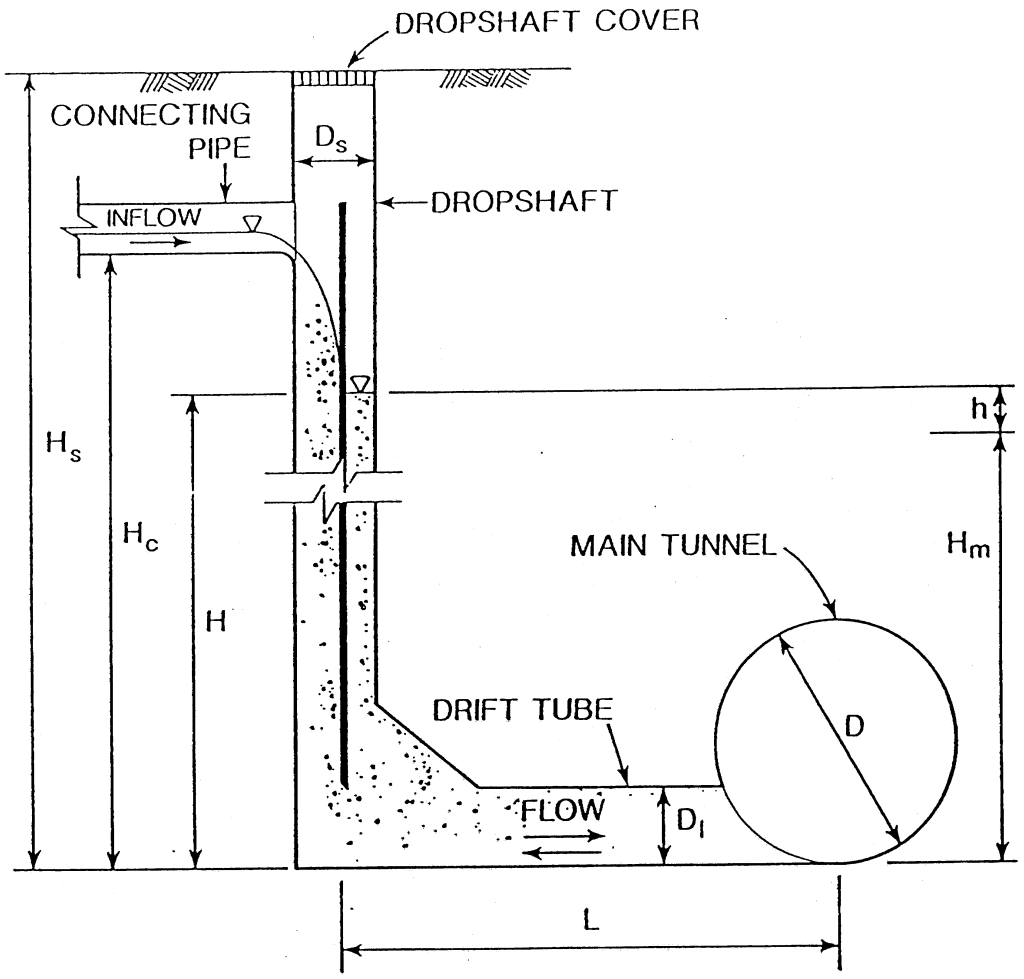

Fig. 28. A sketch of dropshaft–drift tube system for geyser analysis.

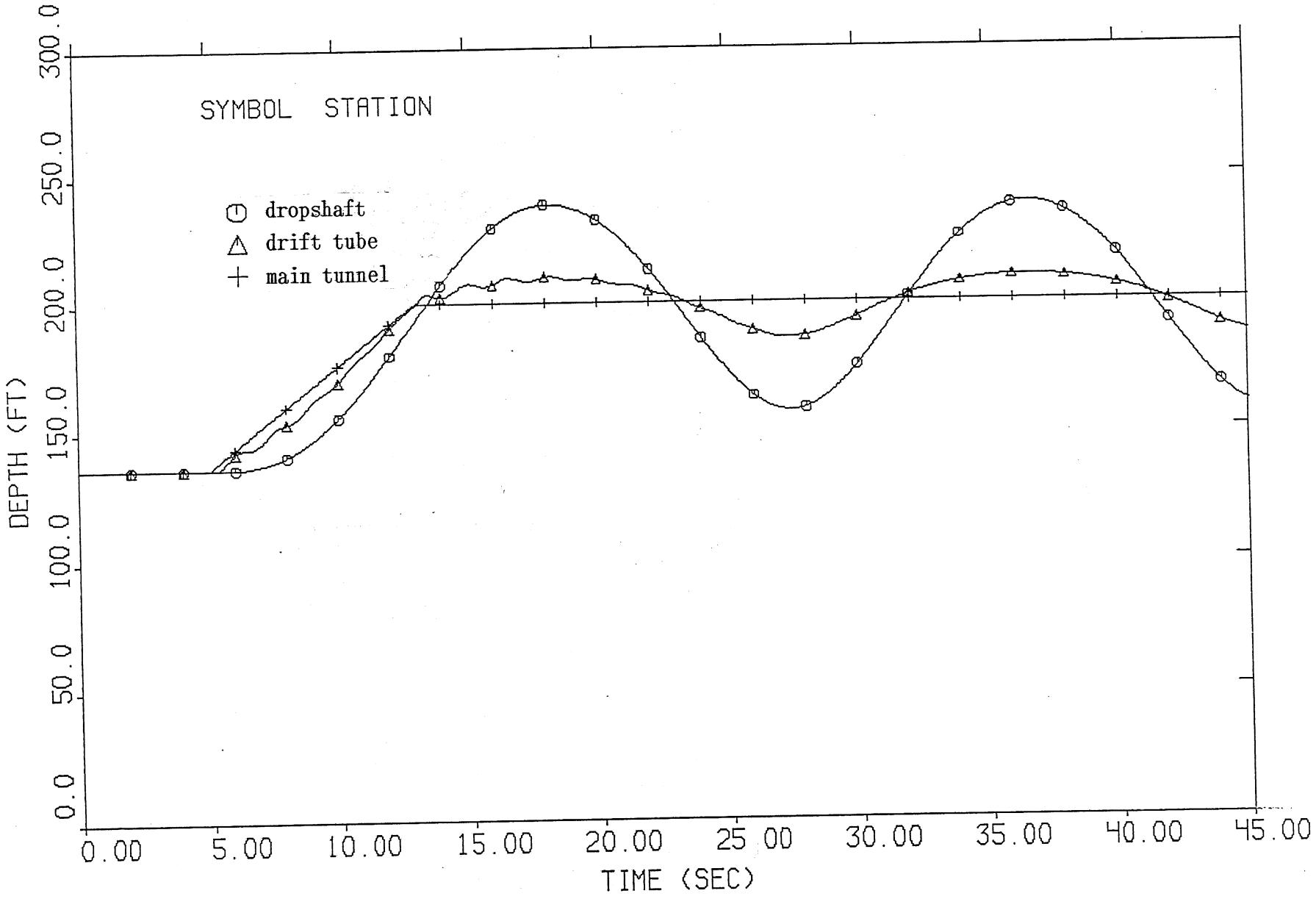

Fig. 29. Time variation of water depth in dropshaft due to tunnel pressure rise. (D_s = 4', L = 150', D_ℓ = 5.59', f_o = 0.00, a = 335 fps).

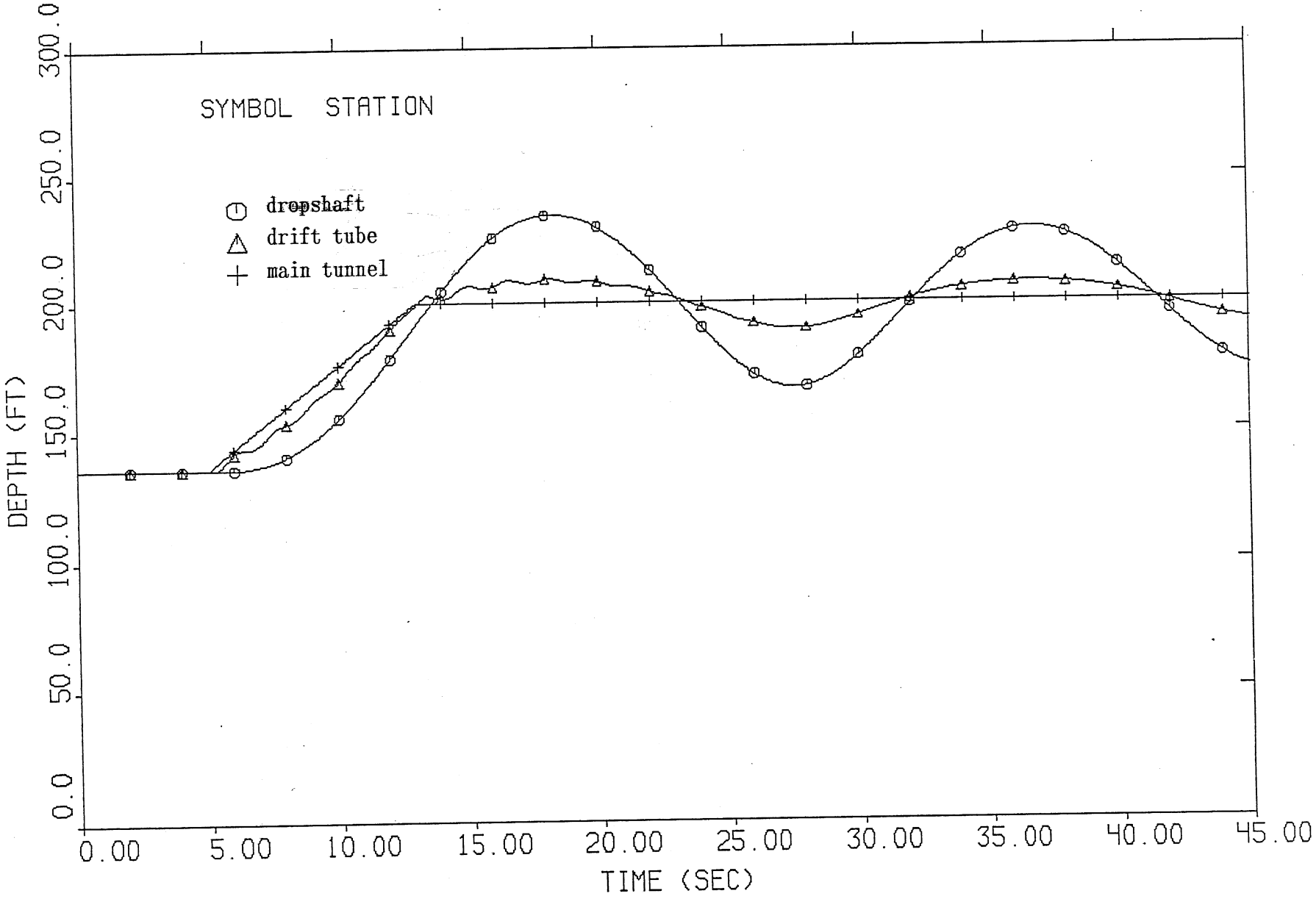

Fig. 30. Time variation of water depth in dropshaft due to tunnel pressure rise. (D_s = 4', L = 150', D_ℓ = 5.59', f_o = 0.02, a = 335 fps).

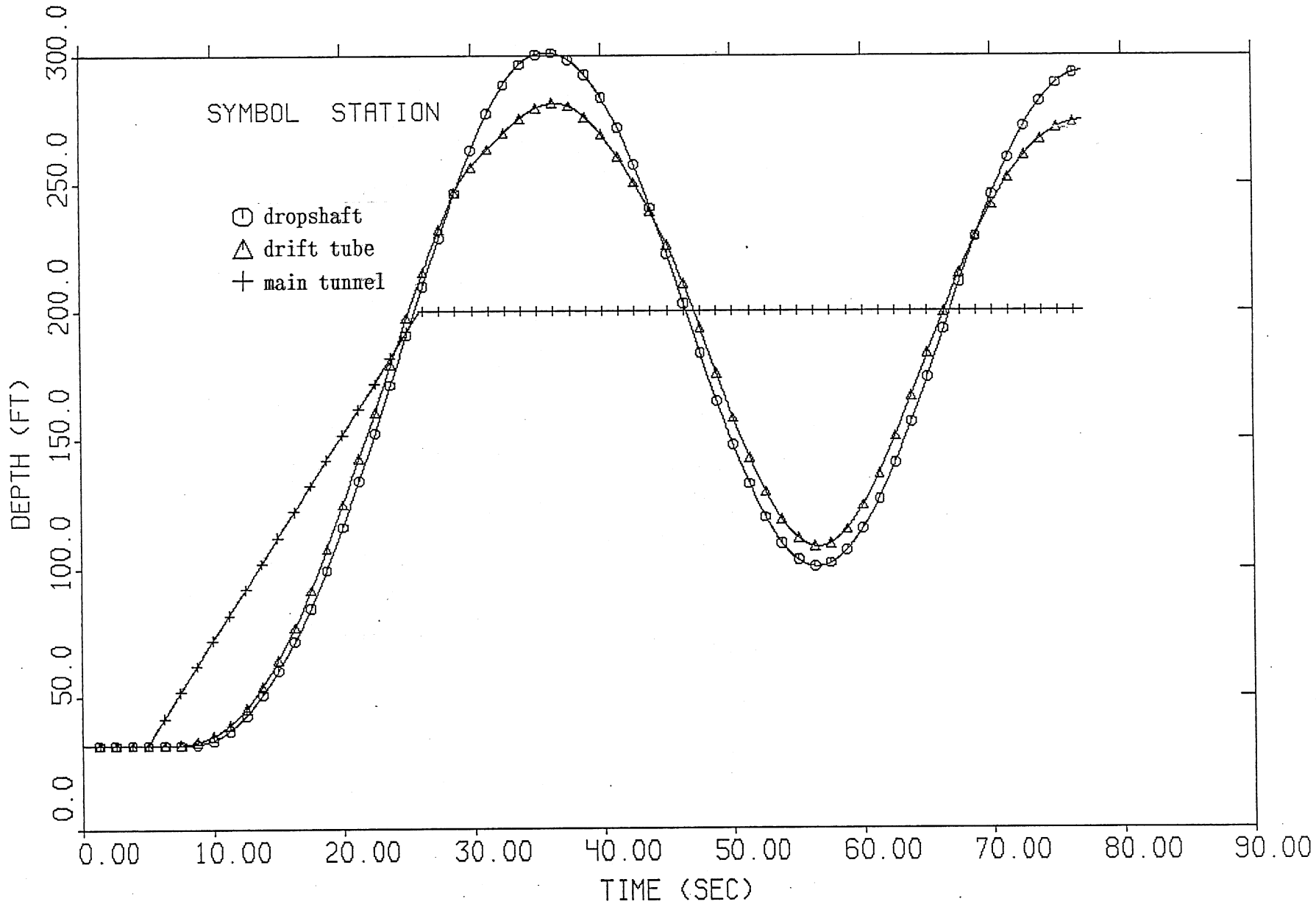

Fig. 31. Time variation of water depth in dropshaft due to tunnel pressure rise. (D_s = 12', L = 1309', D_ℓ = 13.5', f_o = 0.00, a = 335 fps).

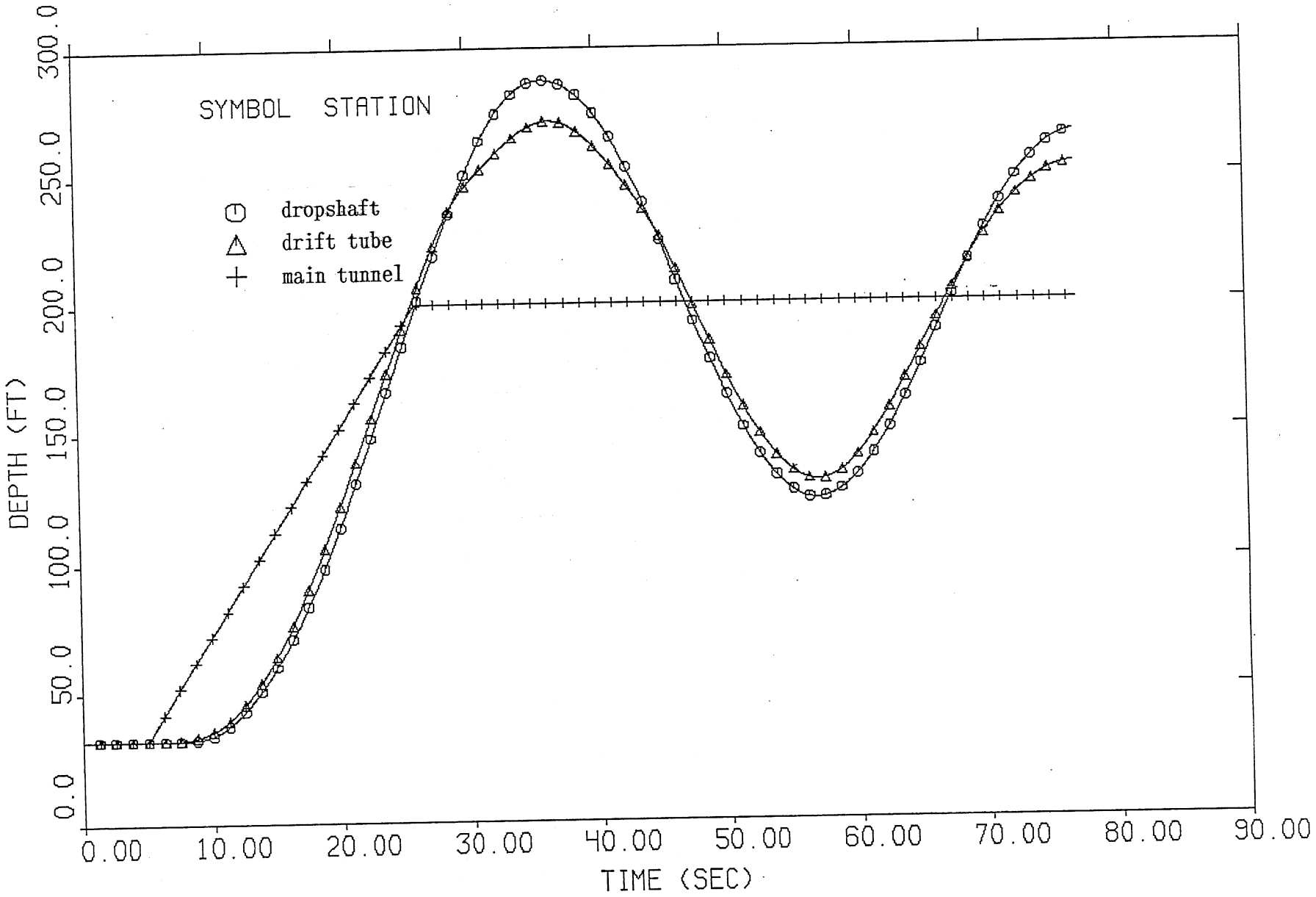

Fig. 32. Time variation of water depth in dropshaft due to tunnel pressure rise. (D_s = 12', L = 1309', D_ℓ = 13.5', f_o = 0.02, a = 335 fps).

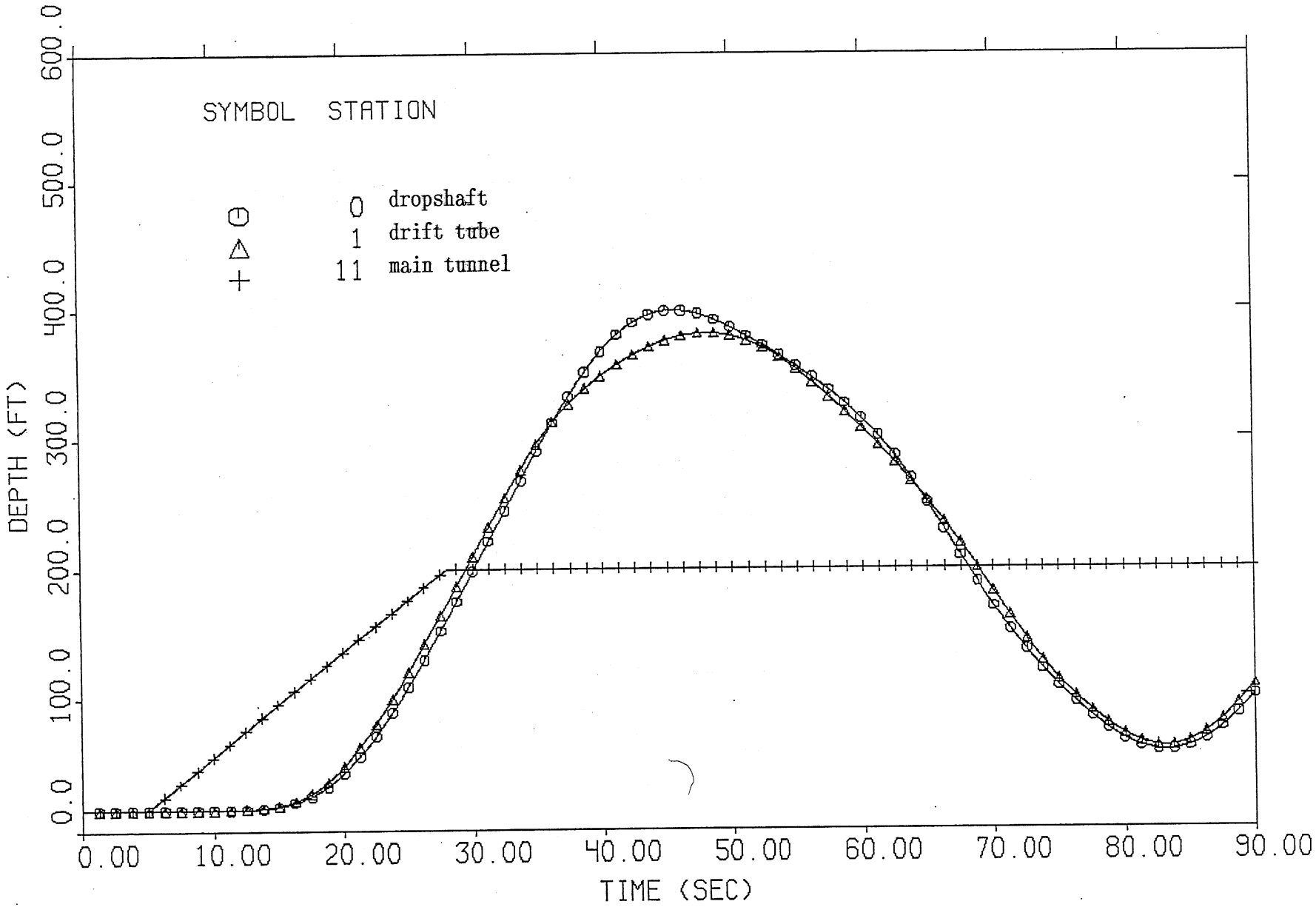

Fig. 33. Time variation of water depth in dropshaft due to tunnel pressure rise. (D_s = 12', L = 1309', D_ℓ = 13.5', f_o = 0.00, a = 100 fps).

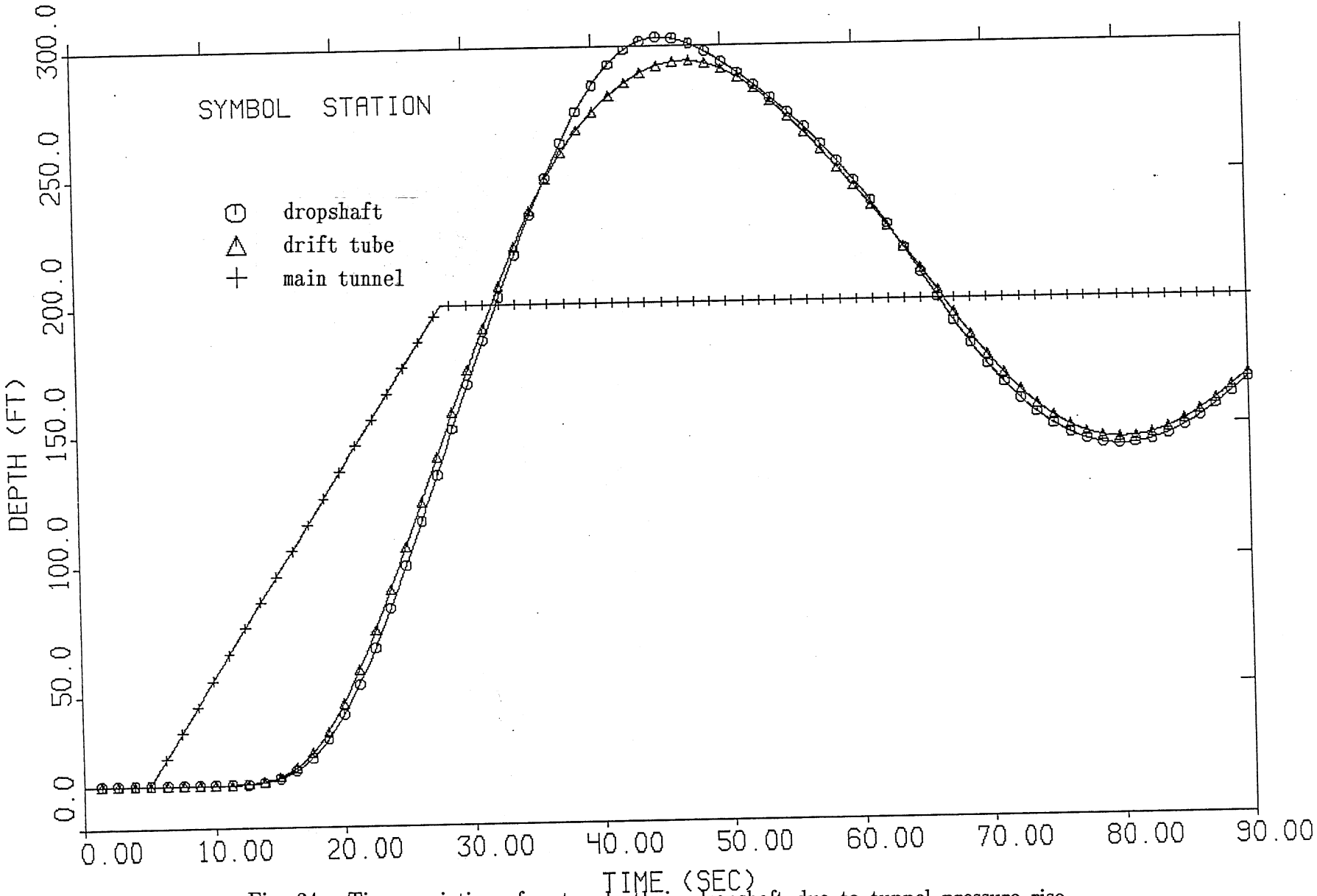

Fig. 34. Time variation of water depth in dropshaft due to tunnel pressure rise. (D_s = 12', L = 1309', D_ℓ = 13.5', f_o = 0.02, a = 100 fps).

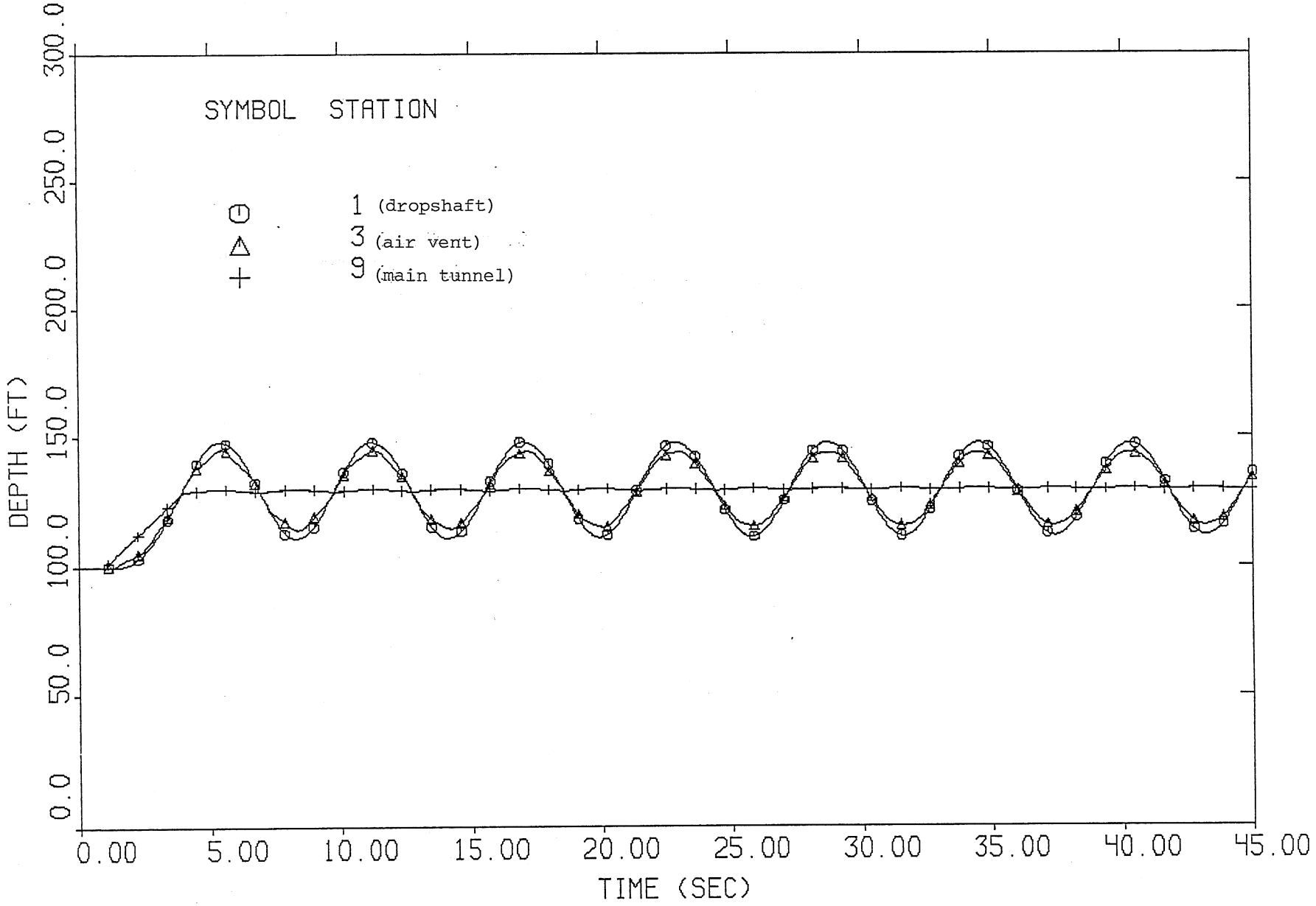

Fig. 35. Time variation of water depth in dropshaft and air vent due to tunnel pressure rise. ($\xi_0 = 0.0$, $\xi_i = 0.0$, $f_0 = 0.0$).

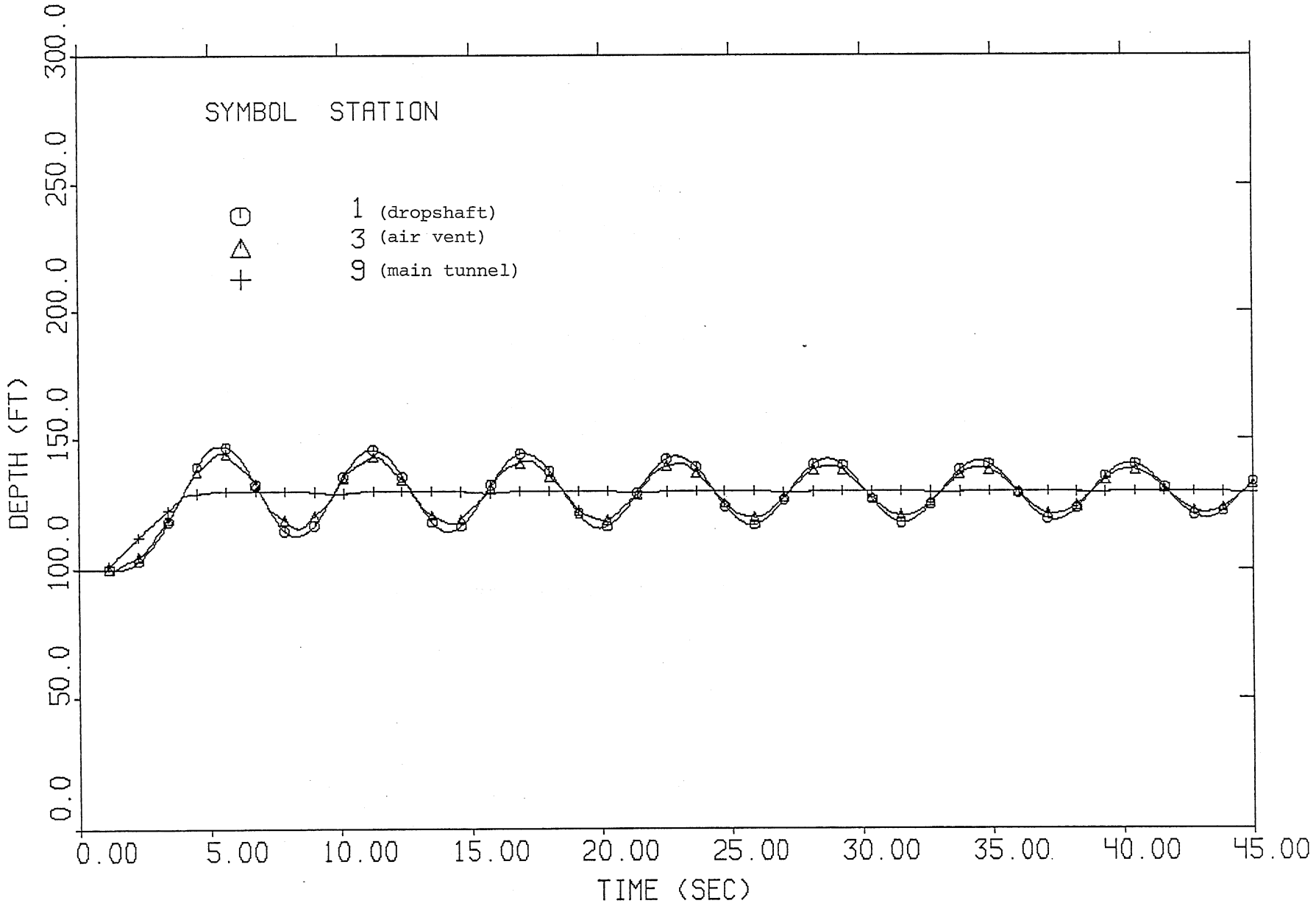

Fig. 36. Time variation of water depth in dropshaft and air vent due to tunnel pressure rise. ($\xi_0 = 1.0$, $\xi_i = 0.5$, $f_0 = 0.012$).

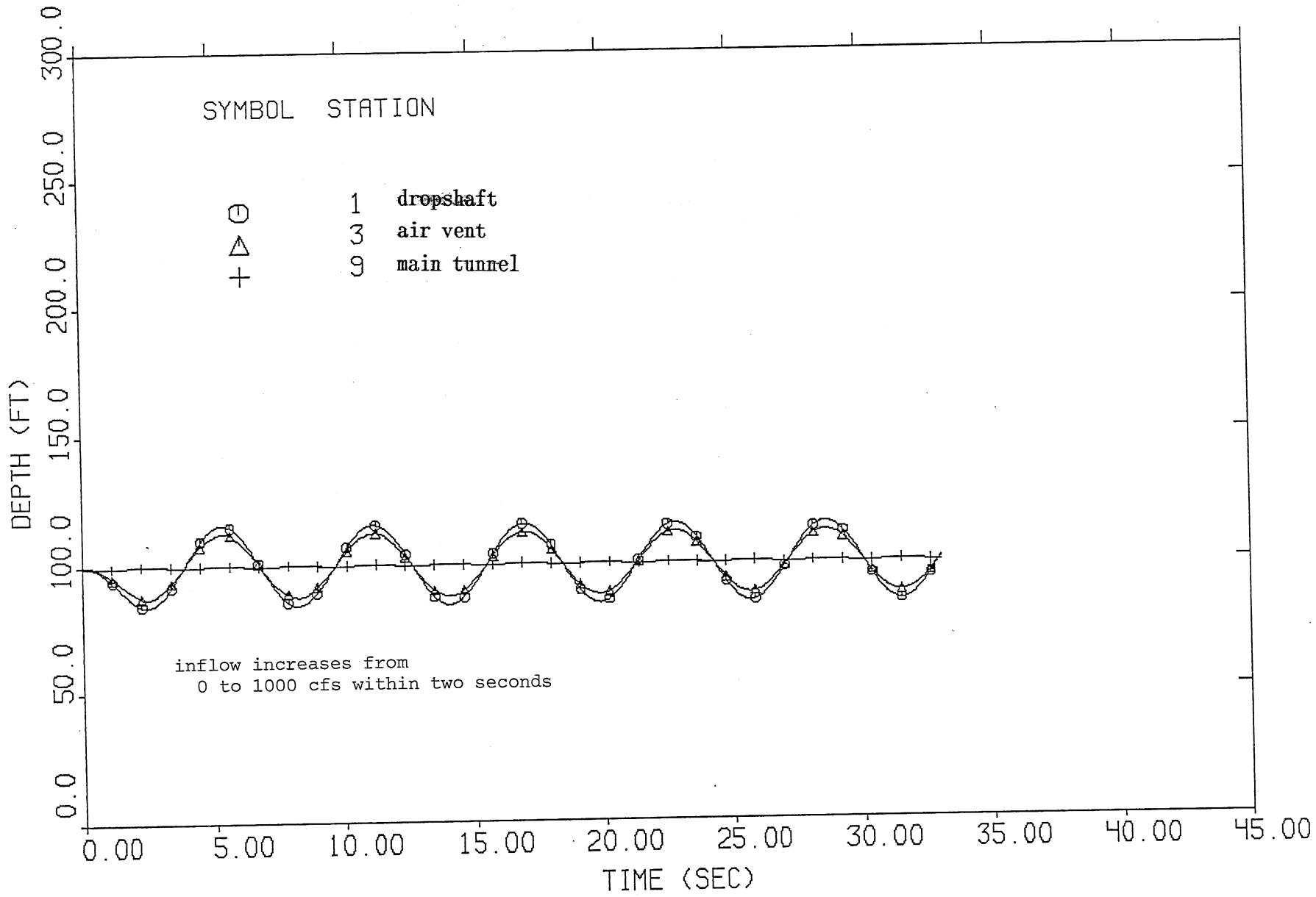

Fig. 37. Time variation of water level in dropshaft and air vent due to sudden opening of gate. ($\xi_0 = 1.0$, $\xi_i = 0.5$, $f_0 = 0.012$).

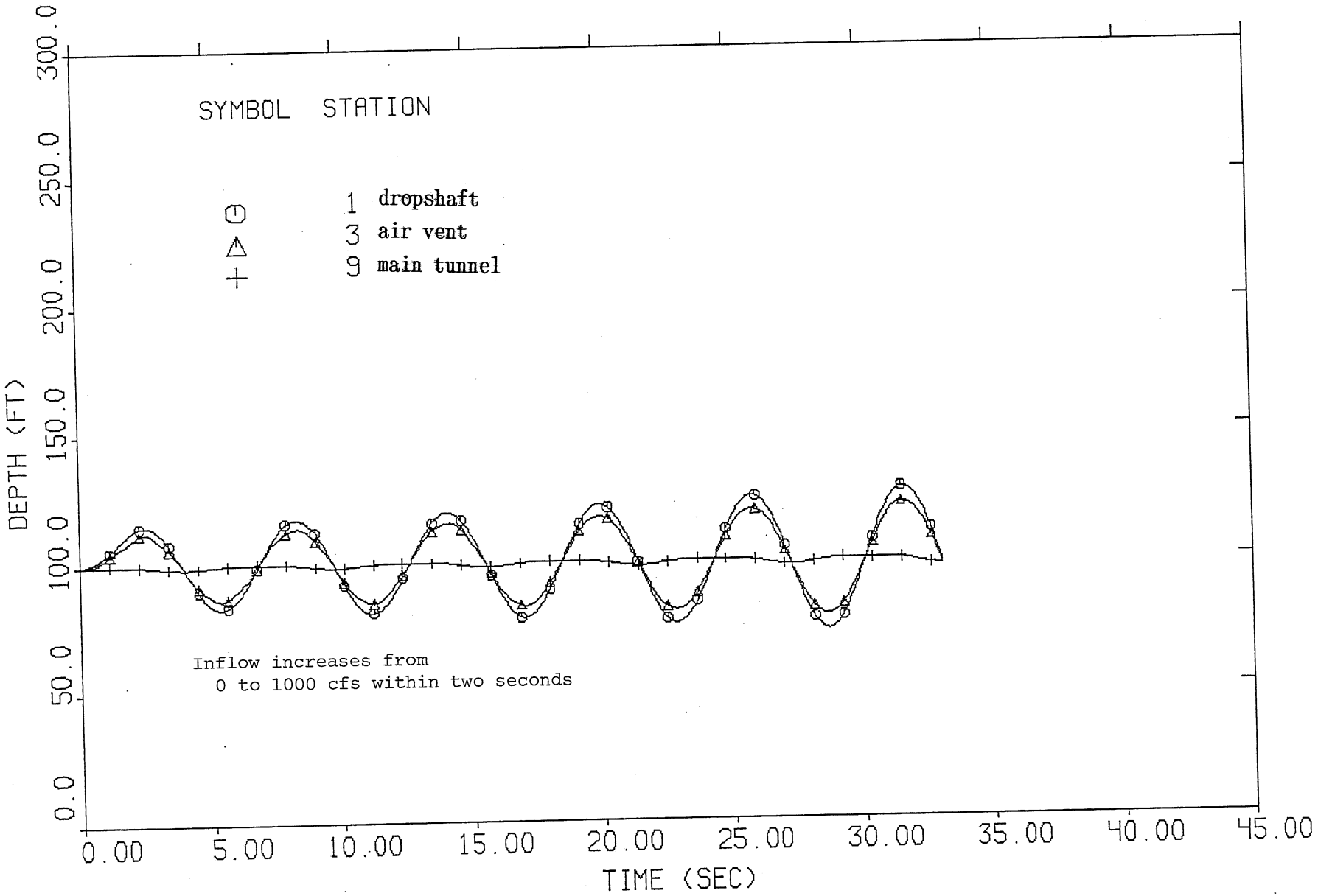

Fig. 38. Time variation of water level in dropshaft and air vent due to sudden opening of gate. ($\xi_0 = 0.5$, $\xi_i = 0.25$, $f_0 = 0.0$).

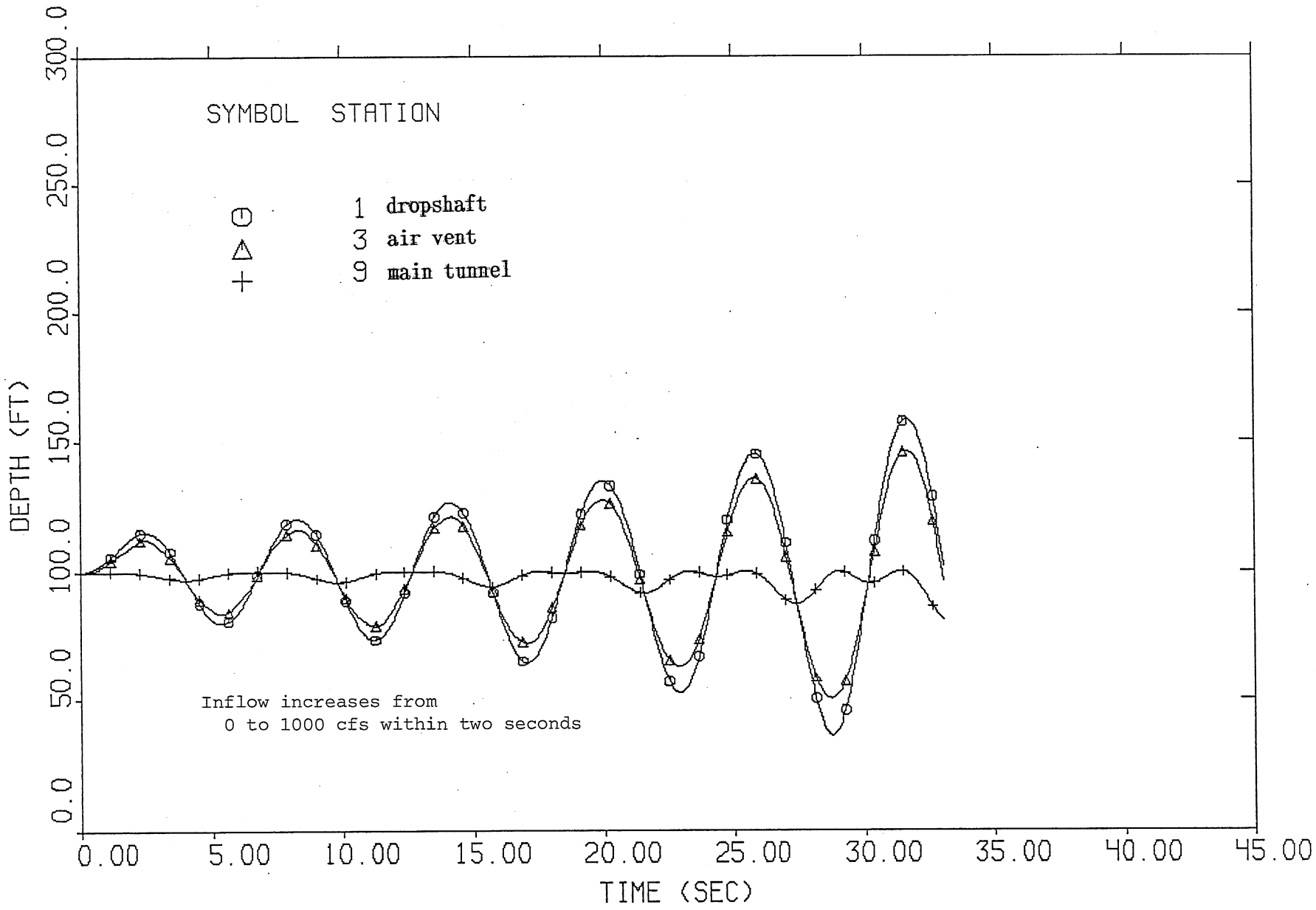

Fig. 39. Time variation of water level in dropshaft and air vent due to sudden opening of gate. ($\xi_0 = 0.0$, $\xi_i = 0.0$, $f_0 = 0.0$).

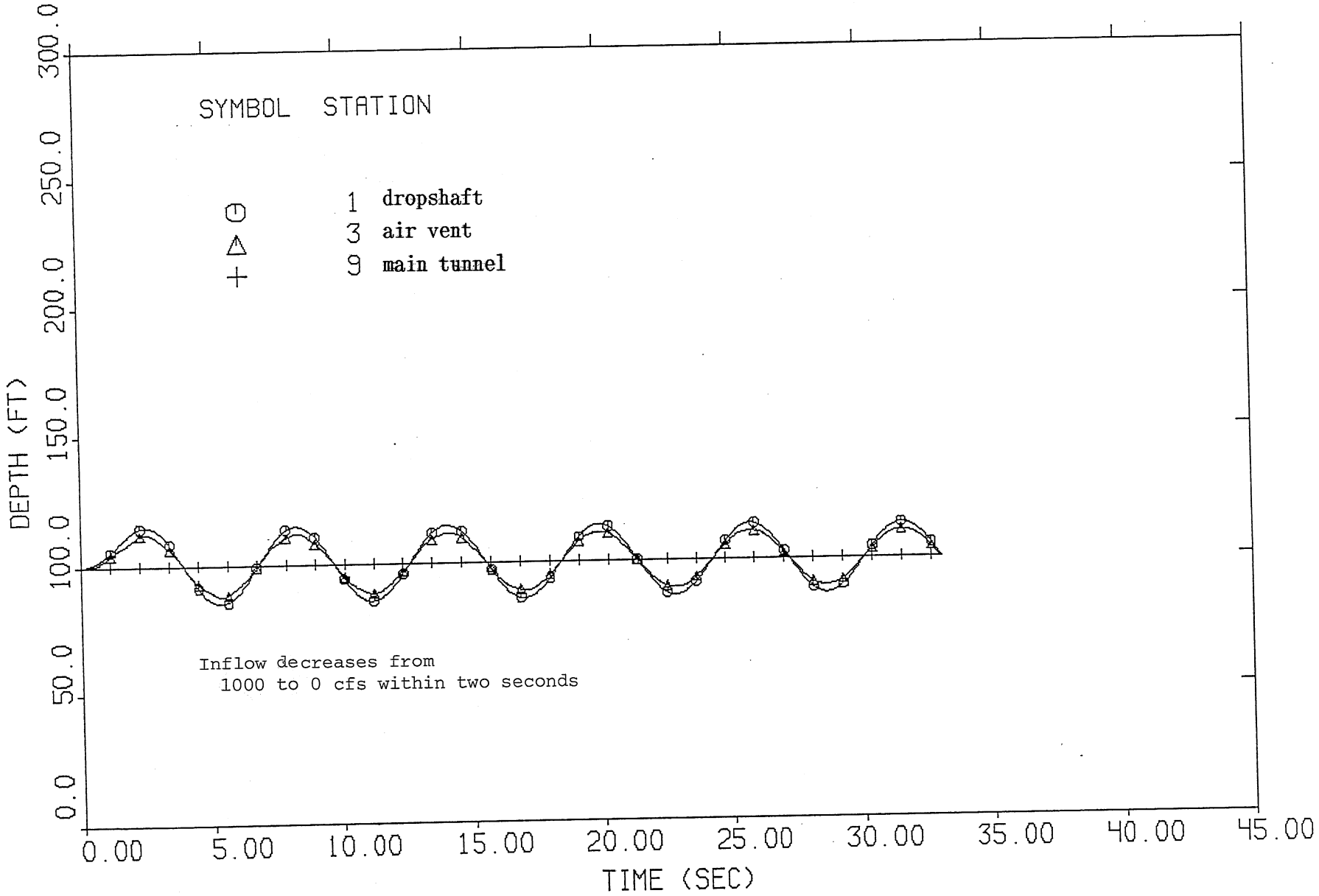

Fig. 40. Time variation of water level in dropshaft and air vent due to sudden closing of gate. ($\xi_0 = 0.0$, $\xi_i = 0.0$, $f_0 = 0.0$).

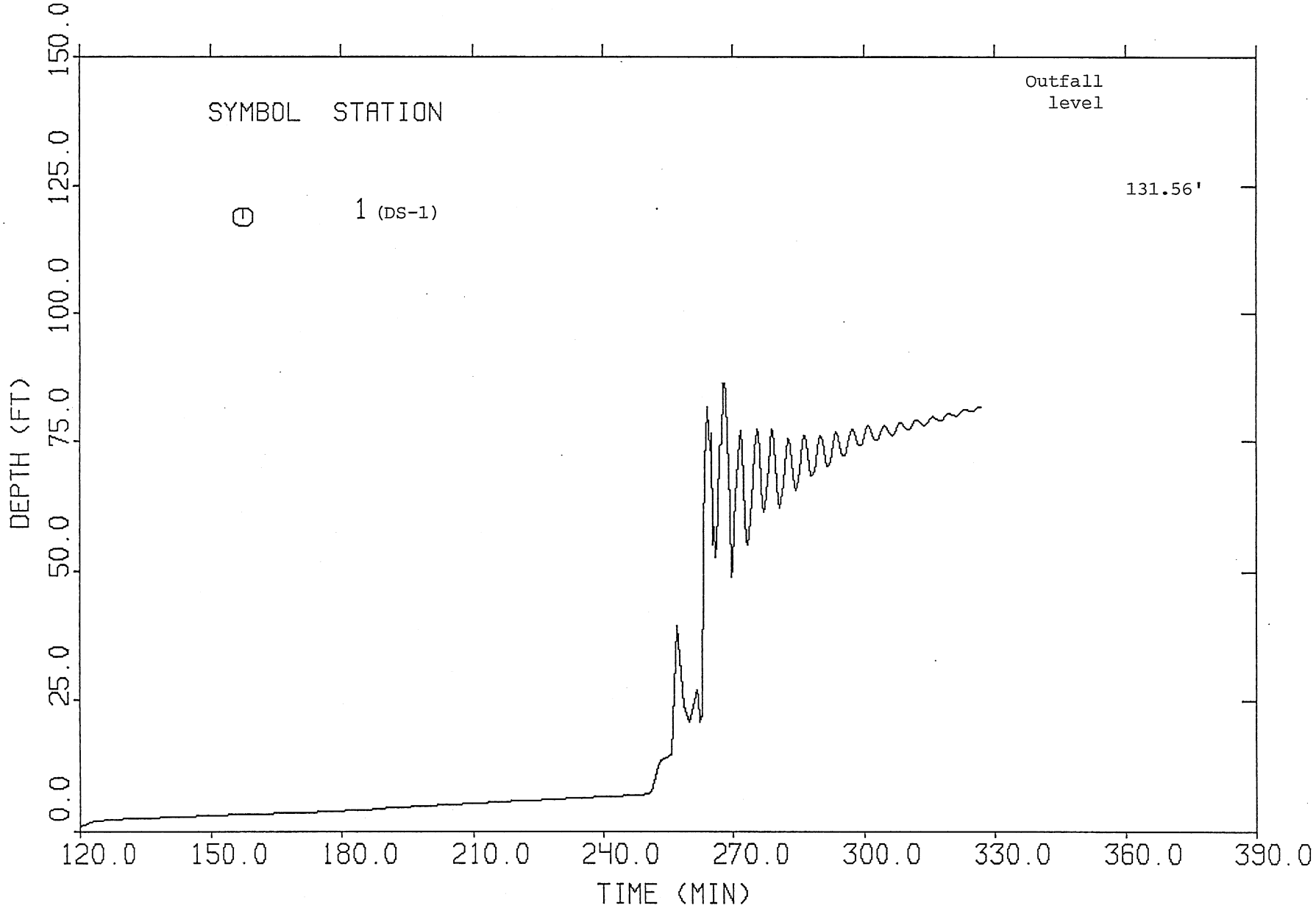

Fig. 41. Time variation of water depth in dropshaft No. 1, with 10% initial storage.

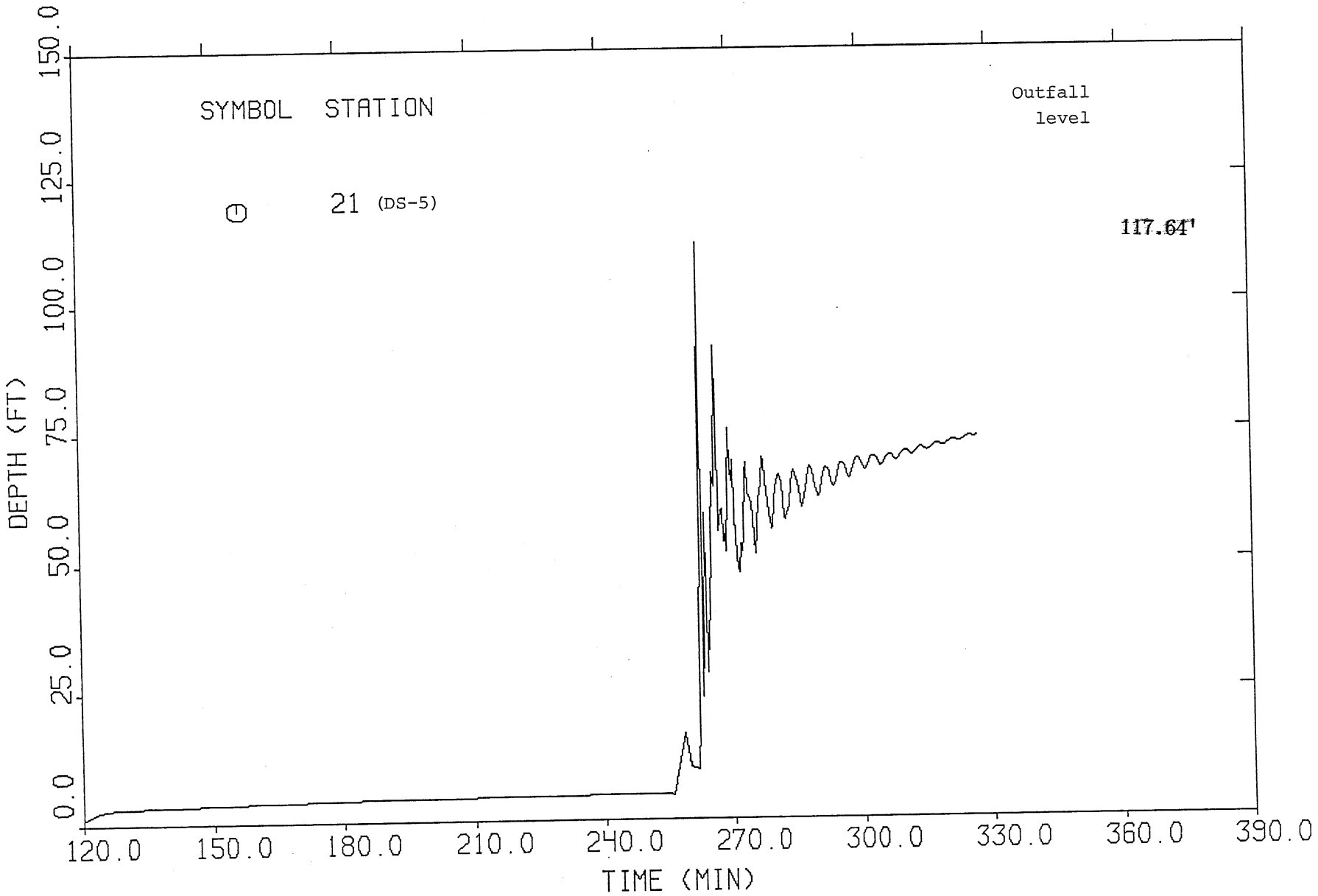

Fig. 42. Time variation of water depth in dropshaft No. 5, with 10% initial storage.

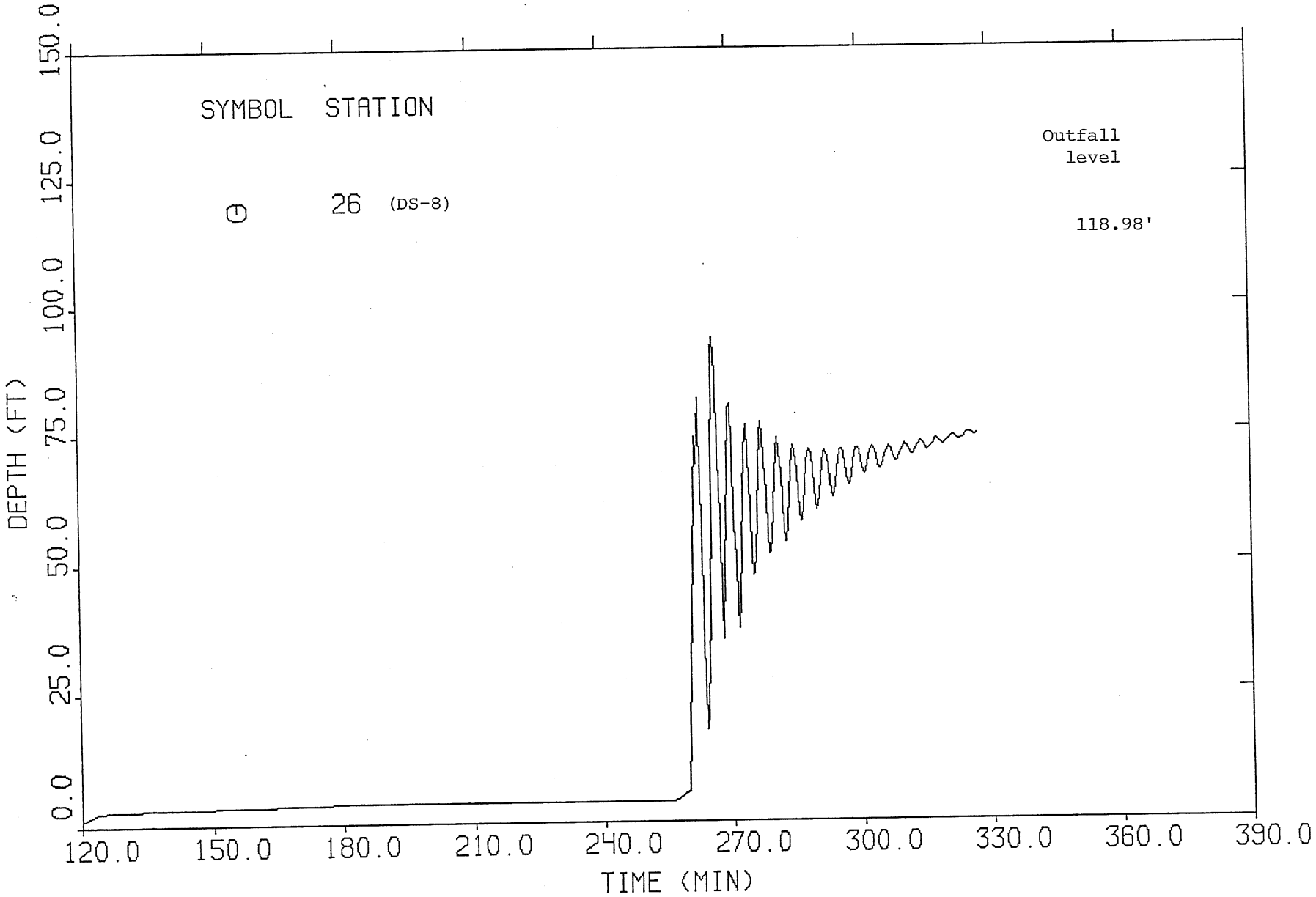

Fig. 43. Time variation of water depth in dropshaft No. 8, with 10% initial storage.

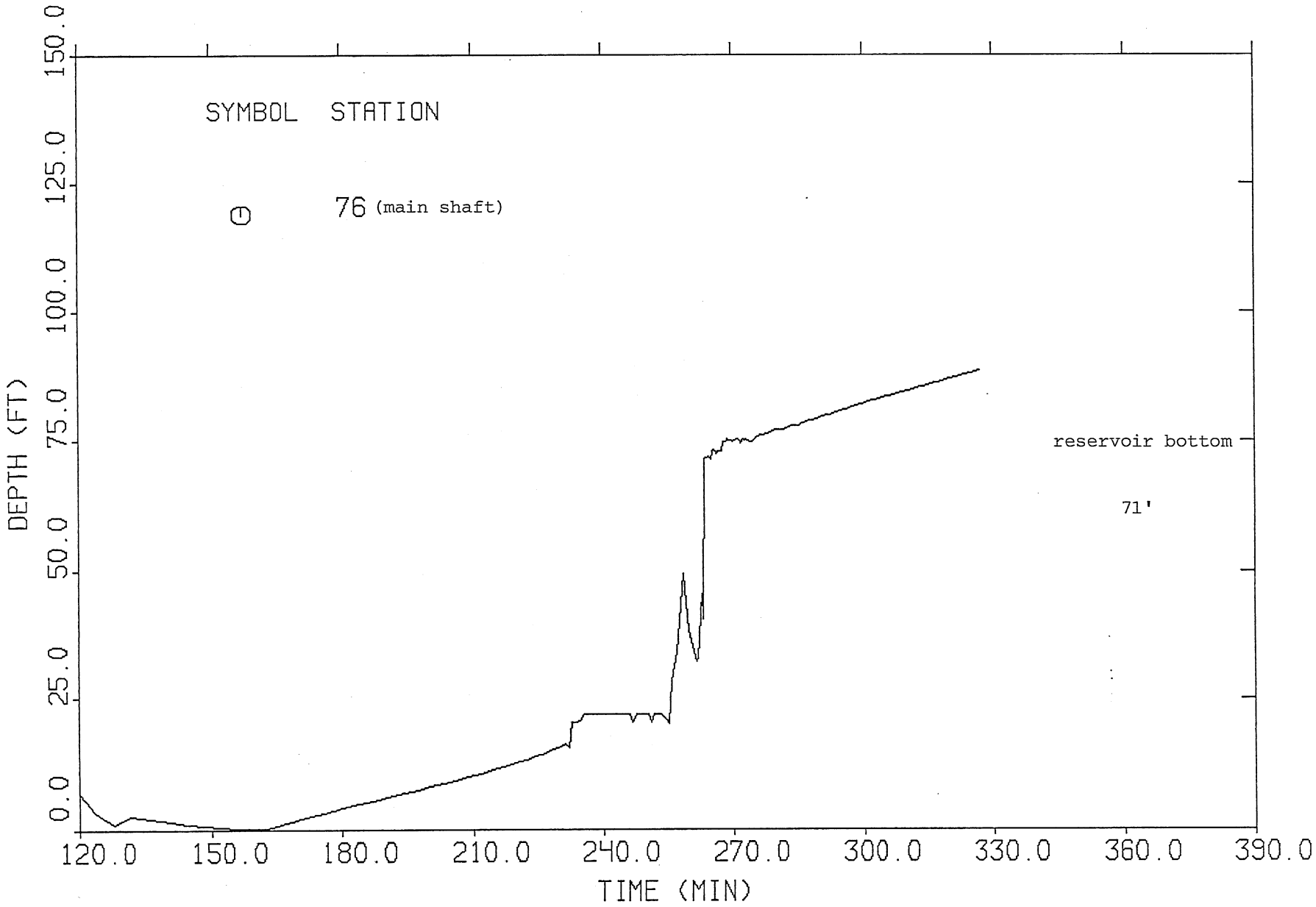

Fig. 44. Time variation of water depth in main shaft, with 10% initial storage.

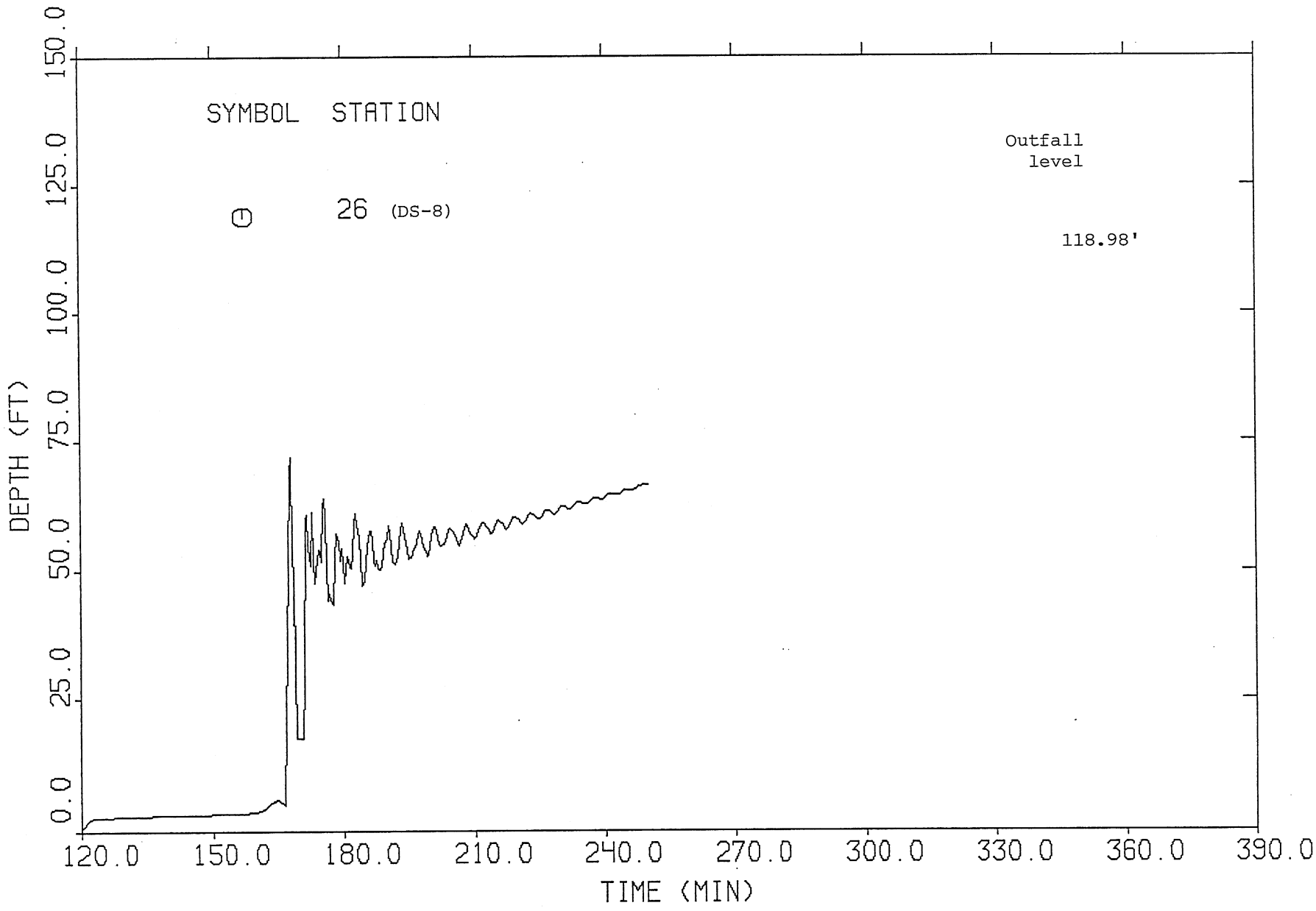

Fig. 45. Time variation of water depth in dropshaft No. 8, with 50% initial storage.

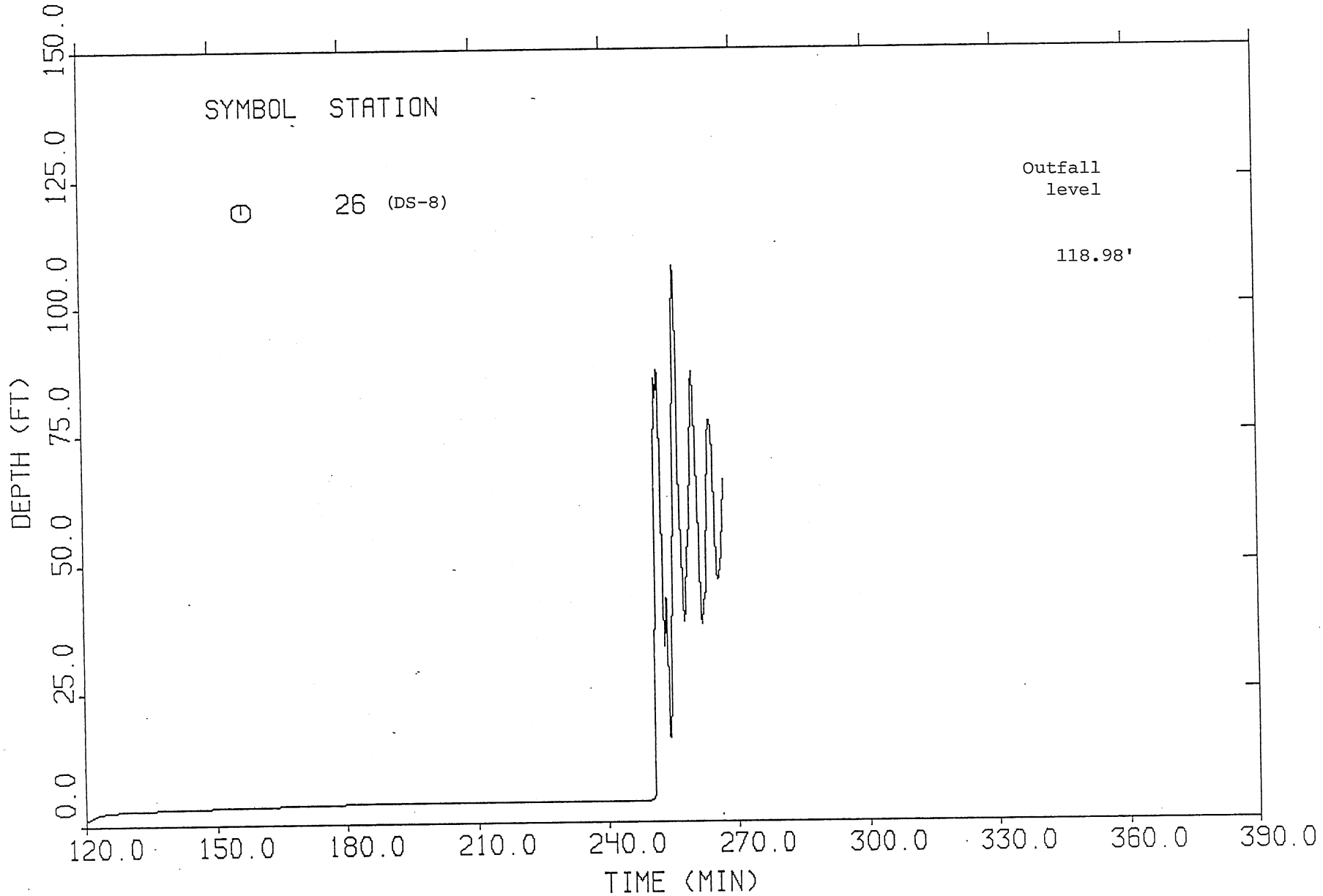

Fig. 46. Time variation of water depth in dropshaft No. 8, with diameters of DS–1, DS–5, and DS–8 increased to 18 feet.

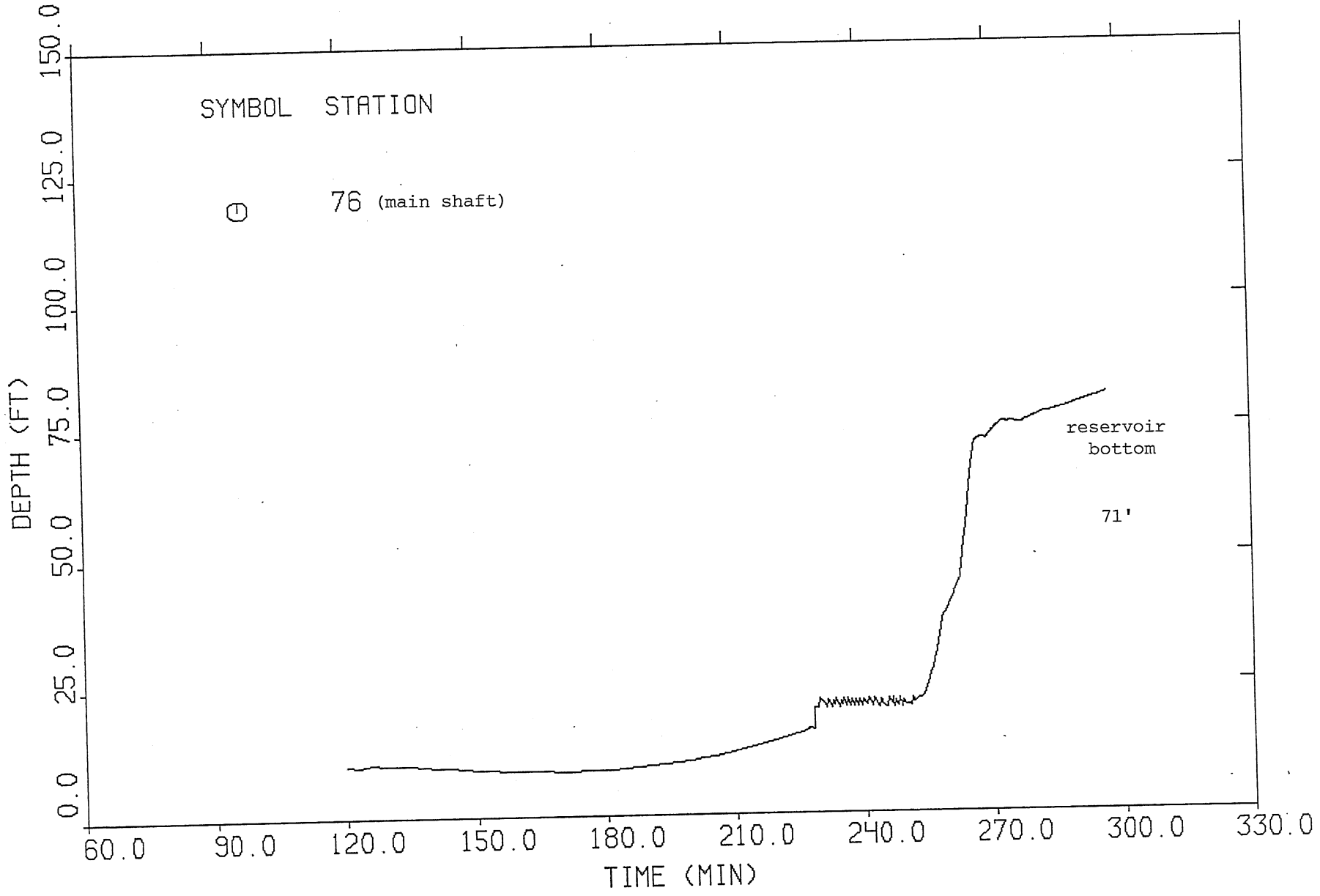

Fig. 47. Time variation of water depth at mainshaft which is enlarged to 150–foot diameter.

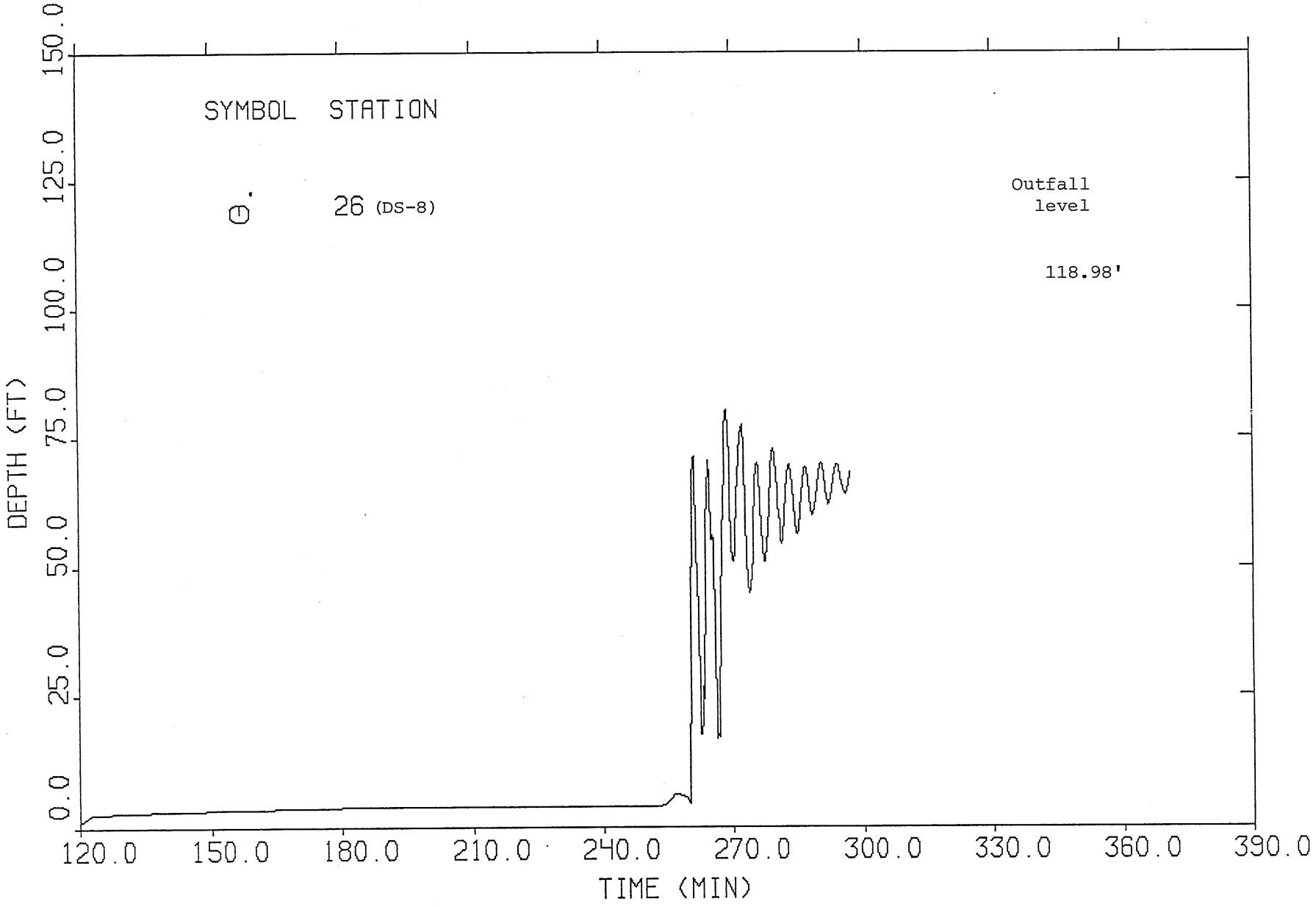

Fig. 48. Time variation of water depth at DS–6 with diameter of main shaft enlarged to 150 feet.

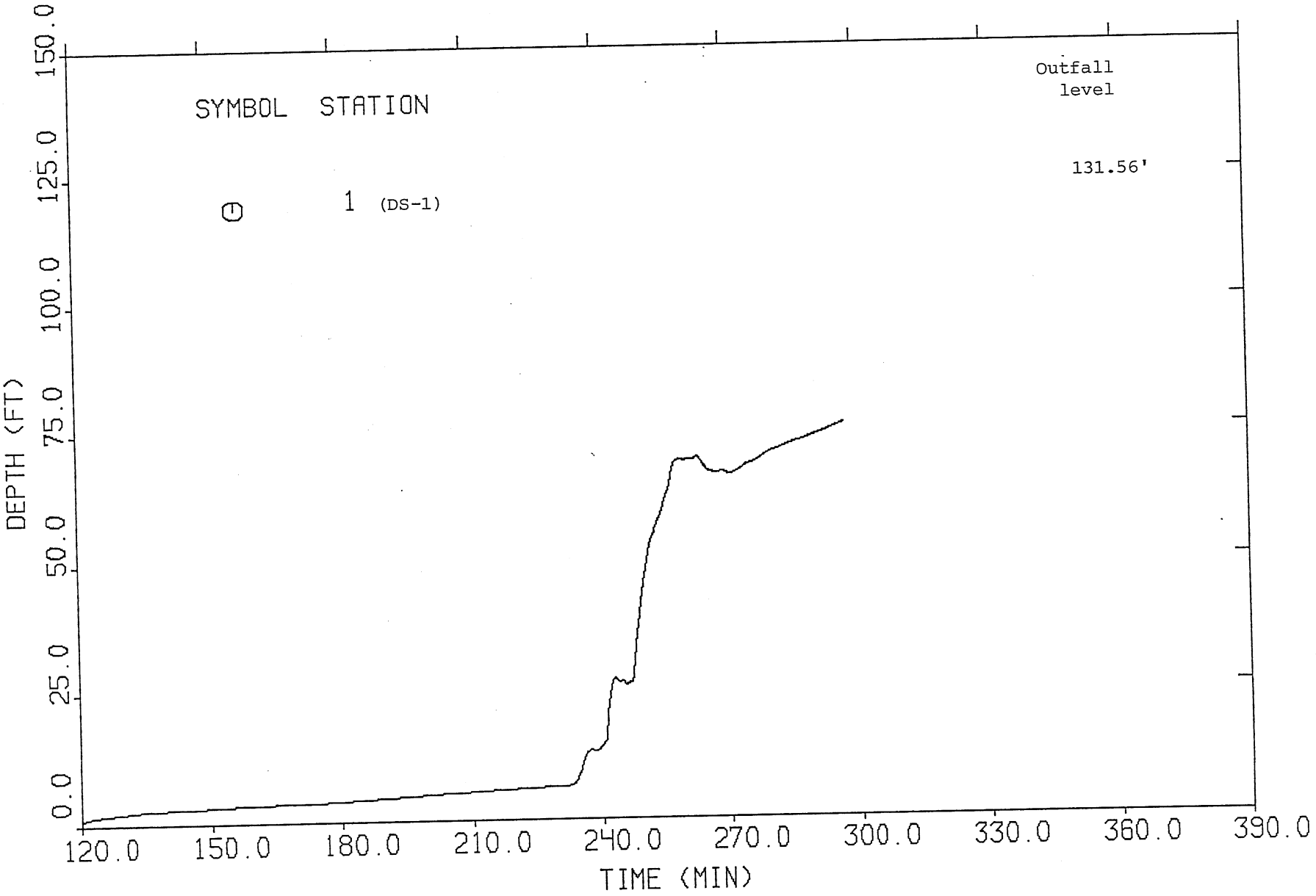

Fig. 49. Time variation of water depth at DS–1, which is enlarged to 150–foot diameter.

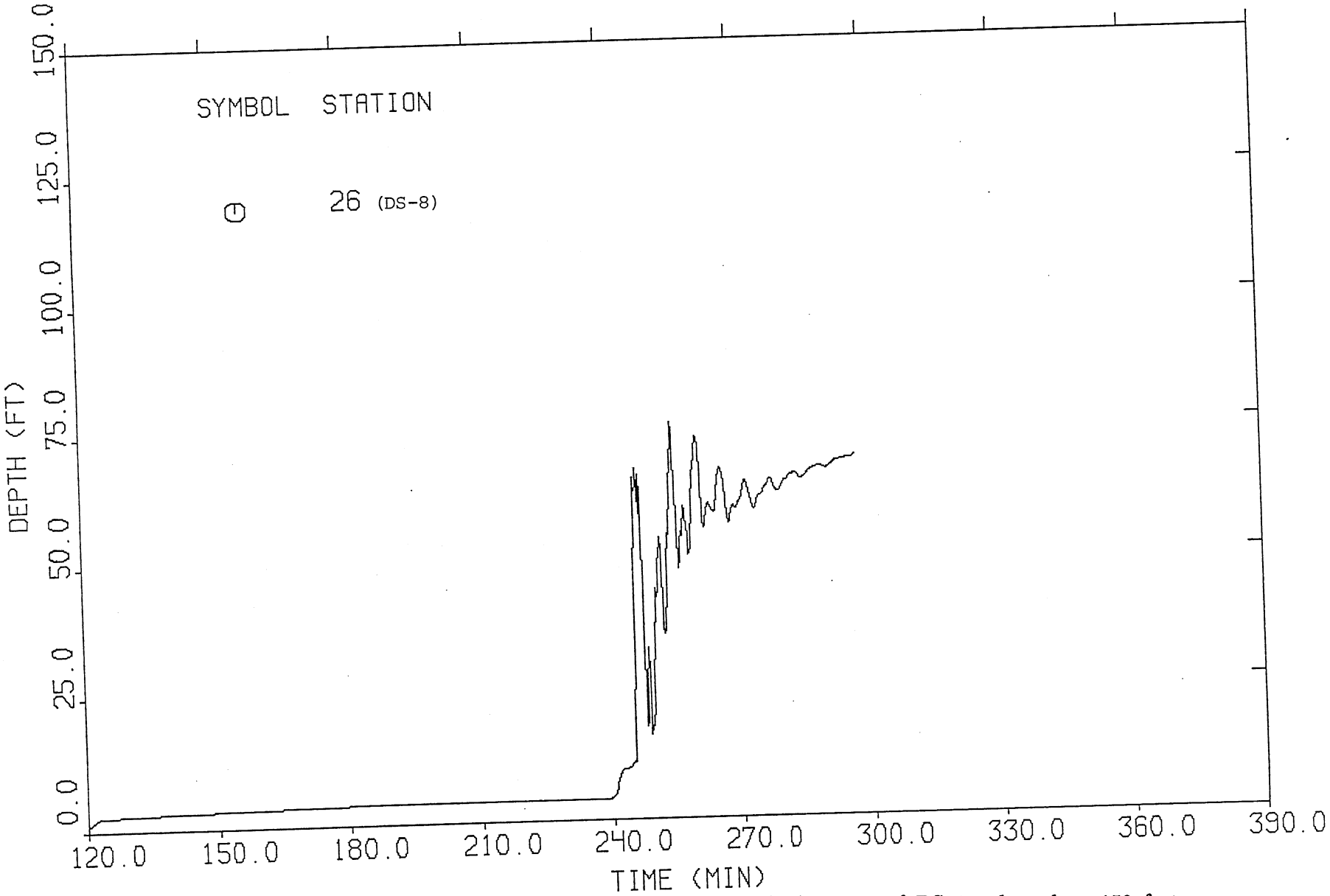

Fig. 50. Time variation of water depth at DS–8, with diameter of DS–1 enlarged to 150 feet.

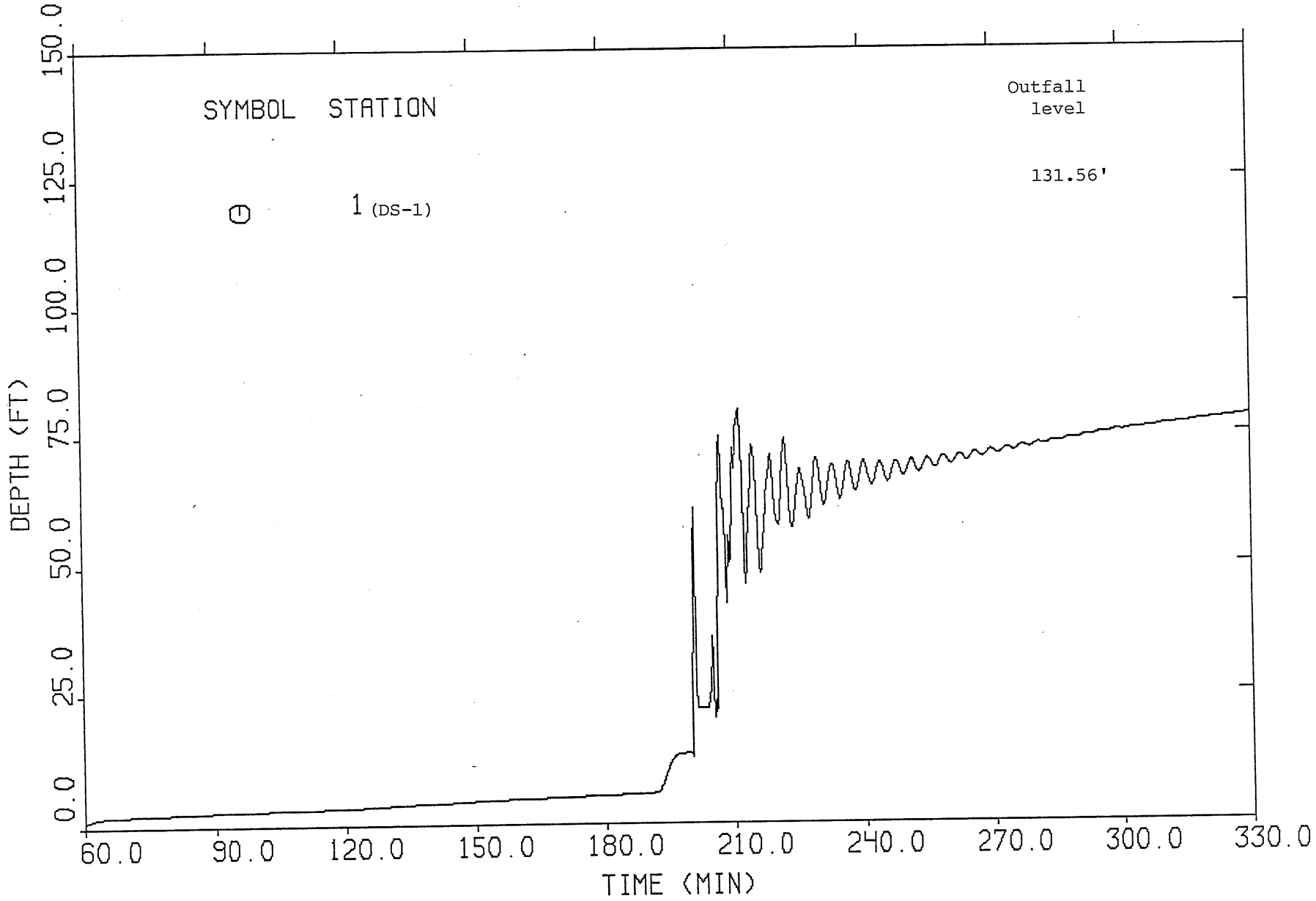

Fig. 51. Time variation of water depth at DS–1, 25–year, 6–hour storm.

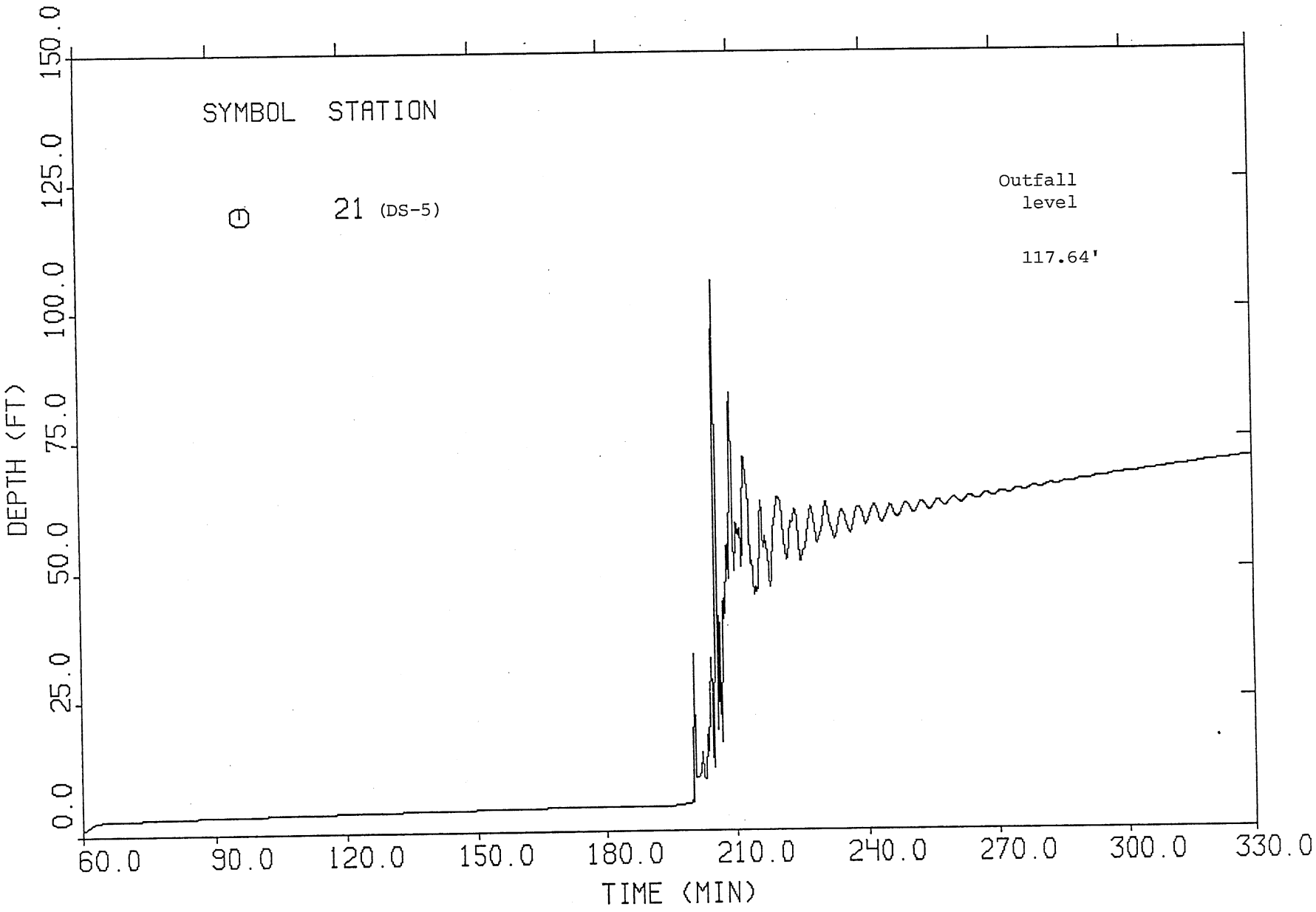

Fig. 52. Time variation of water depth at DS–5, 25–year, 6–hour storm.

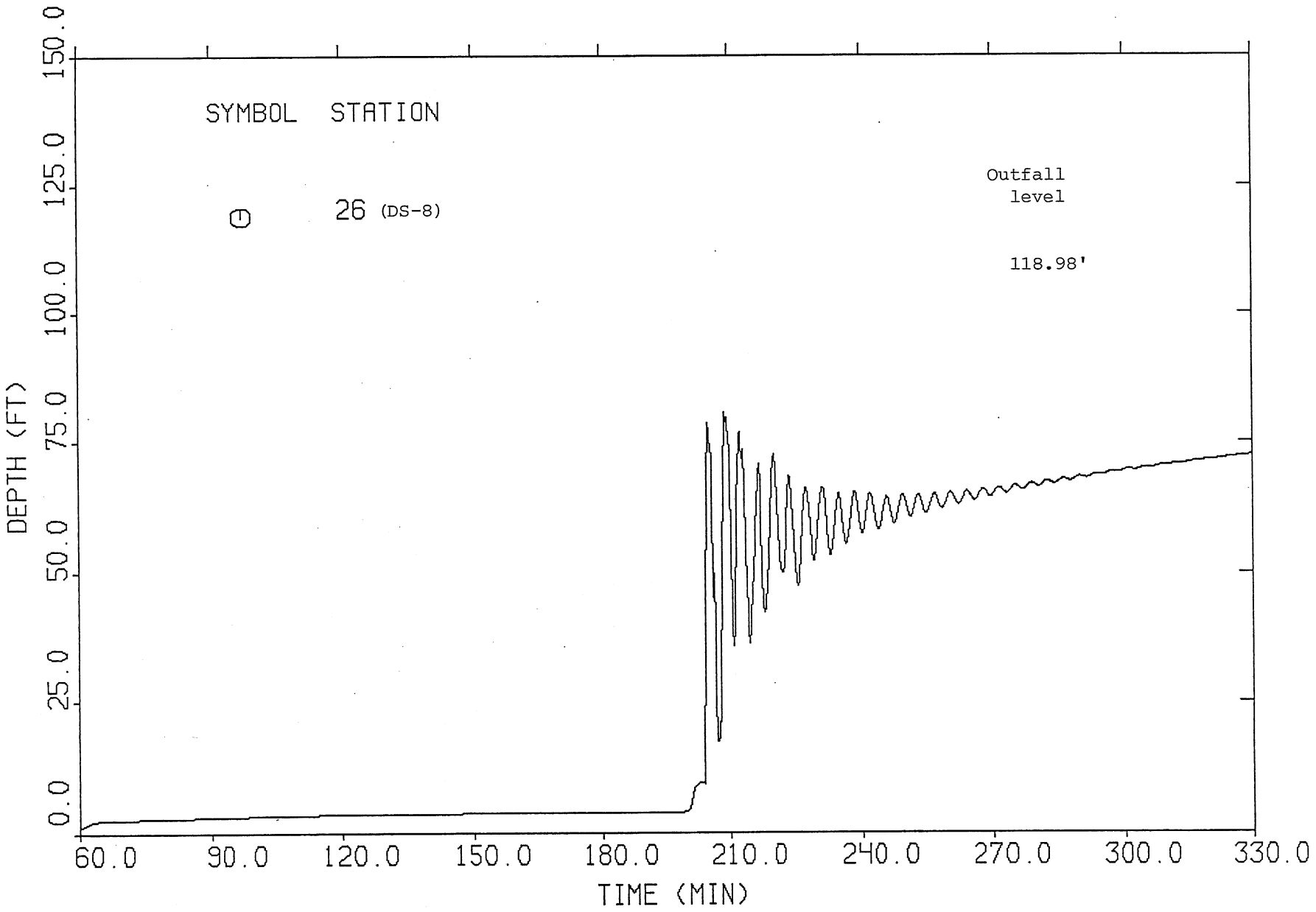

Fig. 53. Time variation of water depth at DS–8, 25–year, 6–hour storm.

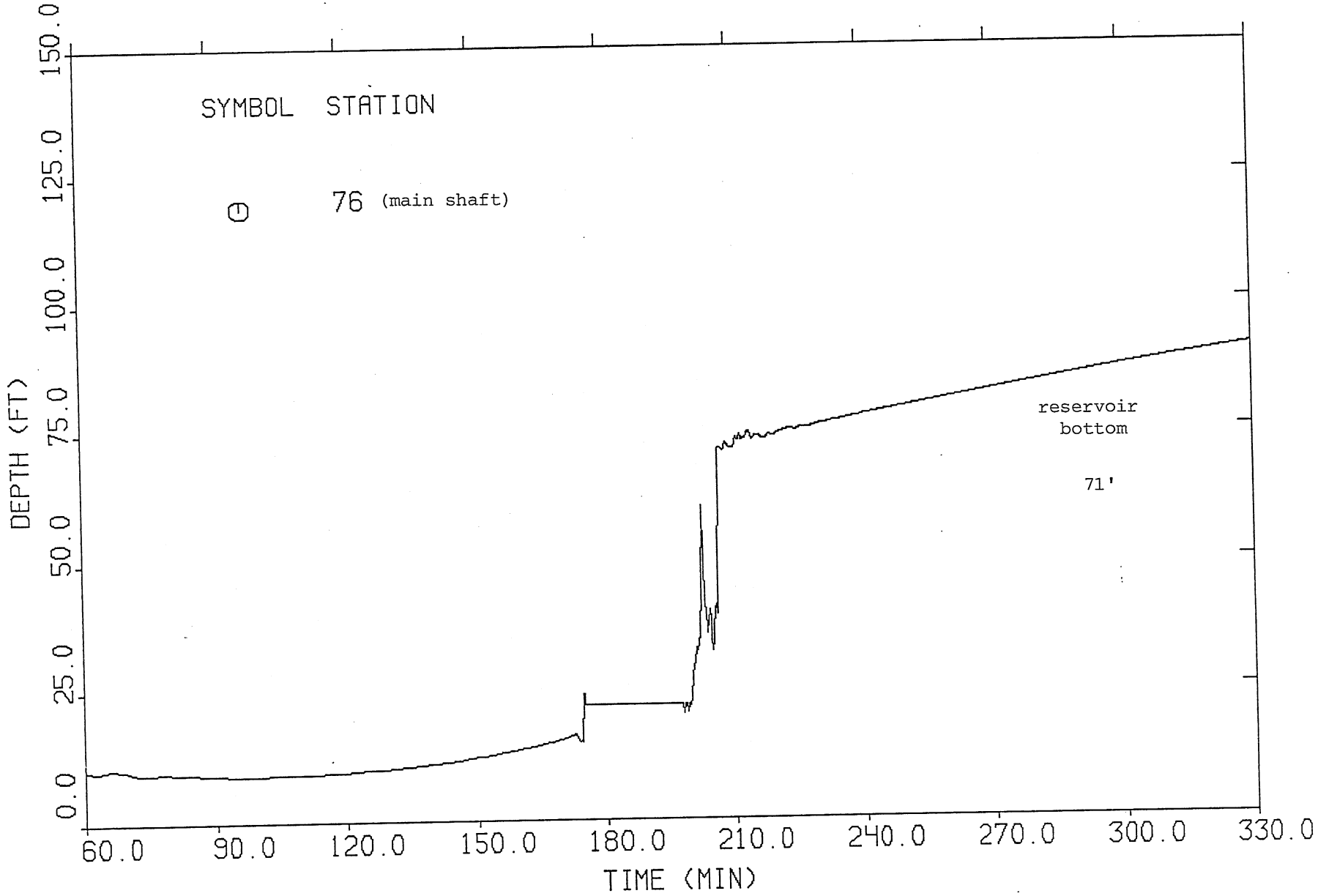

Fig. 54. Time variation of water depth at main shaft, 25–year, 6–hour storm.

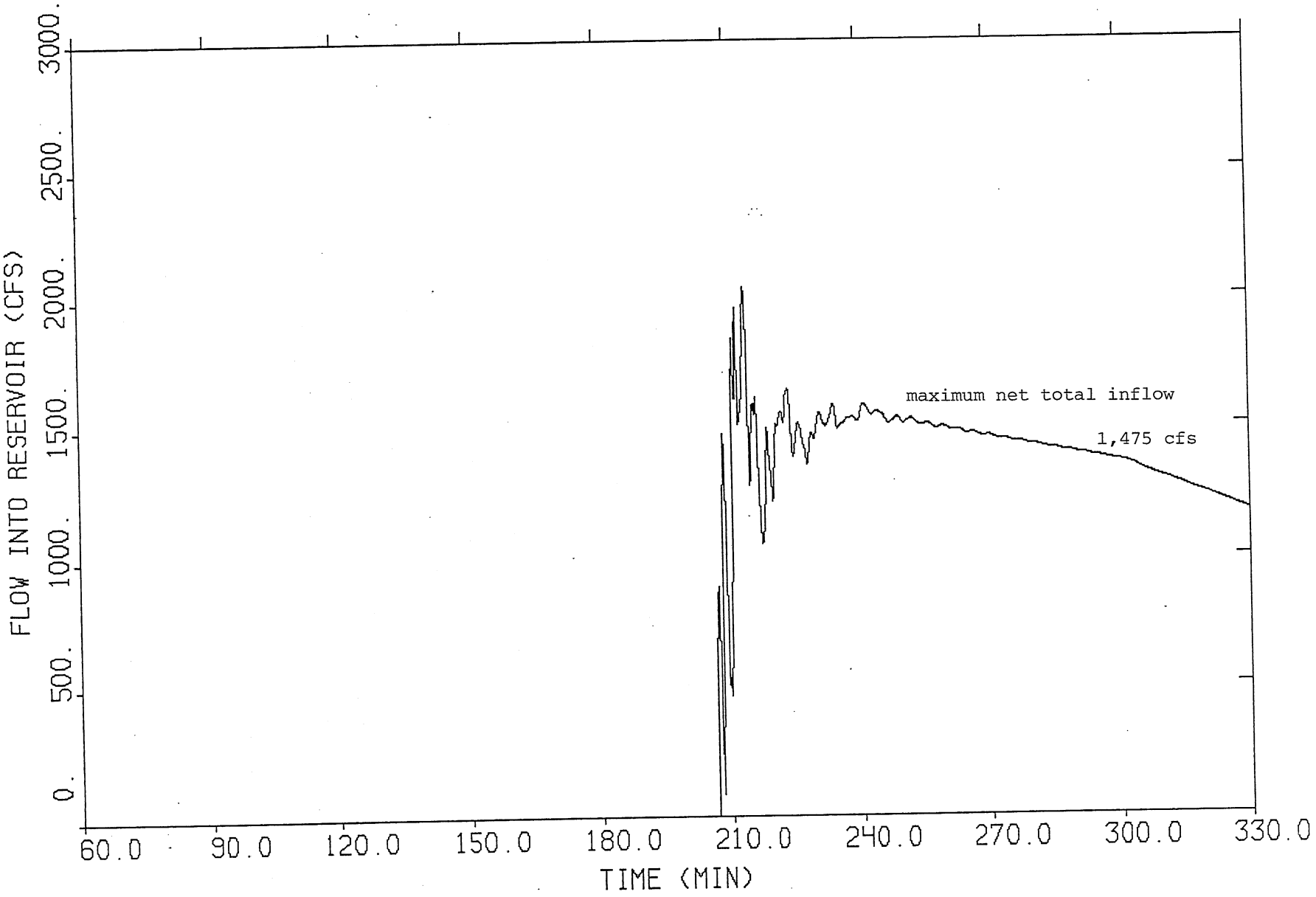

Fig. 55. Outflow hydrograph to terminal reservoir, 25–year, 6–hour storm.

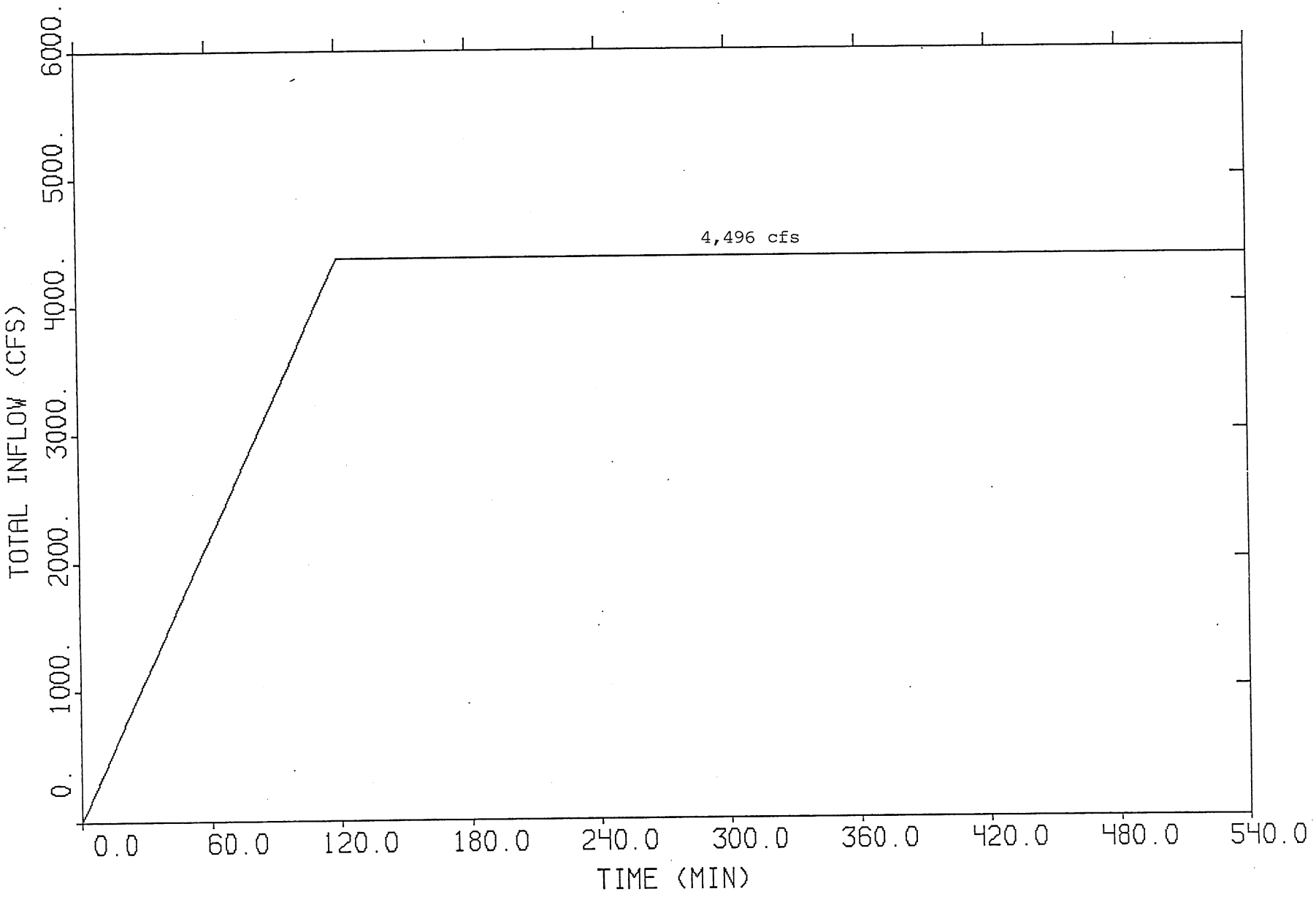

Fig. 56. Hydrograph for total design dropshaft inflow.

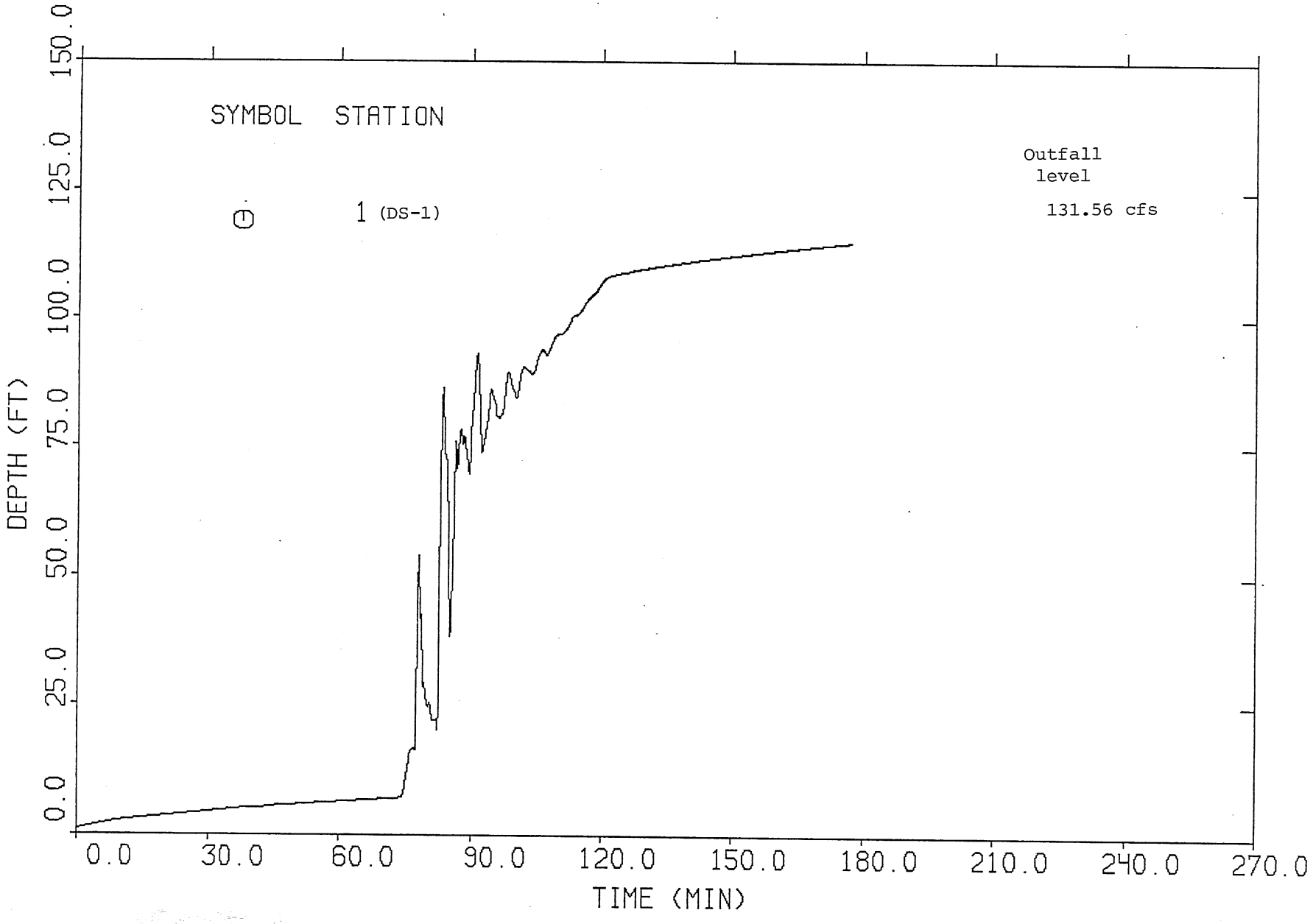

Fig. 57. Time variation of water depth at DS–1, design dropshaft inflow.

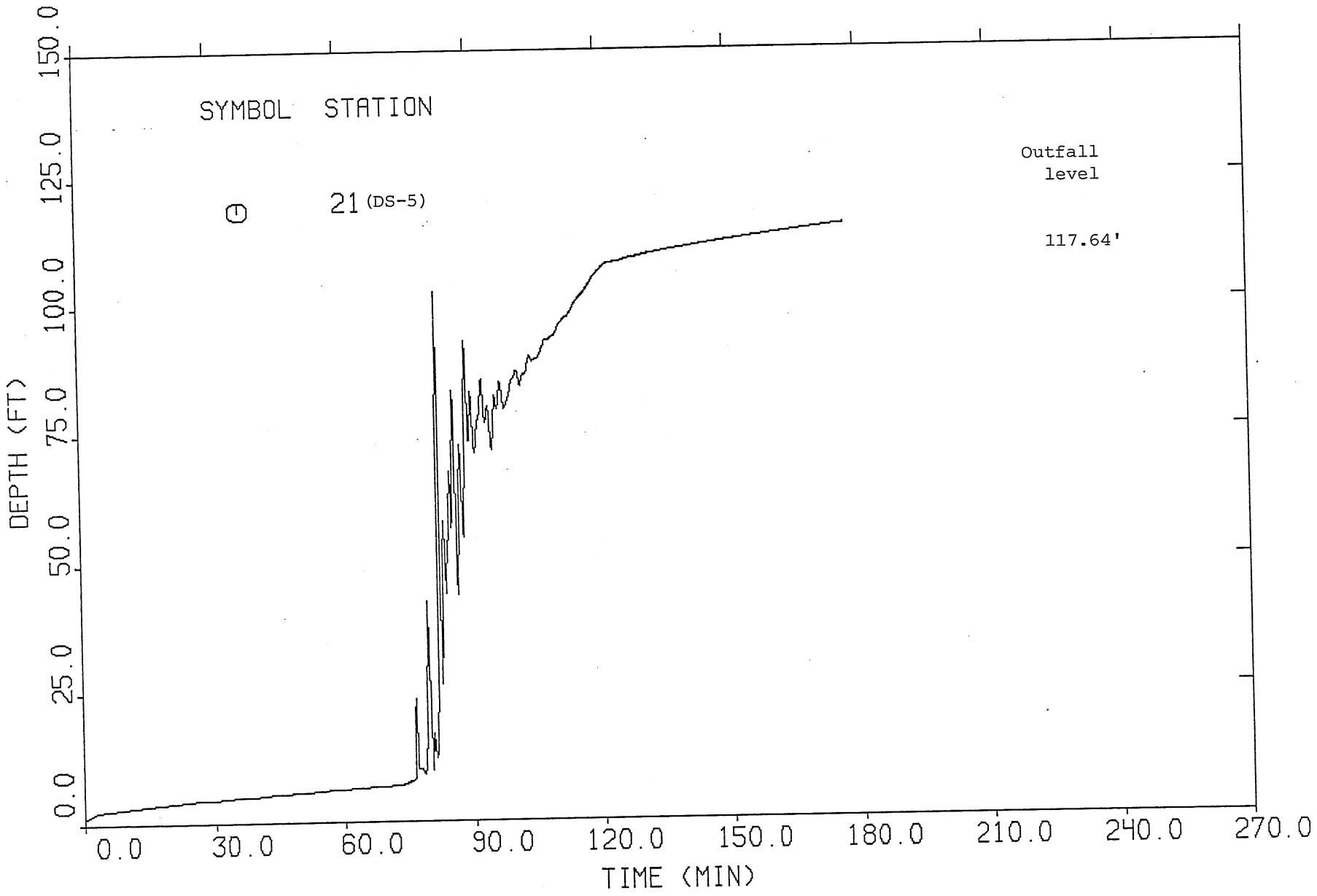

Fig. 58. Time variation of water depth at DS–5, design dropshaft inflow.

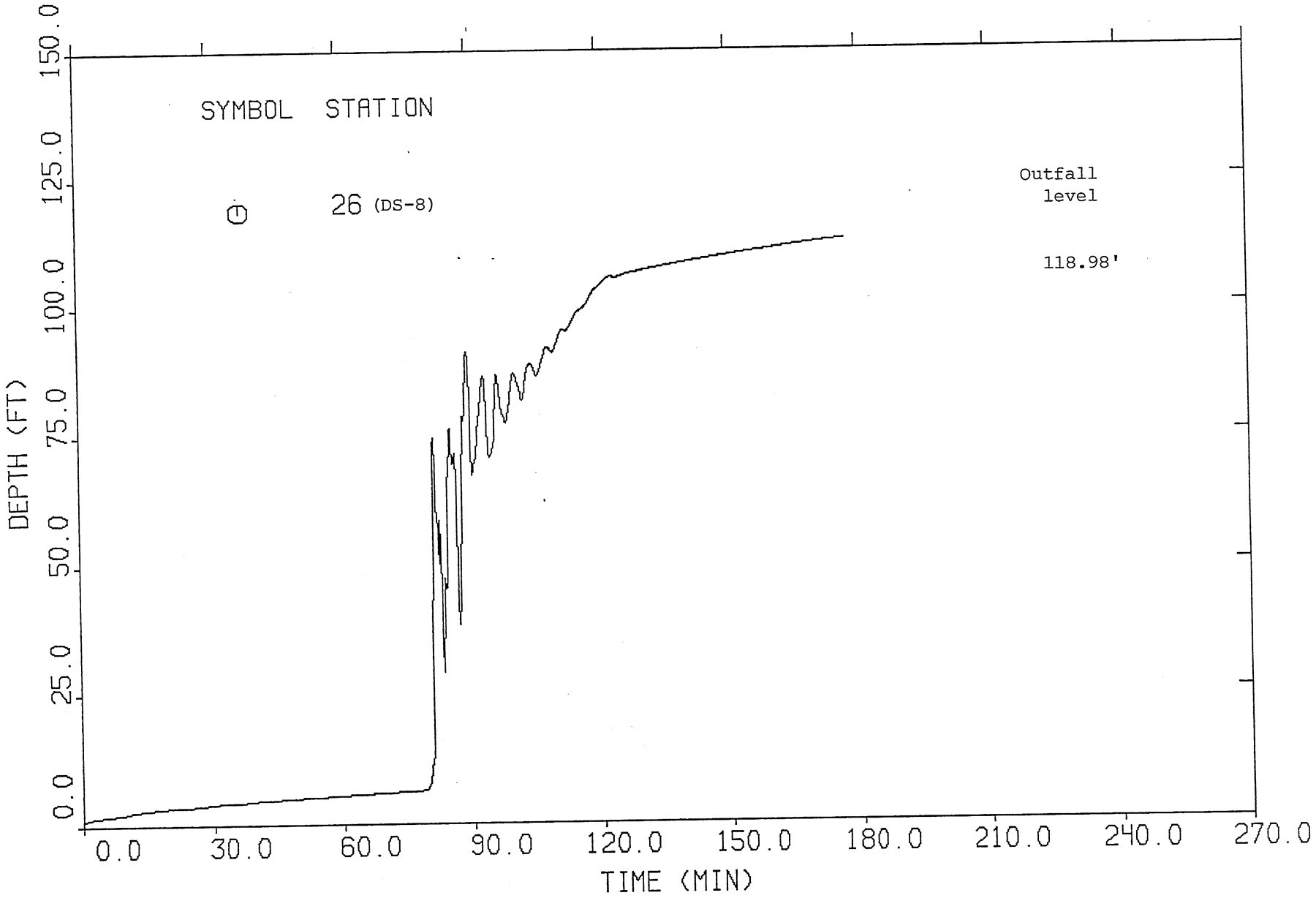

Fig. 59. Time variation of water depth at DS–8, design dropshaft inflow.

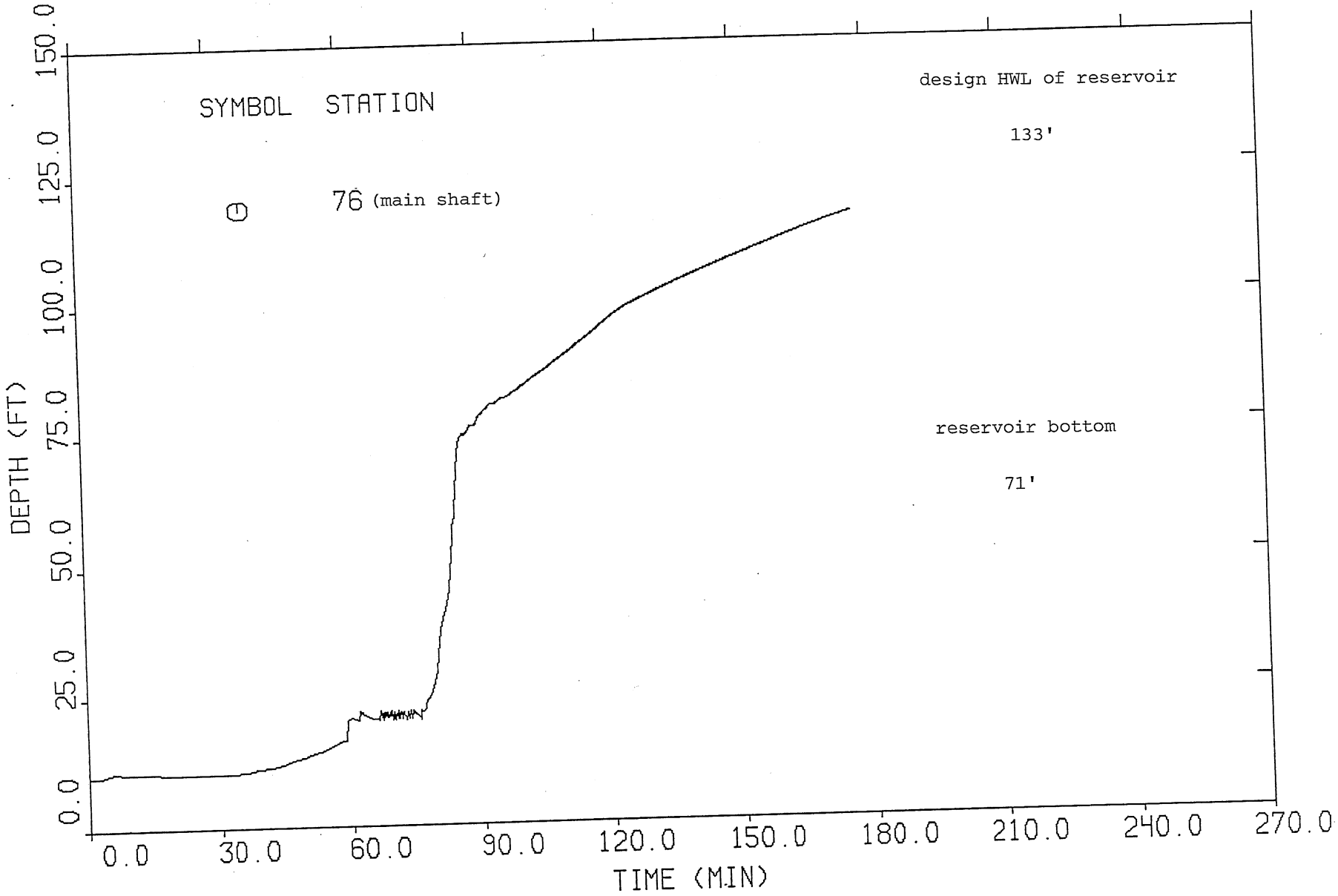

Fig. 60. Time variation of water depth at main shaft, design dropshaft inflow.

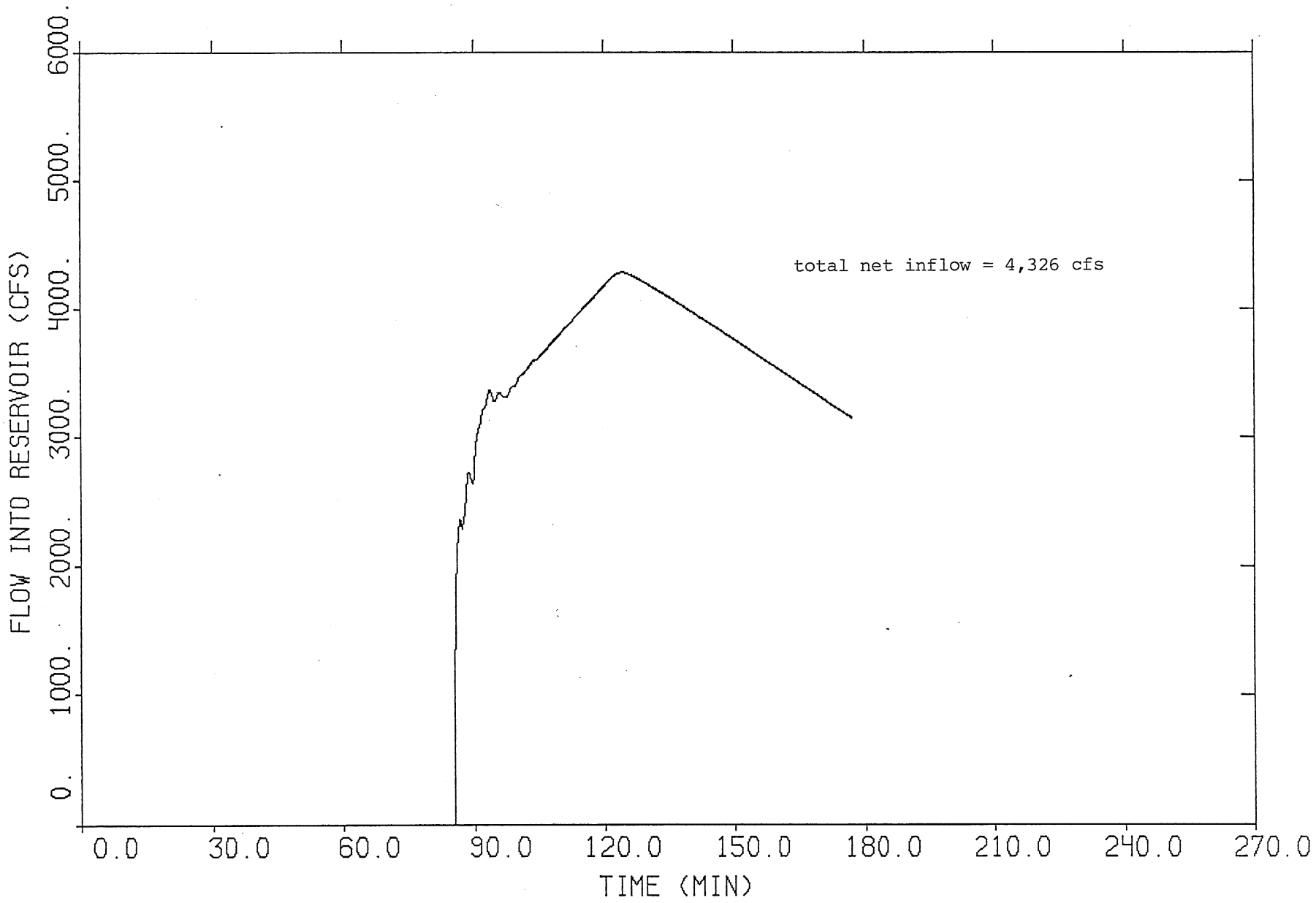

Fig. 61. Outflow hydrograph to terminal reservoir, dropshaft design inflow.

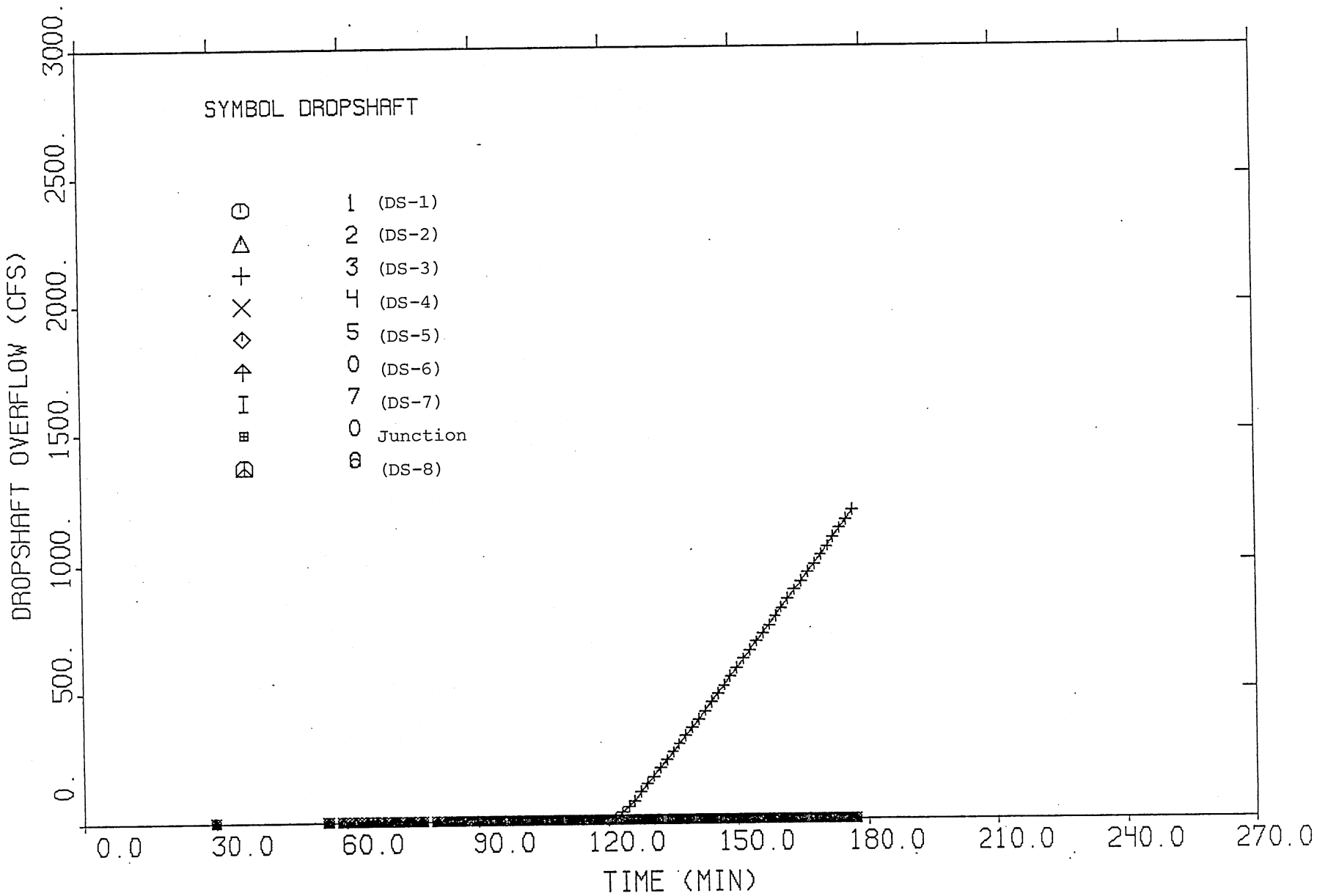

Fig. 62. Overflow hydrograph at Ds–3, dropshaft design inflow.